Modelling Fatigue Deterioration and Retrofitting in Bridge Management Systems

by

Jeremie Raimbault

A thesis

presented to the University of Waterloo

in fulfillment of the

thesis requirement for the degree of

Master of Applied Science

in

Civil Engineering

Waterloo, Ontario, Canada, 2016

Author's Declaration

I hereby declare that I am the sole author of this thesis. This is a true copy of the thesis, including any required final revisions, as accepted by my examiners.

I understand that my thesis may be made electronically available to the public.

Abstract

Similar to any other structure exposed to the elements, bridges deteriorate and degrade over time. This deterioration can result in costly maintenance and repair if it is addressed properly or damage and even loss of life if it is neglected. Due to an increasing number of bridges and limited funds, more economical and efficient bridge management systems (BMSs) were created for planning maintenance and rehabilitation projects. However, the element classifications used in these are broad, and the transition probabilities are based only on inspection history and experience. In particular, the most important form of loading, cyclic loading from trucks, and its effects on fatigue-susceptible features of a bridge such as welds is not considered. Fatigue damage is difficult to measure in the field, as it can take decades to develop, and even in a laboratory setting is time consuming. Computer models have been developed and calibrated from laboratory data, but modelling fatigue is very complicated as it may require consideration of non-linear material behaviour and crack closure effects in order to ensure accurate predictions, and performing Monte Carlo Simulation (MCS) to obtain statistics of crack growth requires thousands or millions of trials. This large computational cost makes computer simulations impractical for the analysis of large stocks of bridge infrastructure. Multiplicative Dimension Reduction Method (M-DRM) is a tool, which can be used to calculate the statistical parameters of the response of a function with a massive reduction in the number of computations required. However, it is not known if techniques such as M-DRM will reduce the computational cost to a sufficient extent to permit the analysis of many structures. One possible solution would be to use simple BMS-like models to simulate fatigue deterioration and the various management actions. This would involve the calibration of a Markov chain, which uses a set of probabilities and current information to predict the condition of an element in the future. However, it is not known if this simplistic approach will be sufficiently accurate in capturing the effects of the various management actions, in order to determine the optimal maintenance strategy.

The research objectives in this thesis are therefore 1) to evaluate the effectiveness of Strain-Based Fracture Mechanics (SBFM) and Multiplicative Dimensional Reduction Method (M-DRM) for predicting the statistics of fatigue crack growth, 2) to compare the computational effort of M-DRM and Monte Carlo Simulation on SBFM in this context, and 3) to calibrate simpler BMS-like Markov chain models and apply them to single welds to assess their accuracy and suitability for modelling fatigue deterioration and making high level fatigue management decisions.

To perform the first objective, SBFM and M-DRM were used to draw fatigue crack growth curves, known as Stress range vs. Number of cycles to failure, or S-N plots, and compare them against existing S-

N curves. Different loading histories were analyzed, both constant amplitude and variable amplitude. The second objective was performed by analyzing the accuracy and difficulty of plotting the S-N curves from the two methods. To perform the third objective, two sizes of Markov chains were calibrated using three different methods: calibration using S-N design curves, calibration using SBFM failure data, and calibration using SBFM crack growth data. To compare these methods, in addition to the curve fits from the calibration methods, a life cycle cost analysis (LCCA) was performed, which assigned costs to different maintenance actions, such as inspection, treatment, repair and replacement, and combined them to form different maintenance strategies. These were then compared to the original graphs for a non-biased comparison method. As these were only calibrated to a Detail Category C, a local stress approach was developed to transform the Markov chains to other detail categories. As fatigue can be affected by other mechanisms, the correlation between elements was investigated, specifically between fatigue and corrosion. An example bridge was then designed, and the deterioration models developed in this thesis applied, with the effect of different maintenance strategies studied.

Several conclusions were drawn from the work performed in this thesis. From the SBFM and M-DRM analyses, loading history does affect the position of the S-N curve, with variable amplitude loading curves falling below the constant amplitude curve. M-DRM can accurately predict the statistics of fatigue crack growth for both for as-welded and treated specimens. The M-DRM analysis was performed using a fraction of the time required to perform the MCS analysis; approximately 2 full days were required to calculate one S-N curve using MCS, compared to less than one hour for M-DRM. M-DRM was also able to perform sensitivity analysis on the variables. Of the three calibration methods for Markov chains, calibration using the probabilistic SBFM crack growth data performed the best when comparing plots of individual condition state probabilities and based on subsequent LCCA. Of the two Markov models used in this thesis, using five and ten condition states, both predicted the same optimal strategy with similar absolute values. The correlation between corrosion and fatigue was also studied and modelled using the Markov chain approach, and it was found that high levels of corrosion can have a significant impact on life-cycle cost, and can even change the optimal fatigue management strategy. Using the full-scale bridge designed in this thesis, by comparing the various management strategies, a cost savings of as much as $2,050,000 over the 100 year life span was obtained by choosing the optimal management strategy. The flexibility and ease of use of the Markov chain models was exploited to easily analyze and modify a number of alternative management strategies, thus demonstrating the usefulness of this approach for modelling the fatigue deterioration and retrofitting of bridges. This work is mainly aimed at bridge infrastructure owners, but the methodology could be applied to any cyclically loaded welded structure.

Acknowledgements

I would like to thank the following persons for their contributions to this work:

- My supervisor, Dr. Scott Walbridge. His experience, knowledge, support, and prompt responses to late night emails have made this work possible.
- Dr. Mahesh Pandey and George Balomenos for their help on understanding and applying M-DRM.
- Dr. Tarek Hegazi and Dr. Rebecca Saari for their comments and insights on the final draft.
- My family, and especially my parents, who have constantly supported and encouraged me in my quest for higher learning.
- Amanda, who has given me so much joy and supported me emotionally, spiritually, and materialistically in the final hard months.
- God, the Author and creator of all things. The more I study and learn, the more I see His fingerprints in the world.

Dedication

To: My parents, my inspiration and reason I am the person I am.

Table of Contents

List of Figures

List of Tables

1.0 Introduction

1.1 Background and motivations

Similar to any other structure exposed to the elements, bridges deteriorate and degrade over time. This deterioration can result in costly maintenance and repair if it is addressed properly or damage and even loss of life if it is neglected. The recent 2013 Report Card for America's Infrastructure [ASCE, 2013] found that one in nine bridges in America are structurally deficient, and require $20.5 billion annually to properly maintain, $8 billion more than what is currently being spent. A 2005 report indicated that the cost of upgrading and renewing the existing urban roads and bridges in Canada was around $66 billion [Statistics Canada, 2009]. Failure to properly maintain bridges can lead to catastrophic collapses, such as the recent Laval, Quebec and Minnesota bridge collapses in 2006 and 2007 [Johnson, Couture, & Nicolet, 2007][Holt & Hartmann, 2008].

During the 1960s and 1970s, this maintenance challenge was addressed as the need arose. Due to an increasing number of bridges and limited funds, more economical and efficient bridge management systems (BMSs), such as Pontis [Thompson et al., 1998], were created for planning maintenance and rehabilitation projects. In order to model deterioration and management actions such as maintenance or repair of large numbers of bridges, the deterioration modelling in Pontis is necessarily simplistic in nature to make computation times manageable. Pontis divided a bridge into 120 elements and assigned condition states (CSs) to these elements from one to five, with one being "in perfect condition" and five being "replacement required". Based on theoretical deterioration modelling and inspection history, probabilities of moving from one CS to another during one year were developed. With this information, future CSs could be predicted using a Markov chain approach, where the transition probabilities are applied to the probabilities of being in each CS in the preceding year to obtain new probabilities of residing in a given CS. However, the element classifications used in Pontis are broad, and the transition probabilities are based only on inspection history and experience. In particular, the most important form of loading, cyclic loading from trucks, and its effects on fatigue-susceptible features of a bridge such as welds is not considered.

Fatigue, or damage due to long-term cyclical loading, is one of the ways in which bridges can deteriorate over time. While the number of catastrophic bridge failures caused by fatigue is not enormous, significant fatigue damage and member or connections failures frequently occur in bridges [Kuehn et al, 2008]. Prior

to such failures, fatigue damage is difficult to measure in the field, as it can take decades to develop, and cracks are typically very small for most of the fatigue life. Fatigue testing in a laboratory setting is time consuming, as samples can undergo millions of cycles to failure, which can take weeks or months for a single sample, depending on the load level and testing speed. Computer models have been developed and calibrated from laboratory data, but modelling fatigue is very complicated as it may require consideration of non-linear material behaviour and crack closure effects in order to ensure accurate predictions.

A range of management actions exist for dealing with detected or anticipated fatigue problems, including: reinforcement to reduce stress ranges, detail modification to reduce stress concentrations, member replacement, load restrictions, gouging and re-welding detected fatigue cracks, increased inspection, and a range of post-weld treatments for increasing fatigue performance. Post-weld treatments employ various means to improve the fatigue performance of the welds – a particularly fatigue-prone part of any structure – using various means, such as grinding or dressing to remove defects and improve the weld profile, or impact treatment (e.g. by peening or high frequency mechanical impact (HFMI) treatment – see Figure 1.1) to introduce compressive residual stresses, which reduce crack growth rates.

Figure 1.1: Improving the fatigue performance of a weld by HFMI treatment

Various analytical means exist for predicting the effects of management actions on fatigue performance. These range from relatively simple, design code-like deterministic checks involving the calculation of a design stress range, which is compared with a fatigue resistance for the detail category of interest (i.e. the "Classification Method") to more advanced techniques employing fracture mechanics and/or probabilistic

methods. One of the more advanced models in the second category is Strain Based Fracture Mechanics (SBFM), which considers both non-linear material behaviour and crack closure effects. SBFM can be used to make deterministic predictions, or in a probabilistic framework, in which all of the input parameters have statistical distributions with a mean, standard deviation, and distribution type. Monte Carlo Simulation (MCS) can then be used to determine the statistics of fatigue growth. However, this requires thousands if not millions of simulations, which required significant computational effort. While a high degree of accuracy in predicting the effects of various fatigue management actions can be achieved with a calibrated SBFM model, applying probabilistic SBFM using MCS to large numbers of welds on large numbers of bridges to make high level management decisions is impractical.

Multiplicative Dimension Reduction Method (M-DRM) is a tool, which can be used to calculate the statistical parameters of the response of a function. The largest advantage of M-DRM over MCS is a massive reduction in the number of computations required, for a three variable problem there are only 16 calculations required, compared to the thousands or millions for MCS. M-DRM also allows for sensitivity analysis of the input variables. M-DRM can be used with advanced analytical models, including SBFM models, to help deal with the large computational effort required by MCS.

In summary, fatigue deterioration is a significant problem in bridges, which is currently not being considered in bridge management systems (BMSs). Advanced models exist for predicting the effects of fatigue management actions. However, the computational cost associated with these models makes them impractical for the analysis of large stocks of bridge infrastructure. Techniques (such as M-DRM) exist for reducing the computational cost of these advanced models. However, it is not known if these techniques will reduce the computational cost to a sufficient extent to permit the analysis of many structures. One possible solution would be to use simple BMS-like models to simulate fatigue deterioration and the various management actions (i.e. using a Markov chain approach). However, it is not known if this simplistic approach will be sufficiently accurate in capturing the effects of the various management actions, in order to determine the optimal maintenance strategy.

1.2 Research objectives

Based on the background and problem statement presented in the preceding section, the research described in the current thesis was undertaken with the following objectives:

1) To evaluate the effectiveness of Strain-Based Fracture Mechanics (SBFM), used in conjunction with the Multiplicative Dimensional Reduction Method (M-DRM), for predicting the statistics of fatigue crack growth in as-received and retrofitted (impact treated) welds;
2) To compare the computational effort of M-DRM vs. MCS in this context and assess the suitability of SBFM/M-DRM analysis for making fatigue management decisions; and
3) To calibrate simpler BMS-like Markov chain models and apply them to single welds and full-scale structures with many welds to assess their accuracy and suitability for modelling fatigue deterioration and making high level fatigue management decisions.

In conducting the analytical research related to the first objective, special attention was paid to modifications to the deterministic SBFM code required so that M-DRM could be performed both in the finite and the infinite life domain. In conducting the research related to the third objective, practical methods for considering a number of issues were explored, including: the modelling of multiple deterioration mechanisms (e.g. corrosion and fatigue) on single elements (e.g. a welded steel bridge girder) and the modelling of correlated behaviours between elements.

1.3 Scope

The research presented in this thesis is entirely analytical in nature. The results of previous laboratory experiments are used to validate the presented analysis. The BMS-like models developed through this research have all been created using Microsoft Excel. The SBFM analysis (using MCS or M-DRM) has been performed using a previously-developed, deterministic FORTRAN code. The fatigue management actions modelled in this analytical research are limited to: inspection, gouging and rewelding, reinforcement, and impact treatment (by needle peening). However, the presented methodologies are thought to be relevant to a much wider range of management actions.

1.4 Structure of thesis

This thesis is organized in six chapters. Chapter 2 presents a literature review covering the following topics: fatigue of welds, deterministic and probabilistic fracture mechanics, M-DRM, and BMSs. In Chapter 3, probabilistic SBFM analyses of as-received and impact treated welds are performed using MCS and M-DRM. Modifications to the SBFM code to enable analysis by M-DRM in both the finite and infinite life domains are discussed, and the benefits of using M-DRM are critically assessed. In Chapter 4, Markov chain-based models, similar to those used in in existing BMSs such as Pontis, are calibrated

using the probabilistic SBFM output from Chapter 3, and then used to model fatigue deterioration and management of individual welds. In Chapter 5, the models developed in the previous chapters are applied to an example full-scale bridge. Finally, in Chapter 6, the main findings and conclusions of this research are presented along with recommendations for future research.

2.0 Literature review

In the following sections, a literature review is presented of the key topics covered in the current thesis. These include: fatigue analysis and design, strain-based fracture mechanics (SBFM), probabilistic fracture mechanics, bridge management systems (BMSs), and fatigue assessment and retrofitting methods.

2.1 Fatigue analysis and design overview

In a perfect world, all metal would be smooth and free of defects. However, this is not the case in real structures, as manufacturing techniques, construction processes and even small variations in the structure of the metal can cause discontinuities and small defects. These defects by themselves are not a problem. However, repeated stress changes in the surrounding material can cause cracks to initiate and grow over time, which, if left unchecked, can eventually cause ductile or brittle fracture of the element.

There are a couple criteria, which govern the severity of a crack. Figure 2.1 shows different crack locations in metal specimens, with one being the least severe and five being the most.

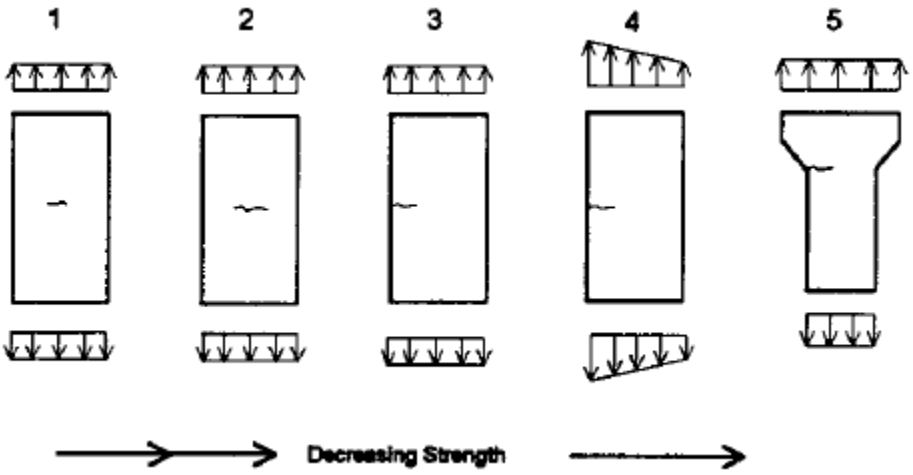

Figure 2.1: Crack severity [Kulak and Smith, 1993]

Case 1 shows a small crack in the center of an element under tension loading. Increasing the crack length, as shown in Case 2, results in a decrease in strength (or increase in crack severity). Moving the crack to an unrestrained edge, as shown in Case 3, allows for greater crack opening and closing, which further decreases the strength. This problem can be magnified by uneven loading, with bending stresses able to

open the crack even more, as shown in Case 4. Finally, any sort of stress concentration, here shown by a change in geometry in Case 5, can decrease the strength significantly.

Figure 2.2 shows a more detailed look at the crack tip. Due to the discontinuity introduced by the crack, the stress field must flow around it, which results in a significant stress concentration at the tip. The peak stress is theoretically infinite, and so the material cannot behave elastically. Instead, a plastic zone forms at the crack tip. This repeated process of an increase in the magnitude of the stress field surrounding the crack causing it to open, relieving the crack surfaces of stress, then creating crack-tip plastic straining, is the basic method by which cracks can grow in and ultimately weaken structures.

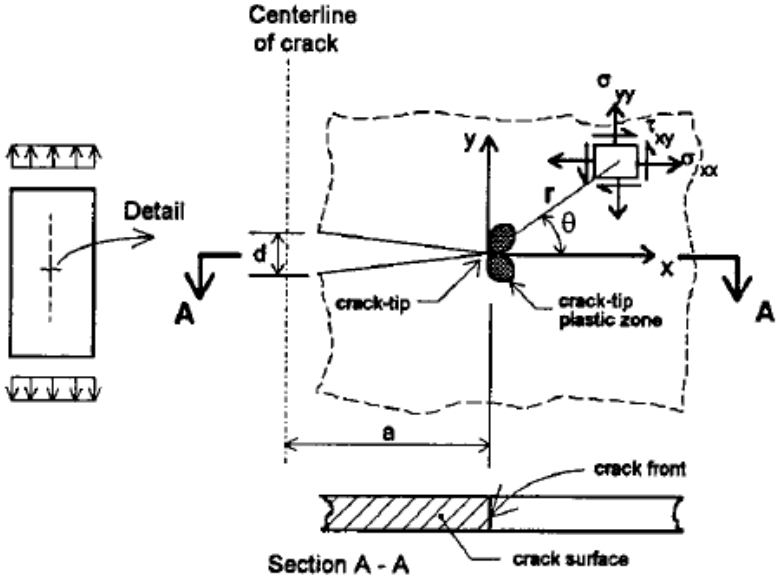

Figure 2.2: Crack details [Kulak and Smith, 1993]

By neglecting the plastic zone, a simplified model can be considered. The stress at the crack tip can be calculated in terms of coordinates r and θ, for the stress in the y-direction ($\theta = 90$), the stress is:

$$\sigma_{yy} = \frac{\sigma\sqrt{\pi a}}{\sqrt{2\pi r}} \tag{2.1}$$

The numerator is often referred to as the stress intensity factor (SIF), K, which can be used to describe any combination of stress and crack length. The factor K is dependent on geometric and loading conditions, and so the equation can be modified to include other terms:

$$K = WY\sigma\sqrt{\pi a} \tag{2.2}$$

where Y is a geometric correction factor, which accounts for such things as plate edges and curved crack fronts, and W accounts for non-uniform stresses along the crack length due to the applied load, residual stresses, thermal effects, etc. These equations assume linear-elastic material behaviour, and require the plastic zone to be small (< 2% of the plate thickness) to produce satisfactory results.

When a crack is sufficiently large, the remaining cross section may fail either by ductile or brittle fracture. Ductile fracture occurs if the stress in the remaining material exceeds the strength of the material. It is normally preceded by significant evidence of plastic deformation. Brittle fracture can occur prior to ductile fracture if the stress intensity factor (SIF) K exceeds the fracture toughness of the material. As the name implies, it occurs with little warning or evidence of prior plastic deformation. Fracture toughness can be measured using the Charpy impact test, in which a small bar is struck and fractured by a swinging hammer, and the energy lost by the hammer due to the fracturing of the material is measured as a change in swing height. This energy is then related to the toughness of the steel [ASTM E23-12c, 2009].

This toughness can be used to determine a critical crack length, a_{cr}, after which the remaining cross section will fracture in a brittle manner. For steel, the fracture toughness depends on a number of factors, such as the ambient temperature. The engineer should ensure that the properties of the section combined with the inspection frequency permit detection of cracks well before they reach a_{cr}.

It is uncommon for newly constructed elements to have cross section geometries that they are already prone to brittle fracture. Thus, where fracture tends to be a greater concern is when a small initial crack grows, or propagates, through the repeated application of stress cycles, into critical cracks, which are sufficiently large to cause failure by fracture. This process is called “fatigue”.

Fatigue is becoming more and more relevant in design and maintenance. Improvements in metallurgy have resulted in stronger steel grades, which allow for higher stresses under service loading. While these steels allow bridges to carry higher static loads, they generally do not result in a significant performance improvement under cyclic (or fatigue) loading. In addition, modern steel structures generally use welding as the primary method of attachment. Welding tends to result in significant reductions in fatigue performance, due to the introduction of defects and tensile residual stresses as a result of the welding process. Welds also tend to occur at locations where stress concentrations are present. The number of aging structures, which are past their design fatigue life, is also increasing. The combination of these factors creates the need for suitable methods to detect and assess fatigue cracks.

Linear elastic fracture mechanics (LEFM) can be used to determine the relationship between the crack length, *a*, and number of cycles, *N*, as shown in Figure 2.3, for the purpose of fatigue life prediction.

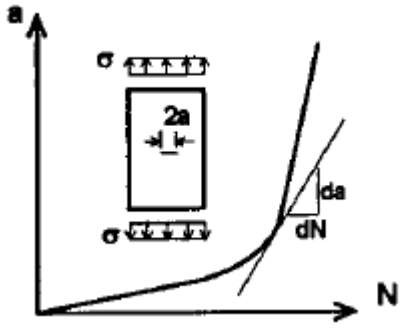

Figure 2.3: Crack length (a) plotted against the number of cycles (N) [Kulak and Smith, 1993]

Equation (2.2) can be modified to consider cyclic loading as shown follows:

$$\Delta K = WY\Delta\sigma\sqrt{\pi a} \tag{2.3}$$

where $\Delta\sigma$ is equal to the difference between the maximum and minimum stress in the stress cycle (i.e. $\sigma_{max} - \sigma_{min}$). We can relate ΔK to d*a*/d*N*, as shown in Figure 2.4, using the Paris-Erdogan law:

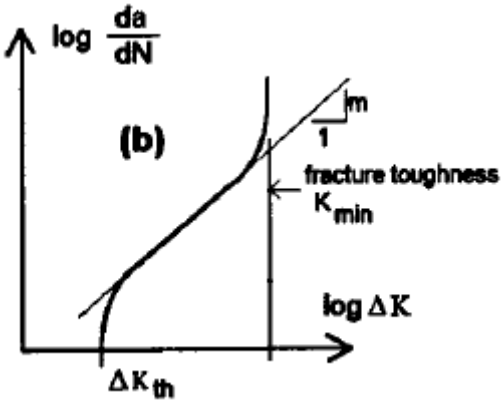

Figure 2.4: ΔK vs log da/dN

At very low growth rates, the curve becomes vertical at ΔK_{th}, or the threshold stress intensity factor. Below this rate the loading is not sufficient to grow the crack, and so the fatigue life is infinite. Above ΔK_{th} the curve straightens to a constant slope *m*, and becomes vertical again near the fracture toughness. The Paris-Erdogan law [Kozin & Bogdanoff, 1989] can be used to approximate the slope in the middle region:

$$\frac{da}{dN} = C\Delta K^m \tag{2.4}$$

where C and m are constants based on the material behaviour. By integrating Equation (2.4) from an initial defect size to a final critical crack length, an estimate of fatigue life can be obtained.

For constant amplitude (CA) loading, in which the maximum and minimum stress levels are the same for each cycle, this stress range, $\Delta\sigma$, is easy to define. However, real loading is normally not that simple, for example when a truck drives over a bridge, each axle will cause a peak, and each peak will have a different magnitude based on the axle weights and spacing. There are methods available for converting variable amplitude (VA) loading histories, such as the one shown in Figure 2.5a, to equivalent CA histories. Two of them, shown conceptually in Figure 2.5b and 2.5c, are rainflow and reservoir analysis. Rainflow analysis is the most popular method, due to the relative ease with which it can be codified [Anthes, 1997, Downing & Socie, 1982], and the close relationship between the cycles counted using the rainflow method and the cycles that would be associated with the closing of hysteresis loops in a nonlinear stress-strain analysis.

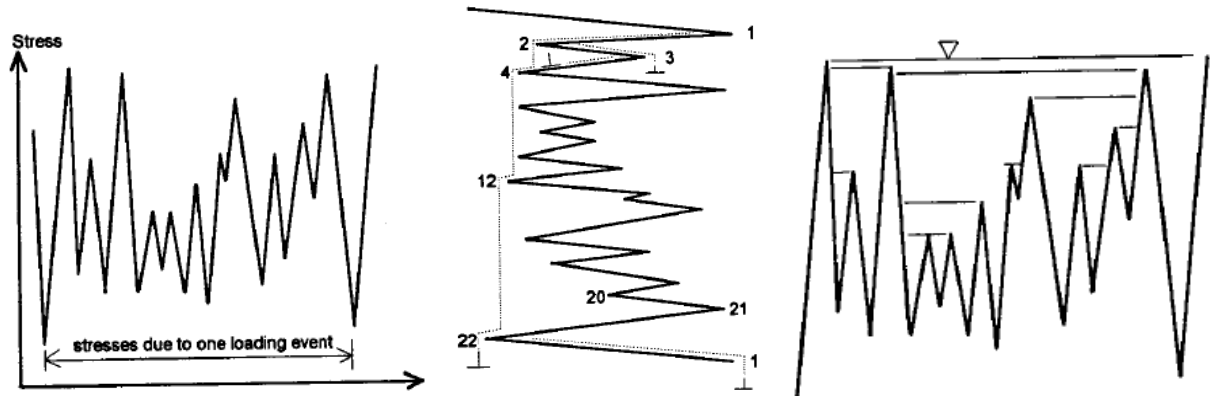

a) Variable amplitude example *b) Rainflow analysis* *c) Reservoir analysis*

Figure 2.5: Variable amplitude (VA) loading analysis

Critical locations from the point of view of fatigue in structures such as bridges generally do not consist of axially loaded plates, such as those shown in Figure 2.1. They are generally associated with sudden changes in geometry at locations such as connections, and therefore have significant stress concentrations, associated with them. A practical approach for considering the effect of these stress concentrations in design is the so-called “Classification Method”, wherein common connection geometries are classified according the severity of the “stress concentration factor” (SCF) that they produce. In this context, the SCF is the ratio of the local stress divided by the global stress that would be present if the sudden change

in geometry weren't there. Once the "detail category" for a given connection geometry is known, it can be designed for fatigue using the appropriate stress-life (S-N) design curve. Figure 2.6 shows an example of a set of S-N curves used for the fatigue design of steel structures in Canada.

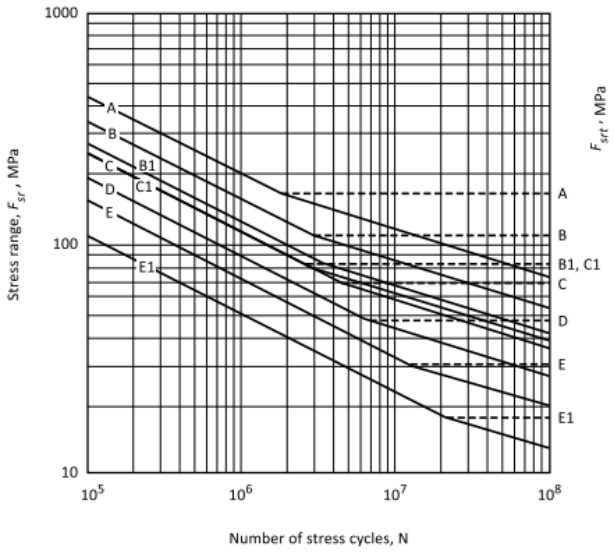

Figure 2.6: S-N Curves [CSA, 2009]

The lines in Figure 2.6 represent the 97.7% survival probability, and each line, denoted A through E1, represents a detail category. The S-N curves can be read in two ways, the first is from the x axis. If a designer has a bridge (for example) with 10,000 loading cycles per year on a Detail Category C, and they want it to last 100 years, they look at the 10^6 line, look at the intersection with the Detail Category C line, which shows the welds cannot have a stress range higher than about 102 MPa to ensure a 97.7% survival probability. The second way to read the graph is from the y axis. If the designer has a Category E detail which has a stress range of 100 MPa, they trace that line horizontally until they reach $N \approx 3 \cdot 10^5$ cycles. They therefore know that they have a 97.7% chance of the detail surviving this long.

The slopes of the design curves in Figure 2.6 at higher stress levels, m, is 3. This slope is constant down to the constant amplitude fatigue limit (CAFL). This is the limit below which a crack will not grow under constant amplitude loading, because the stress intensity factor (SIF) is less than the threshold, ΔK_{th}. This is represented by the dashed horizontal line on the S-N curve. The solid line which continues past the CAFL point has a slope of $m' = 5$, and is used to calculate the cumulative damage for VA loading when some peaks in the stress history are above the CAFL and some below. These slopes and design curves are typical for steel structures. Different curves are used for other materials, such as aluminum.

In order to determine the detail category of a connection for the purpose of fatigue design, most codes summarize the common connection geometries into tables, with text and sketches describing the connection geometry, orientation of the connection with respect to the loading direction, and the type of loading (e.g. axial or flexural). Figure 2.7 shows a sample of a Detail Category C connection from CSA S16-14 [CSA, 2014]. Other detail category definitions can be found in this and other design codes.

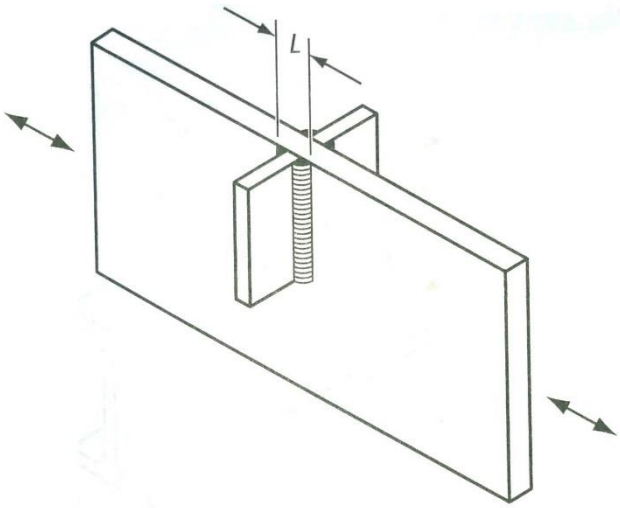

Figure 2.7: Detail Category C [CSA, 2014]

2.1.1 Strain-Based Fracture Mechanics (SBFM)

As mentioned earlier, by integrating Equation (2.4), it is possible to make fatigue life predictions. This is the essence of linear elastic fracture mechanics (LEFM)-based fatigue analysis. While useful for many practical applications, this approach ignores a number of factors that may be significant in some cases, including the effects of nonlinear material behaviour, residual stresses, and crack closure effects. Strain Based Fracture Mechanics (SBFM) is an alternative to LEFM, which can be used to consider these effects. SBFM models have been developed for the fatigue analysis of smooth metal components, largely through research conducted in the last 30 years at the University of Waterloo [Lam, Topper, & Conle, 1998] [Topper & Lam, 1997] [MacDougall & Topper, 1997] [Khalil & Topper, 2003]. Recent efforts to apply these models to welded connections are summarized in [Ghahremani & Walbridge 2011]. The governing equation employed by these models is based on the Paris-Erdogan crack growth law, modified to consider crack closure and the presence of a threshold stress intensity factor (SIF) range:

$$N = \int_{a_i}^{a_c} \frac{\mathrm{d}a}{C \cdot \mathrm{MAX}\left(\Delta K_{eff}{}^{m} - \Delta K_{th}{}^{m}, 0\right)} \tag{2.5}$$

where a_i and a_c are the initial and critical crack depths and C and m are material constants. The effective stress intensity factor range, ΔK_{eff}, is calculated using the following equation:

$$\Delta K_{eff} = K_{\max} - MAX\left(K_{op}, K_{\min}\right) \tag{2.6}$$

where K_{max} and K_{min} are the SIFs at maximum and minimum for a given applied load cycle, and K_{op} is the SIF corresponding to the crack opening stress level for that cycle. The main difference between LEFM and SBFM is in the calculation of the SIFs, K. Previously Equation (2.3) was used to calculate the SIFs. However, in SBFM the following equation is used for calculating K:

$$K = Y \cdot E \cdot \varepsilon \cdot \sqrt{\pi a} \tag{2.7}$$

where ε is the local strain at crack depth, a, and Y is a correction factor to account for the crack shape, free surface, and the finite thickness of the plate. To calculate the stresses and strains for each load cycle, a Ramberg-Osgood material model is used with parameters K' and n'. Strain histories at various depths below the surface of the weld toe and crack closure are considered using established models [Newman 1994, Dowling 2007], which use the maximum stress level, stress ratio, flow stresses, and the plastic constraint factor. Figure 2.8 illustrates the cyclical loading analysis process:

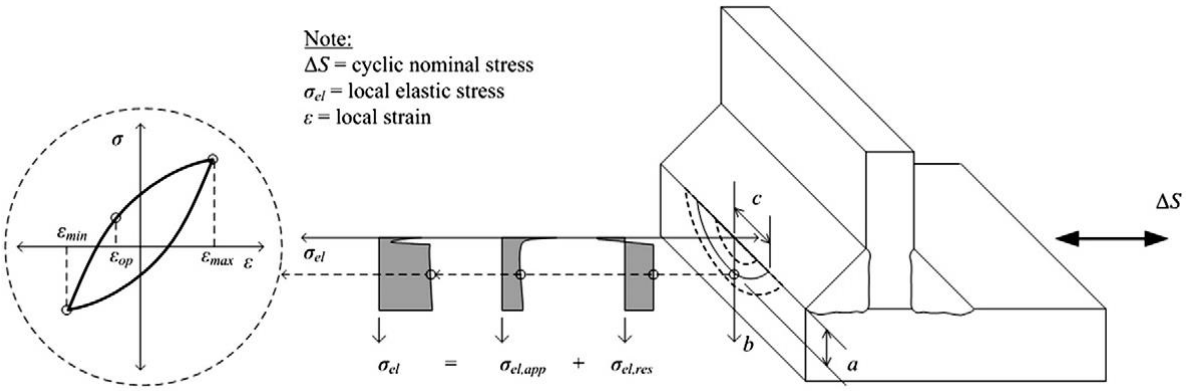

Figure 2.8: Explanation of stress-strain analysis according to SBFM [Ghaharemani & Walbridge, 2011]

The local elastic stress, σ_{el}, is a function of the local elastic residual stress, $\sigma_{el,res}$ due to welding or impact treatment, and the local elastic stress due to the applied load, $\sigma_{el,app}$. The local elastic stresses are calculated using a factor that is similar in many respects to an SCF, k_p:

$$k_p = \frac{K_{el}}{Y \cdot \sqrt{\pi a}} \tag{2.8}$$

where K_{el} is the elastic SIF accounting for non-uniform stress distribution. It is calculated as follows:

$$K_{el} = \int_0^a k_{el} \cdot m(b,a,c) \cdot db \tag{2.9}$$

where $m(b,a,c)$ is a weight function as described in [Shen & Glinka, 1991], b is depth below the surface and k_{el} is the SCF for an uncracked weld toe. The local elastic stress is therefore calculated as:

$$\sigma_{el} = k_p \cdot S \tag{2.10}$$

The local non-linear stress-strain history is calculated using a nominal stress (S) history. Each time a stress-strain hysteresis loop is closed, the local minimum, maximum, and crack opening strains are calculated. ΔK_{eff} is then calculated, and the fatigue life is determined using Equation (2.5).

For the analysis of welds retrofitted using residual stress-based impact treatments, the SBFM model offers advantages over linear elastic fracture mechanics (LEFM) in terms of its ability to model the evolution of the residual stresses under VA loading conditions [Ghahremani & Walbridge 2011].

2.2 Probabilistic fracture mechanics

LEFM and SBFM analysis can be performed either in a deterministic framework (i.e. fixed values assigned to each input parameter) or a probabilistic one (i.e. with each input parameter assigned a mean, standard deviation, and distribution type, in order to obtain a statistical distribution for the output, for example, the number of cycles to failure). In the follow sections, two approaches for performing the probabilistic fracture mechanics analysis are discussed: the classical Monte Carlo Simulation (MCS) approach and the Multiplicative Dimension Reduction Method (M-DRM).

2.2.1 Monte Carlo Simulation (MCS)

Monte Carlo Simulation (MCS) is a method used to determine the probability of failure of a function. Further descriptions can be found in a number of references, for example [Ang & Tang, 1984][Melchers, 1999], but a brief overview will be provided here. The process of MCS involves evaluating a function numerous times with randomly selected values for the variables, z_i. The probability of failure can then be calculated using the following equation:

$$p_f = \frac{n(G(z) \leq 0)}{N_t} \tag{2.11}$$

where N_t is the total number of calculations performed, and $n(G(z) \leq 0)$ is failure, or when the limit state was violated. To generate responses to the function, a random number u_i between zero and one is selected for each variable z_i, which can have any type of distribution, here assumed to be normal. The random number u_i is then transformed into the variable z_i using the following equation:

$$z_i = F_{zi}^{-1}(u_i) \tag{2.12}$$

where $F_{zi}^{-1}()$ is the inverse of the CDF for the variable z_i. The process by which random selection of variables generate responses is shown in Figure 2.9.

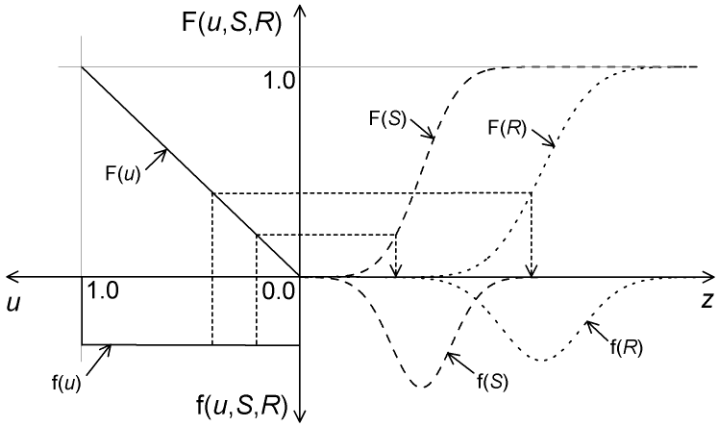

Figure.2.9: MCS [Walbridge, 2005]

Here, two random numbers, u_i, are selected from a uniform distribution, f(u). These are then transformed into the solicitation, S, and resistance, R, using Equation (2.12). The response from this set of random numbers results in the solicitation being greater than the response, and thus failure did not occur.

After this process is repeated numerous times, the probability of failure p_f can be estimated according to Equation (2.13). The more trials performed, the greater the accuracy of the estimation. An advantage to this method is that the probability of failure can be calculated without analysis of the function, it can be treated as a black box, and so is simple to execute. However, many trials are required to achieve an accurate probability of failure, which can be computationally expensive, especially when each trial itself is complex. There are methods available to reduce the number of trials required, such as importance sampling and the use of antithetic variates, which are discussed in detail in [Ang & Tang, 1984][Melchers, 1999], however these still require many iterations.

2.2.2 Multiplicative Dimension Reduction Method (M-DRM)

The Multiplicative Dimension Reduction Method (M-DRM) is an alternative to MCS, which is expected to offer considerable advantages in terms of calculation efficiency. This improved efficiency can be critical – in particular when performing analysis of problems where the computational effort associated with a single, deterministic calculation is high, such as SBFM analysis.

There have been several methods derived for dealing with statistical analysis of multivariate problems, in order to avoid the high computation cost of classical MCS. The first-order reliability method (FORM) [Hasofer & Lind 1974] is an alternative approximate method, but this approach lacks generality when dealing with the response of many variables [Schueller & Pradlwarter 2007]. Similar problems occur for variations of FORM, including the second-order reliability method (SORM), the first-order third-moment reliability method, and the response surface approach [Zhao & Ono 2001].

The method of moments can be used to find an approximate solution to a multivariate problem [Taguchi 1978]. By calculating the first four moments of the response, mean, variance, skewness and kurtosis, the parameters of that distribution can be back-calculated. However, the calculation of moments involves multi-dimensional integrals, which are very complex. Research in the past has looked at the efficient evaluation of these integrals using point estimate methods [Taguchi 1978], [Rosenblueth 1981], Taylor series approximation and non-classical orthogonal polynomial approximations [Kennedy & Lennox 2001]. More recently, high-dimensional model representation [Li et al. 2001] and the dimensional reduction method [Rahman & Xu 2004], [Xu & Rahman 2004] have been used, in which the multivariate function is decomposed into orthogonal component functions. The principle of maximum entropy [Jaynes 1957] was introduced to deal with the issue of sensitivity of tail probabilities, but this required significant computational effort in the moment calculations when dealing with a large number of constraints. The

recent emergence of fractional moments [Inverardi & Tagliani 2003], [Milev et al. 2012] has made these calculations easier. A fractional moment is a moment of the order of real as opposed to whole numbers, which can be combined together to determine information about the resultant distribution.

M-DRM [Zhang, 2013] is a combination of fractional moments and the maximum entropy principle, and is a more efficient method of performing statistical analysis than MCS. The main benefit this method has over MCS is the massive reduction in number of trials needed. Given a problem with three variables, for example, instead of the thousands of iterations required for MCS, only 16 calculations are required for M-DRM. A second benefit is the additional analysis options available. With only mean and standard deviation results available from MCS, M-DRM allows for sensitivity analysis.

M-DRM uses Gaussian quadratures, which are commonly used for multi-dimensional integration. The type of Gaussian quadrature varies depending on the type of distribution, with Gauss-Hermite used for Normal and Lognormal distributions, and Gauss-Laguerre used for Exponential and Weibull distributions. These quadratures are based on the approximation of integrations evaluated at known Gauss points. The number of points corresponds to the number of orders desired, with five being the most common.

Table 2.1: Weights (wj) and points (zj) for 5th order Gaussian quadrature [Balomenos & Pandey 2013]

Gaussian Rule	**N**	**1**	**2**	**3**	**4**	**5**
Gauss-Legendre	wj	0.24	0.48	0.57	0.48	0.24
	zj	-0.91	-0.54	0.00	0.54	0.91
Gauss-Hermite	wj	0.01	0.22	0.53	0.22	0.01
	zj	-2.86	-1.36	0.00	1.36	2.86
Gauss-Laguerre	wj	0.52	0.40	0.08	0.004	2.3E-5
	zj	0.26	1.41	3.60	7.09	12.64

Similar to how a normal random variable, *X*, can be related to the standard normal random variable, *Z*, using the following expression:

$$X = \mu + \sigma \cdot Z \tag{2.13}$$

with μ equaling the mean value and σ equaling the standard deviation, the Gauss-Hermite points can be obtained as follows:

$$X_j = \mu + \sigma \cdot z_j \tag{2.14}$$

where z_j is taken from Table 2.1.

To perform M-DRM, all of the variables except one are held at their mean value while each variable is varied one at a time according to the five Gaussian quadratures using Equation (2.14). For an example with three variables, denoted as α, β, λ, a total of 16 calculations are required, five for each of the three variables, and one final calculation with all variables held at their mean values. The first moment for each variable is then calculated as follows:

$$\rho_\alpha = \sum_{i=1}^{5} w_j \cdot R(\alpha_i, \beta_0, \lambda_0) \tag{2.15}$$

where w_j are the Gaussian weights according to Table 2.1, and $R(\alpha_i, \beta_0, \lambda_0)$ is the resultant value achieved by varying α by each Gaussian Point according to Equation (2.14), and holding β and λ at their mean values. The second moment for each variable is then calculated similarly as follows:

$$\theta_\alpha = \sum_{i=1}^{5} w_j \cdot R(\alpha_i, \beta_0, \lambda_0)^2 \tag{2.16}$$

Equations (14)-(16) are explained in Figure 2.10.

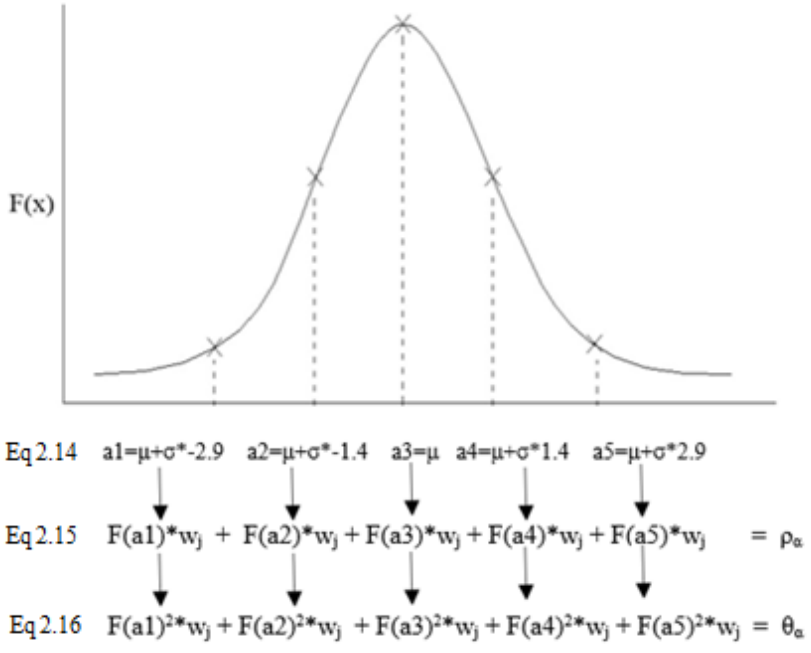

Figure 2.10: Graphical explanation of M-DRM

The mean of the result can then be calculated using the following expression:

$$\mu = \rho_{avg}^{(1-n)} \cdot \rho_\alpha \cdot \rho_\beta \cdot \rho_\gamma \tag{2.17}$$

where n is the number of variables, three in this case, and ρ_{avg} is the result of holding all variables at their mean. The second moment of the result is calculated by:

$$\theta = \theta_{avg}^{2\cdot(1-n)} \cdot \theta_\alpha \cdot \theta_\beta \cdot \theta_\gamma \tag{2.18}$$

These are then used to calculate the standard deviation of the result as follows:

$$\sigma = \sqrt{\theta - \mu^2} \tag{2.19}$$

A sensitivity analysis can also be performed. The primary sensitivity, *S*, can be calculated for each variable using:

$$S_\alpha = \frac{\dfrac{\theta_\alpha}{\left(\rho_\alpha\right)^2} - 1}{\left[\dfrac{\theta_\alpha}{\left(\rho_\alpha\right)^2} \cdot \dfrac{\theta_\beta}{\left(\rho_\beta\right)^2} \cdot \dfrac{\theta_\gamma}{\left(\rho_\gamma\right)^2}\right] - 1} \tag{2.20}$$

The global sensitivity, *Sg*, is calculated as:

$$Sg_\alpha = \frac{1 - \dfrac{\theta_\alpha}{\left(\rho_\alpha\right)^2}}{1 - \left[\dfrac{\theta_\alpha}{\left(\rho_\alpha\right)^2} \cdot \dfrac{\theta_\beta}{\left(\rho_\beta\right)^2} \cdot \dfrac{\theta_\gamma}{\left(\rho_\gamma\right)^2}\right]} \tag{2.21}$$

In summary, M-DRM can offer significant reduction in computational time compared to MCS. M-DRM also allows for additional properties, such as sensitivity, to be calculated.

2.3 Bridge Management Systems (BMSs)

Bridge management systems (BMSs) are computer programs used by bridge owners to make high level decisions concerning maintenance planning for large stocks of bridge infrastructure. The software can be used to perform various tasks, such as: storing inspection reports, archiving historical maintenance data, and simulating alternative management strategies to find the one that results in the lowest life-cycle cost of maintaining all of the bridges in a transportation network. The deterioration modelling performed in BMSs is generally highly simplistic in nature, due to the enormous number of calculations required to simulate deterioration of many elements on the many bridges in a transportation network and the high level of uncertainty in the site-specific parameters associated with each bridge element. In the following sections, analysis methods commonly employed to model deterioration in BMSs are reviewed.

2.3.1 Markov chains

The Markov Chain is a statistical method developed by Andrey Markov, which uses a set of probabilities and current information to predict the condition of an element in the future [Grinstead & Snell, 2012]. To predict the deterioration of an element using a Markov chain, condition states (CSs) are first defined for the element, for example: CS1 could represent "perfect condition" and CS5 could represent "failure". Five CSs is the most common. However, it is possible to use a different number, in which case the last CS normally represents "failure". Within each time period there will be a probability of the element residing in a specific CS. The sum of the probabilities associated with all of the CSs within the time period is one. Next, the probabilities of movement between CSs between each time period is defined. For an element with *n* CSs, *n-1* of these probabilities of movement are required. Table 2.2 shows sample transition probabilities for a five CS Markov chain model:

Table 2.2: Sample transition probabilities

Condition State:	**Transition Probability, q_i**
CS1	0.1
CS2	0.2
CS3	0.3
CS4	0.4

The probabilities listed in Table 2.2 are the probabilities of moving to the next CS. The probability of staying in the same condition state is $1-q_i$. These probabilities of movement can be also summarized in a matrix, also known as the Transition Probability Matrix, or TPM. The sample is shown in Table 2.3

Table 2.3: Sample Transition Probability Matrix (TPM)

	CS1	**CS2**	**CS3**	**CS4**	**CS5**
CS1	0.9	0.1	0	0	0
CS2	0	0.8	0.2	0	0
CS3	0	0	0.7	0.3	0
CS4	0	0	0	0.6	0.4
CS5	0	0	0	0	1

The probabilities below the diagonal all are zero, as it is assumed the condition cannot improve without intervention, but will rather stay in its current state or deteriorate. The probabilities on the diagonal are for staying in the same CS, the ones to the right the probability of moving to that CS. The other probabilities in the top-right corner of the TPM are often also set to zero, based on the assumption that the probability of jumping two CSs in a single time step is negligible [McCalmont, 1990]. The probability associated with CS5 is unity, as the element cannot deteriorate any further, and so gets trapped in that CS. This process of deterioration is shown in Figure 2.11:

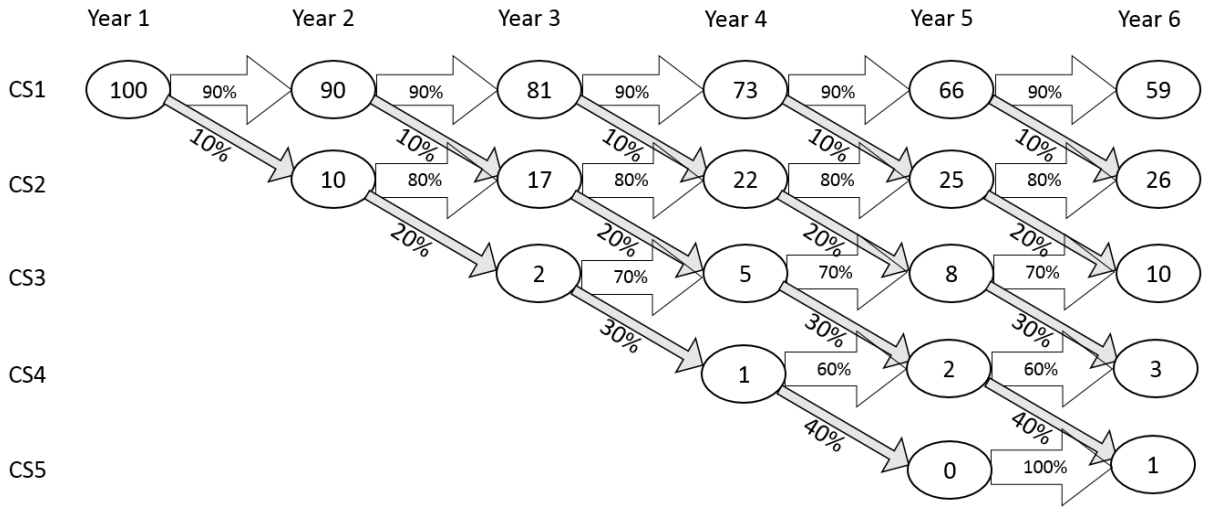

Figure 2.11: Markovian deterioration

For this example, it was assumed that in Year 1 there is a 100% probability of being in CS1. For Year 2, there is therefore a 90% chance the probability stays in CS1, and 10% moves to CS2, with no possibility of being in CS3-5. For Year 3, there is again a 90% chance the probability stays in CS1 and a 10% chance of moving down to CS2. The probability of the elements already in CS2 in Year 2 have an 80% chance of staying, and so this is added to the probability moving from CS1, resulting in a 17% chance of being in CS2 in Year 3. The remaining 20% of the elements in CS2 in Year 2 deteriorate to CS3 in Year 3. A similar procedure continues for the remaining years, and this can be continued for any desired analysis period. Note that the sum of the probabilities of being in each CS in each year should add up to 100%. This is not exactly true in Years 4, 5, and 6 in this example due to rounding errors. The probability of residing in each CS at any year can be calculated as:

$$q_n = q_0 \cdot T^n \tag{2.22}$$

where q_n is the vector of probabilities of being in each CS in year n, q_0 is the initial probabilities of being in each CS, T is the TPM, and n is the number of years.

So far in this section a Markov chain with five condition states has been used, however any number of condition states can be used for a Markov chain. Table 2.4 shows the number of condition states used in BMSs around the world, as shown the number varies from three to nine and beyond.

Table 2.4: Number of condition states in BMSs [Adey et al., 2010]

No.	Country	Name	Number of condition states								
			3	4	5	6	7	8	9	100	Not given
1	Canada	OBMS		1							
2	Canada	QBMS		1							
3	Denmark	DANBRO				1					
4	Finland	FBMS		1							
5	Germany	GBMS									1
6	Ireland	Eirspan		1							
7	Italy	APTBMS			1						
8	Japan	RPIBMS			1						
9	Korea	KRBMS			1						
10	Latvia	Lat Brutus		1							
11	Netherlands	DISK				1					
12	Poland	SMOK				1					
13	Poland	SZOK				1					
14	Spain	SGP								1	
15	Sweden	BaTMan	1								
16	Switzerland	KUBA			1						
17	USA	ABMS							1		
18	USA	Pontis									1
Total			1	5	4	4	0	0	1	1	2

Markov chains allow for very easy manipulation of the probabilities of being in each CS to simulate actions such as inspection, repair, and replacement. For example, replacement can be modelled by shifting the probabilities of being in each CS back to q_0. Strengthening or treatment can also be considered by changing the TPM to reflect the expected reduction that will result in the deterioration rates. Inspection and repair can similarly be modelled using slightly more sophisticated assumptions.

Markov chains are therefore a very useful tool to be used for predicting the deterioration of structures [Elhakeem & Hegazy, 2005]. They assume that the elements essentially have no "memory" and only deteriorate based on their CS in the previous year. They can therefore be used to model a structure starting half-way through its service life without knowing its full history. The ability to assign CSs to elements means clear definitions for deterioration, which can be easily related to inspection results. The Markov chain analysis can be easily modified to model actions such as inspection, repair, and replacement.

2.3.2 Calibration of Markov chains

The predictive abilities of a Markov Chain depend primarily on the Transition Probability Matrix, or TMP. The best approach for calibrating this TMP depends on what kind of data is available. According to (Tran, 2007), there are two types of data, regular data and snapshot data. Regular data could be data from inspection histories carried out at short intervals, where the movement between CSs can be clearly modelled. Snapshot data is data that does not paint a clear picture of the degradation process, usually because of infrequent and non-uniform inspections. For example, say a previous inspection report has an element in CS2 (out of 5), and 6 years later is now in CS4. It is unknown if the element went directly from 2 to 4, or spent some time in 3. TPMs are difficult to determine from snapshot data, and so statistical methods such as the Bayesian Approach are required to deal with the uncertainty. Often expert opinions, in addition to inspection data, are taken into consideration using this method (Tran, 2007).

(Karunarathna, et al., 2013) outlines three main methods for estimating the transition probabilities that go into a TPM: Regression Non-linear Optimizing (RNO), Bayesian Approach (BA), and Markov Chain Monte Carlo (MCMC) with Metropolis-Hasting Algorithm (MHA).

Regression Non-Linear Optimizing (RNO):
RNO is the most commonly used method (Carnahan et al., 1987; Jiang et al., 1988; Veshosky et al., 1994; Morcous, 2006; Morcous et al., 2010 and Bu et al., 2012). Regression analysis is used to fit a curve to the

inspection history data, often a 3rd order polynomial. Next, Performance Indices (*PI*) are calculated, where *PI* = 6 – *CR*, where *CR* is Condition Rating. So *PI* 5 corresponds to brand new components (*CR* = 1), and *PI* 1 is a component requiring replacement. The Expected Performance Index (EPI) can then be calculated by $EPI_{(t)} = C_{(t)} \cdot S$, where *C* is the matrix of probabilities of being in each CS at time *t*, and *S* is the *PI*, or [5 4 3 2 1]. The *EPI* is a single value that represents the condition of the bridge, the higher the value, the better state the bridge is in. The same calculation is done to obtain *PI(t)*, but uses the results from the regression fitting curve of the inspection data. The objective function is then:

$$\text{minimize}\left(\sum_{t=1}^{t=T}\left|PI_{(t)} - EPI_{(t)}\right|\right) \tag{2.23}$$

Bayesian Approach (BA)

BA analysis methods have become more popular in recent years with the development of computer based advanced sampling techniques, and have been used recently to calibrate TPMs (Micevski et al., 2002; Tran, 2007; Ranjith et al., 2013). The objective function is:

$$\text{maximize } \log\left(L\left(\frac{Y}{\theta}\right)\right) = \text{maximize}\sum_{t-1}^{T}\sum_{i=1}^{5} N_i^t \log(C_{it}) \tag{2.24}$$

Where $L(Y/\theta)$ is the likelihood to observe a condition rating data set *Y*, *T* is the largest age, N_i^t is the number of elements in CS*i* at year *t*, C_{it} is the probability in CS*i* at year *t*.

There have been several studies comparing various TPM calibration methods, such as the BA-based Markov Chain Monte Carlo (MCMC), MCMC with the Metropolis-Hasting Algorithm (MHA), Ordered Probit Models, the BA-based nonlinear optimization method, and the percentage prediction method (Tran, 2007; Ranjith et al., 2013). These have concluded that BA-based approaches are the most suitable for predicting future element CS distributions, in particular BA-based MCMC with the MHA.

MCMC with the MHA

When applying the MHA, a proposal density needs to be selected. For this example, a distribution with density, π, is chosen. For given X_n, Y_{n+1} (proposal value) is generated from a preferred density and is accepted with a probability $\alpha(X_n, Y_{n+1})$ given by:

$$\alpha(x, y) = \min\left\{1, \frac{\pi(y)}{\pi(x)}\right\} \quad (2.25)$$

If the proposal value is accepted, then set $X_{n+1} = Y_{n+1}$, otherwise keep X_{n+1} *as* X_n. A Varience-Covarience matrix needs to be assumed, and although the exact values are not required, assuming values too small will result in a long convergence time and high acceptance rate, whereas values too large will result in the TMP values getting stuck in non-optimal places. The matrix can be arbitrarily chosen and tuned until the acceptance rate becomes near to the optimal value of 0.234. After analysis is completed, point estimators and confidence intervals can be calculated.

Comparison

The following is a list of disadvantages to RNO, which (Tran, 2007) argues can be solved with Bayesian Approaches, specifically MCMC and MHA.

1) Reliability is solely dependent on accuracy of formula type used for curve fitting analysis;
2) Linear regression may not be appropriate since there are dependent variables in the system and infrastructure condition ratings are discrete;
3) RNO may stop at local minimum points resulting in incorrect transition probability values;
4) RNO cannot provide confidence limits of the transition probabilities; and
5) The resulting TPMs are difficult to update when new data are available.

Optimization Function used for RNO

As the amount of data already draws a smooth curve, no regression analysis is required. The next step is non-linear optimization, which requires an objective function to optimize. (Tran, 2007) uses Performance Indices (PIs), a measure of current performance, in the analysis of the degradation of sewer pipes. Alternatively, (Wirahadikusumah et al., 2001) used an Overall Structural Grade (OSG), which is a general rating from 1 to 5, and simply minimized the difference between the actual and predicted OSG using the following expression:

$$\text{minimize} \sum_{t=1}^{N} \left| Y(g) - E[y(t, P)] \right| \quad (2.26)$$

where *Y(t)* is the sewer condition at stage *t*, expressed in OSG units, and *E[y(t,P)]* is the expected value of sewer condition at stage *t* as predicted by the Markov chain model using transition probability matrix, *P*.

(Bu et al, 2012) uses a similar process, with the objective function given as:

$$\text{minimize} \sum_{t=1}^{N} \left| A(t) - E(t) \right| \tag{2.27}$$

where the probability of resting in each CS, *Q(t)*, is multiplied by the vector *R = [100,70,50,20]*. *A(t)* then uses *Q(t)* estimated from regression, and *E(t)* estimated from the Markov chain. This paper goes one step further to verify the result with the Chi-square goodness of fit test:

$$x^2 = \sum_{i=1}^{k} \frac{(E_i - A_i)^2}{E_i} \tag{2.28}$$

Which is then compared to a significance level $\alpha = 0.05$.

(Ranjith, 2013) uses the following objective function:

$$\sum_{n=1}^{N} \left| Y_n(t) - E(t_n, P) \right| \tag{2.29}$$

where *Yn(t)* and $E(t_n,P)$ are condition ratings for the different elements. These are then confirmed using the Chi-square goodness-of-fit test.

The common Markov chain calibration procedure in this literature review of BMSs is to calculate a single number, which represents the current state of the bridge, often multiplying the probabilities of lying in each CS with a weighted vector, with higher weights for better performances. The objective function is then simply to minimize the difference between the Markov model and the produced value.

2.3.3 Bridge management software and common practice

In 2006 it was reported that over 40% of the bridges in Canada are over 50 years old [Bisby & Briglio, 2004]. The trend of increasing bridge age is only increasing in Canada:

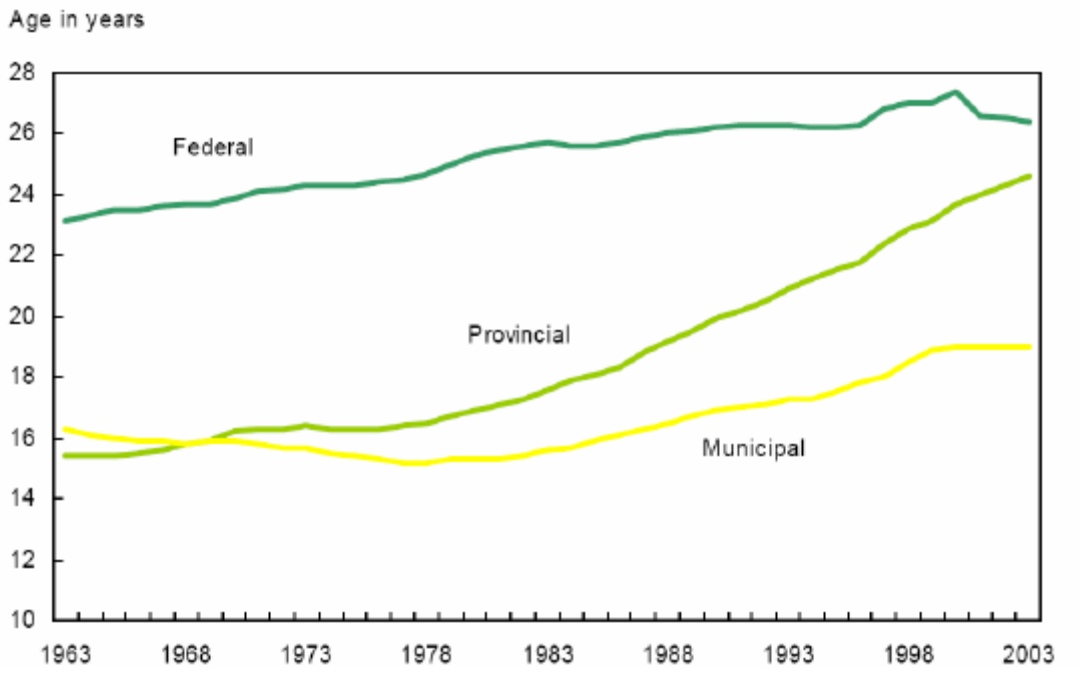

Figure 2.12: Average age of bridges [Hammad et al., 2007]

As shown in Figure 2.12, the average age is increasing in all three jurisdictions. These older bridges require significant inspection, maintenance, repair, and replacement to ensure a functioning transportation network, which requires significant funding, which may not be available.

During the 1960s and 1970s, bridge maintenance was performed reactively as the need arose. However, a series of bridge failures during the 1960s prompted investigation into bridge deterioration, and data was collected from the 1970s to 1990s. During this time, the U.S. Federal Highway Administration (FHWA) in cooperation with state Departments of Transportation (DoTs) developed a generic Bridge Management System, which led to the Pontis system [Thompson et al., 1998]. Pontis "is both a software system and an organizing framework to help bridge managers make the transition from collecting and processing raw safety inspection data to a more sophisticated approach of optimizing the economic efficiency of the bridge network". Pontis divides a bridge into 120 elements, such as concrete deck, steel girders, expansion joints, etc., and assigns CSs to these elements from one to five, with one being perfect condition, and five meaning "replacement required". The element is assigned an initial CS vector (q_0) for a new element (or an older element, in the case of an existing bridge). Pontis then uses the Markov chain approach to predict the deterioration of the element over time. Pontis also has the capability to model different maintenance strategies, and associated with these are different TPMs, as well as an initial costs per maintenance intervention. The total life cycle cost is then calculated as follows:

$$V(i) = \left[C(i,a) + a\sum_{j} P_{ij}(a)V(j) \right] \quad (2.30)$$

where *i* is the CS observed today and *j* is the CS predicted one year in the future, *V(i)* is cost expected as a result of being in state *i* today, *C(i,a)* is initial cost of action a taken in state *i,* α is discount factor, P_{ij} *(a)* is the transition probability of state *j* conditional on state *i* and action *a*, and *V(j)* is the cost expected as of next year if state *i* occurs.

Performing maintenance can result in future cost savings, however further benefit can be gained by improving the structure at the same time. For example, increasing the width of a bridge to allow for wider lanes reduces the risk of accidents, or increasing the strength of a bridge with substandard load capacity so that trucks no longer have to take a detour. Pontis can include the benefit of such improvements using the following formula:

$$B = W(B_a + B_v + B_t) \quad (2.31)$$

where *W* is the weight given to user cost, B_a is savings in accident costs, B_v is savings in vehicle operation cost, and B_t is savings in travel time costs, each of which are calculated separately.

Once the current state of a bridge is known, Pontis uses optimization algorithms to determine the best maintenance strategies for the bridge. Bridge maintenance actions are mutually exclusive, for example repairing concrete, painting girders, or installing preventative corrosion systems. These each have an associated incremental cost to perform and long-term incremental benefit. Pontis performs an analysis that ranks the actions in terms of their Incremental Benefit/Cost ratio, and then organizes these into different maintenance strategies, which are a combination of different actions. The associated incremental benefit and cost ratios of these strategies are illustrated in Figure 2.13.

The most cost-effective actions are those yielding the highest incremental benefit/cost ratios. As we move up the curve, we require a higher initial cost for relatively fewer benefits, and so this maintenance strategy is less cost-effective. Most maintenance actions result in a net benefit for the long term cost of the bridge, however to perform all possible maintenance actions would require significant cost, which may not be realistic for a typical maintenance budget. Pontis therefore ranks the maintenance strategies using an Incremental Benefit/Cost method by first assuming zero budget, and then calculates the total cost

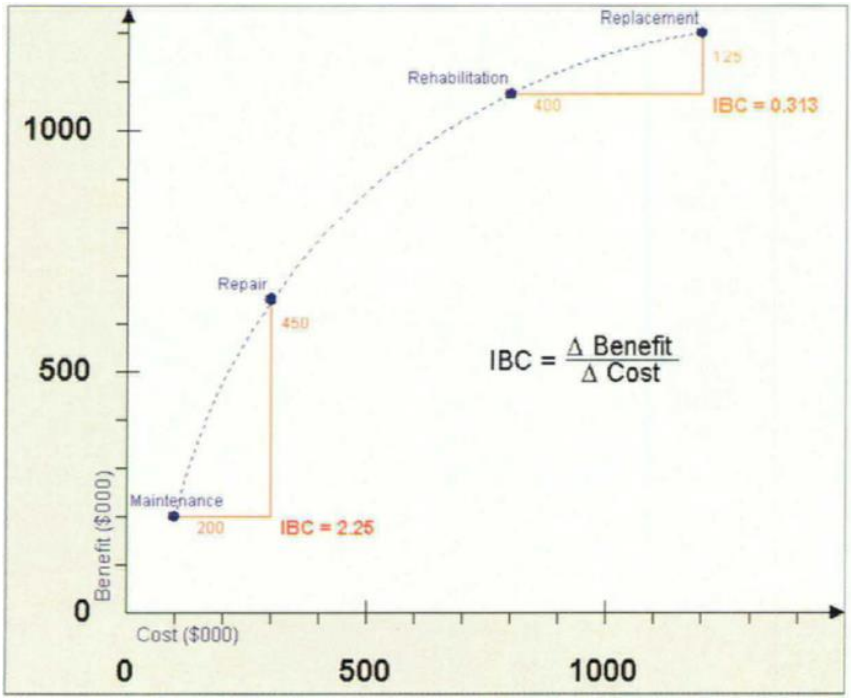

Figure 2.13: Diminishing marginal returns [Thompson et al., 1998]

assuming no maintenance is done. It then increases the maintenance budget in small increments, and finds the combination of actions that yields the most cost-effective maintenance strategy for the budget constraint. The engineer can then look at what budget is available and perform the maintenance suggested.

Another similar Bridge Management Software is BRIGIT [Hawk & Small, 1998], developed in 1996 by the American Association of State Highway and Transportation Officials (AASHTO) in cooperation with U.S. Federal Highway Administration (FHWA). BRIGIT was able to "facilitates the organization of bridge data, provides clear, accurate and timely reporting, can rank bridge populations by a number of user-specified criteria, allows the identification of critically deficient structures, and facilitates the tracking of deterioration trends and repair performance" [Abbott, 1998]. BRIDGIT uses Markovian deterioration predictors and a level-of-service approach to model deterioration, repairs, and costs, and also considers user costs associated with traffic accidents and detouring. BRIDGIT is also able to optimize using multi-period analysis as opposed to sequential period analysis, which means not only is the optimal maintenance action calculated, but also the optimal timing.

BRIDGIT divides a bridge into elements, which are then sorted into the following seven categories: decks, superstructures, piers, abutments, joints, railings, and bearings. These elements are then assigned

up to five CSs, as well as transition probabilities for Markovian deterioration modelling. The deterioration is assumed to be a single-step process, probabilities may not jump more than one CS per year, and that improvements only occur when maintenance actions are performed. Other assumptions include non-time-dependent transition rates, and that the transition probabilities do not vary from year to year. Each CS is then assigned an A/M/U factor, representing whether the element is Acceptable, Moderately acceptable, or Unacceptable, which then triggers repair actions.

In addition to classic elements, such as concrete deck or steel girders, BRIDGIT also models protective systems, such as waterproofing membrane or painting. [Hawk & Small, 1998] acknowledges that the protected and protection elements should deteriorate together as a coupled process, however BRIDGIT uses a simplified direct method to avoid complexity. A protection modifier is defined for each protective element, which represents the decrease in deterioration of the protected element. This modifier can change based on the CS of the protective element. For example, a paint protection system is in CS2, which is associated with a protection modifier of 4. The rate of deterioration of the element protected by this paint is one fourth the rate of deterioration of the unprotected element. The protection system has its own TPM, and as it deteriorates the protection modifier also deteriorates, resulting in the underlying element deteriorating more rapidly as well.

Repairs of elements are modelled by shifting probabilities to higher CSs. BRIDGIT acknowledges that the repairs may not be of the same quality as the original, and that deterioration may occur quicker for the repaired element, and so BRIGIT artificially accelerates the deterioration by moving some of the element percentages to a lower CS. There are two levels of repairs that can be performed, the first removes all unacceptable CS probabilities, the second removes all unacceptable and marginally unacceptable. If the cost of repairs exceeds 70% of the replacement cost, then a replacement action is performed instead, which has higher cost.

As mentioned above, BRIDGIT considers user costs associated with functional deficiencies, and also costs associated with accidents and detours (i.e. user delay costs). One of the deficiencies is deck width, and the associated cost is calculated using Equation (2.32):

$$WC(i,t) = 365 \cdot A\cos tH \cdot W1 \cdot ADT(i,t)^{W2} \cdot L(i)^{W3} \cdot (ALOSW(i,t) - W(i) + 1)^{W4} - W5 \qquad (2.32)$$

where i is each bridge and t is time, WC is the total user cost, *AcostH* is the unit cost due to an accident, *ADT* is the annual daily traffic, L is bridge length, *ALOSW* is acceptable clear deck width *LOS* goal, W is

actual clear deck with, and *W1-W5* are regression coefficients. Other equations are used to calculate costs associated with deficiencies in bridge clearance or load capacity, which incur detour costs. These user costs are then included in the optimization functions for determining the optimal maintenance strategy. More details about optimization and other considerations can be found in [Hawk, 2003].

A third popular BMS is KUBA, based out of Switzerland [Hajdin, 2001]. It also uses a Markovian deterioration process using five condition states, and can also optimize maintenance strategies using similar processes to those employed by Pontis and Bridgit.

There have been several other BMSs programs developed, some privately and some publically. Table 2.5 shows the type of BMS used in each province in Canada:

Table 2.5: BMS details per province [Hammad et al, 2007]

Province:	**Number of Bridges**	**BMS:**
Alberta	13,900	BEADS
British Columbia	20,000	N.A.
Manitoba	1,200	Pontis
New Brunswick	N.A	N.A.
Newfoundland and Labrador	N.A	N.A.
Nova Scotia	4,000	NSBMS
Ontario	3,000	OBMS
Quebec	8,700	QBMS
Saskatchewan	3,020	N.A.
Prince Edward Island	200	PEIBMS

BMSs are also used internationally, a study performed by [Adey et al, 2010] found BMSs used in 15 countries, modelling a combined total of 880,610 bridges and culverts, shown in Table 2.6.

BMSs can not only be used to predict optimal maintenance strategies on single bridges, but also on network of bridges all drawing from the same budget [Elbehairy et al, 2009].

Table 2.6: BMS details per country [Adey et al., 2010]

No.	Country	Name	Bridges	Culverts
1	Canada	OBMS	2'800	1'900
2	Canada	QBMS	8'700	0
3	Denmark	DANBRO	6'000	6'000
4	Finland	FBMS	11'487	3'078
5	Germany	GBMS	0	0
6	Ireland	Eirspan	2'800	0
7	Italy	APTBMS	1'011	0
8	Japan	RPIBMS	750	0
9	Korea	KRBMS	5'317	0
10	Latvia	Lat Brutus	934	845
11	Netherlands	DISK	4'000	600
12	Poland	SMOK	8'290	24'189
13	Poland	SZOK	0	0
14	Spain	SGP	13'252	5'979
15	Sweden	BaTMan	288	300
16	Switzerland	KUBA	5'000	1'250
17	USA	ABMS	9'728	6'112
18	USA	Pontis	500'000	250'000
Total			580'357	300'253

As shown, BMSs are used extensively for modelling and predicting deterioration of bridges in Canada and around the world, and improvements to BMSs in general will therefore have a large impact on the maintenance of bridges to an acceptable level of safety in the most cost-effective manner.

However, fatigue is generally not well modelled in current BMSs. Those BMSs that do include CS definitions for fatigue generally are not capable of modelling fatigue deterioration. Rather, the CS definition is essentially a "flag" that is raised to alert the bridge owner depending on an inspection result, and the effects of further deterioration and/or management actions such as reinforcement or treatment cannot be modelled. Table 2.7 presents the CSs and descriptions for fatigue in Pontis.

Table 2.7: Pontis fatigue condition state descriptions [MDOT, 2007]

Condition State:	**Description**	**Feasible Actions**
1	"Good" Fatigue damage to the bridge has been repaired or arrested. The bridge may still be fatigue prone.	
2	"Fair" Fatigue damage exists which is not arrested (normally, this condition state would be used the first time the element is identified and at any other time when additional fatigue damage occurs.)	• Monitor fatigue damage. • Retrofit detail.
3	"Poor/Serious" Fatigue damage exists which warrants analysis of the element to ascertain the serviceability of the element or the bridge.	• Analyze structure. • Replace element

There are several shortcomings with this information. The first is the number of CSs – only three are used. The second is a lack of clear CS definitions. The difference between CS1, CS2, and CS3 is very subjective, and not governed by a quantitative measure, such as crack depth. There is also no consideration for the effects of preventative maintenance such as impact treatment to slow or arrest crack growth in critical areas. In fact, as mentioned earlier, fatigue deterioration is not modelled at all in this BMS currently or any other, based on the information in the current literature on this subject. Thus, there is a significant need / opportunity to improve future BMSs in this regard. Possible reasons for the current state of affairs include: 1) the difficulty associated with detecting fatigue damage during the early stages of fatigue life, which makes the CS definition a challenge, and 2) uncertainty regarding the degree to which the complex behaviour of fatigue cracks can be adequately represented using the simple deterioration models commonly used in BMSs. An improved fatigue deterioration model could make better use of fatigue inspection data, which is already difficult to acquire as early growth cracks are not detectable from visual inspection, and also improve allocation of maintenance budget funds to optimal projects.

2.4 Previous efforts to model fatigue using Markov chain models

Previous research has been conducted to model fatigue using Markov chain models. One such paper, [Lassen, 1991], investigates the fatigue loading on offshore steel structures by repeated wave loads. A total of 44 samples were loaded under constant amplitude loading at 150 MPa, and the cracks were

measured using an automatic crack monitoring system. The crack length was divided into CSs, ranging from 0.7mm to 3mm. The probabilities of CS movement were then defined based on the results from the fatigue tests and the CS definitions. The Markov chain was then used in an example application modelling the deterioration and potential maintenance strategies of a main float column in an offshore structure. However, this paper uses only one loading stress range, at constant amplitude loading, and for a certain detail geometry, and so applications are limited. In addition, the statistics of small cracks was governed by the ability of the crack measuring devices, and so the transition probabilities at lower crack length may not be accurate.

In [Bogdanoff & Kozin, 1985], a detailed investigation of Markov chains is conducted, including simple stochastic cumulative damage models, nonstationary models, and continuous time versions. It also discusses how to incorporate incomplete inspection data into the calibration process. This reference illustrates examples of how to apply Markov chains to cumulative deterioration models such as corrosion, plastic degradation, and especially fatigue.

More recently, [Walbridge et al, 2012] have investigated the prediction of fatigue in bridges using Markov chains. The authors use a Strain Based Fracture Mechanics model to predict deterioration of a weld in a bridge, using different combinations of stress ranges and design service lives. Different maintenance actions, such as inspection, treatment, repair and replacement are defined, and these are combined to form different maintenance strategies. These are then modelled over a 100 year life span, and total life cycle costs are calculated. A Markov chain was then set up to also calculate life cycle costs, using similar maintenance actions and loading cases, and calibrated to minimize the difference in the costs between the two methods. However, the transition probabilities are not directly related to concrete condition state definitions, as the calibration was performed to the total cost as opposed to crack growth data.

2.5 Fatigue assessment and retrofitting methods

If a fatigue crack is detected or a fatigue concern is raised, based on calculations or previous experience on similar structures, there are several methods available for addressing it. Figure 2.14 presents a summary of common repair strategies, which also considers the cause of the fatigue cracking.

		Repair and strengthening methods							
		grinding	re-welding	surface treatments	adding plates	bolted splices	shape improving	stop holes	modification connection
Causes of fatigue cracking	weld defects	G	G	N	G	E	G	N	G
	lack of fusion	F	G	G	G	E	E	G	E
	cold cracks	F	G	G	F	E	G	G	E
	restraint	F	F	G	G	E	G	G	E
	vibration	F	F	G	G	F	G	F	E
	web gaps	G	F	G	F	N	N	F	E
	geometrical changes	F	F	F	G	E	N	F	G
	web breathing	N	F	F	F	F	N	G	E
		E : Excellent		G : Good		F : Fair		N : Not good	

Figure 2.14: Repair and strengthening of fatigue cracks [Kuehn et al, 2008]

Grinding is removing the crack and the surrounding material completely from the structure by using a grinding tool. This removes the theoretically infinite stress concentration caused by the tip of the crack with a more gradual hole caused by the width of the blade, but may also increase stress due to the corresponding reduction in cross section area. Re-welding is adding welding material over the affected metal. Surface treatments include: tungsten inert gas (TIG) dressing, impact treatment (e.g. hammer peening) or grinding, and largely deal with only a couple of millimeters of depth. These are only able to affect small crack sizes, as cracks larger than the treatment depth are generally not affected by these treatments. Reinforcement by adding plates to connect both sides of the crack can reduce the stress at the crack tip by providing an alternative load path. Bolted splices act in a similar manner to adding plates. Improving the shape can reduce stress concentrations caused by sharp changes in geometry, which can reduce the local stress at the crack area. Drilling “stop holes” can stop or slow the growth of large cracks, by removing the theoretically infinite stress caused by the sharp crack tip by replacing it with a more gradual hole. Finally, modification of the connection detail can reduce the stress in critical areas, which can reduce or arrest crack growth. These modifications normally involve reinforcement to provide an alternate load path or “softening” so that the connection attracts less load.

Impact Treatment of Welds

The methods described in the previous section can mostly be described as reactive maintenance, and rely on a crack being detected. There are a number of preventative maintenance options available, which can be applied prior to crack detection to increase fatigue life. One important category of preventative maintenance treatments is impact treatments, such as needle peening (Figure 2.15), hammer peening, and high frequency mechanical impact (HFMI) treatment (Figure 1.1).

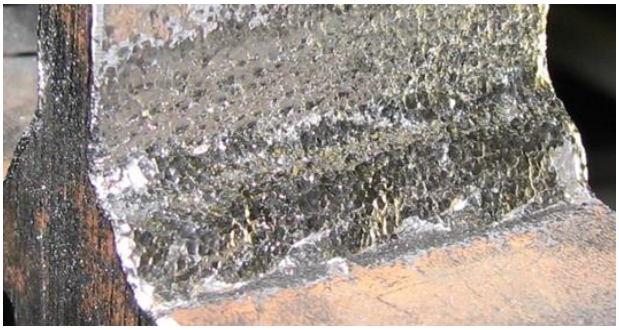

Figure 2.15: Needle peening [Ghahremani & Walbridge, 2011]

Impact treatments work by introducing compressive residual stresses near the surface of the treated weld toe. These have the effect of slowing or arresting crack growth rates at smaller crack depths. Figure 2.16(a) shows a microscopic view of a treated weld toe, with the surface grains compressed due to the impact of the treatment tool. Figure 2.16(b) shows the effect of impact treatment on the residual stresses. The dashed line is for the as-welded specimen, where the residual stresses are near zero or slightly tensile. The solid line is for the impact treated weld, and show a residual stress that is compressive and near the yield strength of the steel. This effect is only for about 1.0 mm near the treated surface.

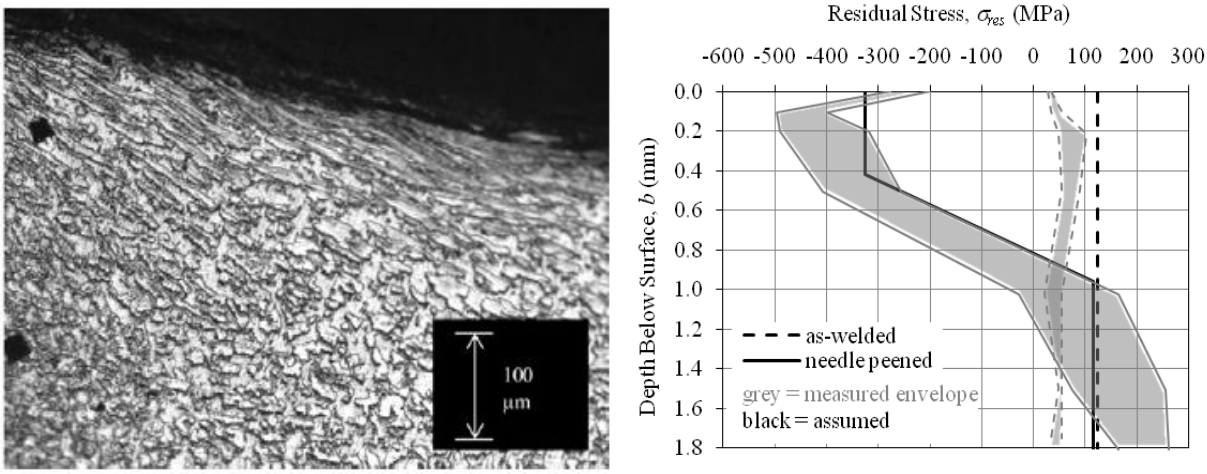

a) microstructure near surface of needle peened weld *b) measured residual stress distributions*

Figure 2.16: Microstructure and residual stresses of needle peening [Ghahremani & Walbridge, 2011]

These treatments are only effective for small cracks or cracks that have not formed yet. These treatments can be used on new welds, or for retrofitting existing welds, so long as they do not already obtain large cracks. Various studies (e.g. [Ghahremani & Walbridge 2011]) have shown that the effects of impact treatments on fatigue performance can be predicted using fracture mechanics models, wherein the residual stresses along the crack path are modified to simulate the effect of the treatment.

3.0 Probabilistic fracture mechanics

In this chapter, probabilistic strain-based fracture mechanics (SBFM) analyses of as-received bridge welds and bridge welds retrofitted by impact treatment (specifically: needle peening) are performed using Monte Carlo Simulation (MCS) and the Multiplicative Dimension Reduction Method (M-DRM). Modifications to the SBFM code to enable analysis by M-DRM in both the finite and infinite life domains are discussed, and the benefits of using M-DRM are critically assessed.

Accurately predicting the fatigue deterioration of welded components can be a computationally expensive undertaking – in particular, in cases where nonlinear material and variable amplitude (VA) loading effects are significant, as modelling these effects may require step-wise introduction of each stress cycle, and "cycle-by-cycle" crack growth analysis. Recent efforts have been undertaken (e.g. [Walbridge et al. 2012]) to model the fatigue behaviour of welds modified by impact treatment using a strain-based fracture mechanics (SBFM) model that employs up to 17 input parameters. This models cycles the material at various points along the crack path, generating non-linear stress-strain hysteresis loops. The strain peaks are then used to calculate the crack propagation with each load cycle. When analyses are performed under complex VA loading histories, even a single deterministic analysis can be tedious.

Determining the statistical properties of fatigue performance is very useful for design. However, to reliably determine these properties experimentally takes many tests, which is both expensive and time-consuming. Deterministic models, such as SBFM models, can be calibrated to experimental results, but they fail to include the variability of the material properties, geometry, defects, loading, etc., of the physical experiments. This variability is important when dealing with reliability in design.

If a probabilistic analysis is performed using Monte Carlo simulation (MCS), then hundreds of thousands of repetitions of the deterministic analysis may be required. In addition, if an entire structure is analyzed, separate simulations may be required for each potential crack initiation site. If the goal is to compare alternative management strategies for the structure (e.g. sequences of inspection and impact treatment retrofitting at various stages during the service life), then the use of the SBFM model ceases to be a feasible option, despite its advantages in terms of accuracy and sophistication.

The multiplicative dimensional reduction method (M-DRM) is a recently-developed statistical method [Zhang 2013], which varies the input variables using Gaussian weights as initial guesses, while holding the other variables constant. Based on an analysis of the results of a small number of trials, not only are

statistical properties, such as mean and standard deviation, calculated, but primary and global sensitivity analysis can also be performed. The main benefit to this method is a reduction in the number of trials required, for example, for a 3-variable problem, instead of the many thousands of trials required to perform an MCS analysis, only 16 are required using M-DRM.

3.1 Monte Carlo Simulation (MCS)

The deterministic SBFM model outlined in Section 2.1 is useful for predicting the fatigue life of one specific weld with one set of input parameters. However, in reality all of the model parameters have a certain amount of variability, from material properties to loading conditions to geometric properties. Deterministic (nominal) values are generally used in design, but construction is never perfect and so the parameters in the field can differ from the design values. Even extremely small variations to parameters such as the initial defect size can have a large impact on the fatigue life.

With this in mind, in the current study, the SBFM model was run as a probabilistic model, in which each of the initial variables had statistical properties including: mean, standard deviation and distribution type. This approach has been used previously to perform probabilistic Linear Elastic Fracture Mechanics (LEFM) analysis of as-received and needle peened welds [Walbridge & Nussbaumer 2008]. In the SBFM model, the additional parameters required to model nonlinear material effects include: the elastic modulus, E, the static yield and ultimate strength, σ_y and σ_u, the cyclic material parameters, K' and n', and a parameter, μ, which models the recovery of the crack opening stress following overloads under VA loading [MacDougall & Topper, 1997].

Given the deterministic model and statistical distributions for the input parameters, MCS can be used to generate histograms of crack depth versus number of load cycles to failure, N, for different stress ranges. This was done in [Walbridge et al. 2012] for the analysis of a transverse stiffener weld in mild steel plate. Table 3.1 shows the statistical properties of each of the input variables assumed in the probabilistic SBFM analysis. A justification of these statistical properties is presented in [Walbridge et al. 2012]. It should be noted that all of the *VAR*() are multipliers applied to the deterministic model parameters to account for various sources of uncertainty.

Table 3.1: Probabilistic SBFM analysis variables

Var.	**μ**	**σ**	**Units**	**Dist.**	**Description**
a_i	0.15	0.045	mm	LN	initial crack depth
$(a/c)_i$	0.50	0.16	-	LN	initial crack aspect ratio
VAR(T)	1.02	0.012	-	N	T = plate thickness
θ_w	39.8	6.9	^{o}	LN	weld toe angle
ρ_w	0.65	0.3	mm	LN	weld toe radius
LN(C)	-29.13	0.55	N, mm	N	Paris law constant
ΔK_{th}	80.0	15.0	N, mm	LN	SIF range threshold
μ	0.002	0.001	-	LN	crack closure parameter
VAR(E)	1.04	0.026	-	N	E = elastic modulus
VAR(σ_y)	1.07	0.053	-	LN	σ_y = yield strength
VAR(σ_u)	1.0	0.077	-	LN	σ_u = ultimate strength
VAR(K')	1.04	0.35	-	LN	K' = Ramberg-Osgood constant
VAR(n')	0.92	0.15	-	LN	n' = Ramberg-Osgood constant
VAR(σ_{weld})	1.0	0.25	-	N	σ_{weld} = welding residual stress
VAR(σ_{pwt})	1.0	0.20	-	N	σ_{pwt} = peening residual stress
VAR(ΔS)	1.0	0.15	-	N	ΔS = nominal stress range
VAR(SCF)	0.93	0.12	-	LN	SCF = stress concentration factor
Note:	*VAR*() denotes multiplier applied to the nominal value.				

The statistical properties in Table 3.1 were run through a random number generator and a value for their parameter was chosen, and that value used as an input for the SBFM model, which resulted in a number of cycles to failure. This procedure was repeated hundreds of thousands of times, each time with a new set of input variables randomly chosen, with the result being a histogram of the number of cycles to failure. Statistical analysis can then be performed on the results, and a mean and standard deviation obtained. This process is repeated using different stress ranges as an input, and using the resultant mean and standard

deviation both the 50% and 95% survival probability S-N curves can be graphed. The 95% survival probability curve is commonly used for the fatigue design of structures such as bridges.

A question for all MCS analyses is how many trials must be performed. More trials will mean greater accuracy, but also greater computational time. To determine how many were required, a large number, 200,000 trials, was chosen as a starting point, and then iterations with fewer trials were performed and compared against the 200,000 until a noticeable difference started occurring.

This comparison was performed using condition states, similar to those used to model the deterioration of structural elements in bridge management systems (BMSs), where CS1 is like new, and CS5 represents failure, etc. The criteria for moving between CSs is the fatigue crack depth, a, with boundary limits shown in Table 3.2.

Table 3.2: Condition state definitions

	Limit:
Condition State 1	$a < 0.15$ mm
Condition State 2	$a < 0.25$ mm
Condition State 3	$a < 1.0$ mm
Condition State 4	$a < 2.5$ mm
Condition State 5	$a \geq 2.5$ mm

MCS was then performed on SBFM, the output divided into condition states, with the results shown in Figure 3.1.

The vertical axis in Figure 3.1 is the probability being in each CS, and the horizontal axis is the number of years of service. For the purpose in this section the actual numbers are not important, rather how close the estimations are with fewer runs. The reason these plots were used for comparison is to capture not just the probability of failure, but also the manner in which the crack grows over time, to ensure that accurate predictions are performed for all crack sizes. Comparing the solid and dashed lines in Figure 3.1, the effect of reducing the number of trials used in the MCS can be seen.

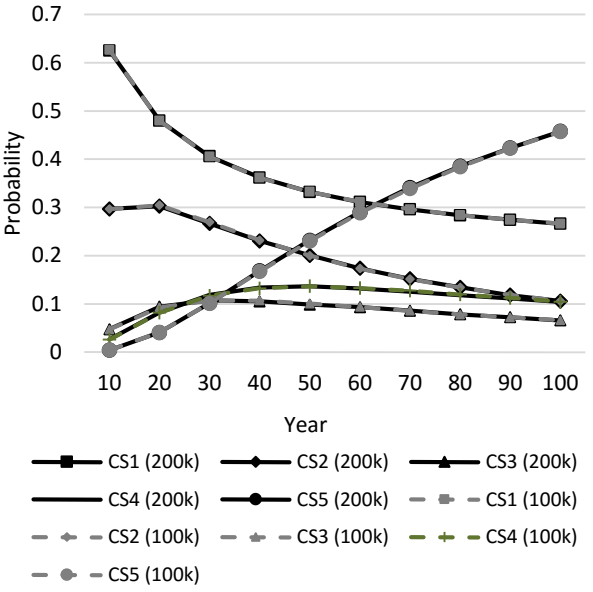

a) MCS Results: 200,000 vs 100,000 runs

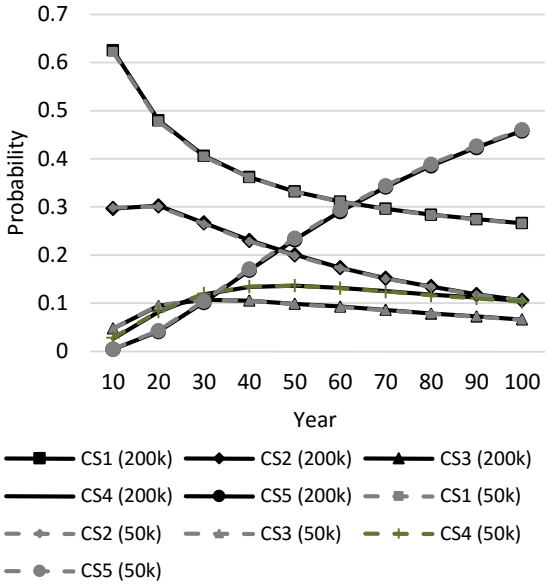

b) MCS Results: 200,000 vs 50,000 runs

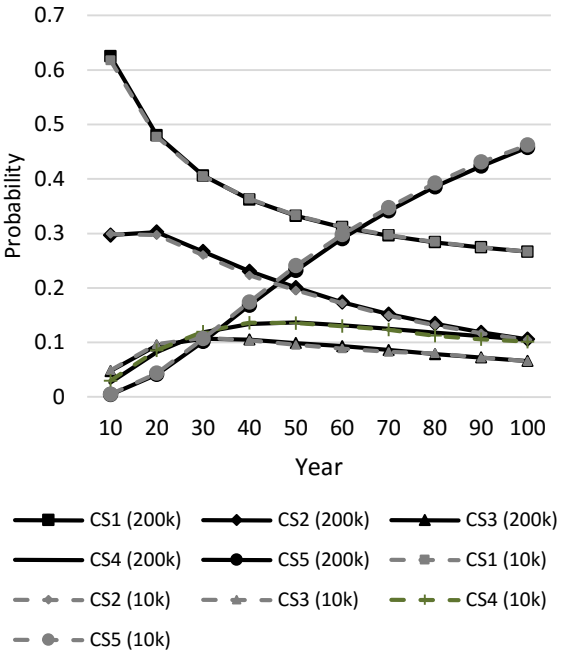

c) MCS Results: 200,000 vs 10,000 runs

Figure 3.1: Monte Carlo Simulation convergence analysis

The threshold for convergence was set such that there is no visual difference from the data produced from 200,000 trials. It can be seen that there is no noticeable change when decreasing from 200,000 to 50,000

trials. However, at 10,000 trials the lines start to shift, particularly for CS5, or failure, and so it appears that 50,000 trials is when the results converge. Using more than 50,000 trials will result in increased computational time with no benefit with regards to accuracy, and somewhere between 50,000 and 10,000 trials the results produced are slightly inaccurate. Therefore, for the remainder of the analyses in this thesis, MCS is performed with 50,000 trials.

The model can now be used to generate survival probability curves. By changing the input stress range, we can obtain the number of cycles to failure for different points along the S-N curve. The most common type of loading seen in analysis is Constant Amplitude (CA) loading, as it is simple to calculate. The CA loading in this thesis uses a load factor S_{min} / S_{max} of 0.1 However, CA loading is not realistic, particularly for bridges, as trucks vary significantly in terms of weight and therefore stress range on the critical members. Figure 3.2 shows a histogram and the cumulative frequency of gross vehicle weights in Ontario:

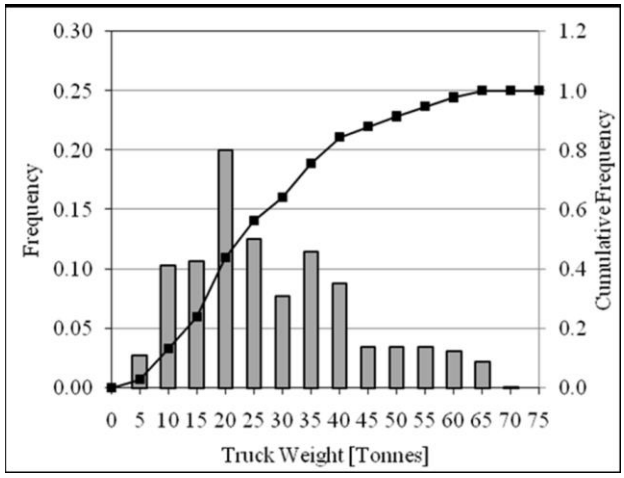

Figure 3.2: Ontario gross vehicle weights [MTO, 1995]

As shown, there is a significant range in weights of trucks that drive over the bridge, and assuming constant amplitude loading is unrealistic. Therefore, two variable amplitude loading histories were developed, the first (ps-m-40) is the measured stresses at the midspan of a 40 m span, and the second (ps-r-15) the stresses at the reaction of a 15 m continuous girder. Figure 3.3 shows the influence lines for the stresses for each of the histories:

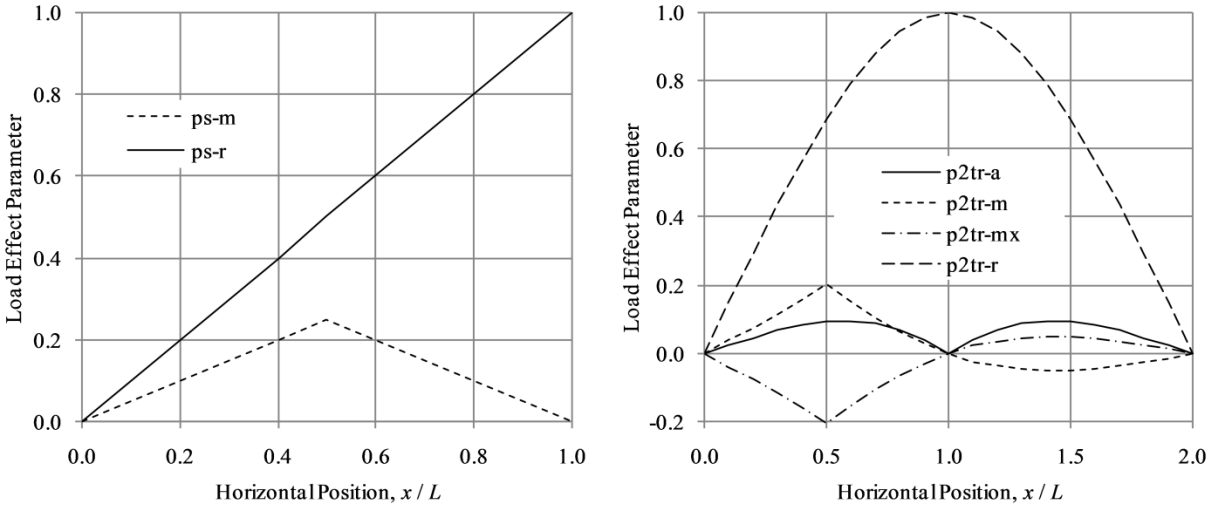

a) 1 span simply supported girder *b) 2 span continuous girder*

Figure 3.3: Truck influence lines [Ghahremani, 2010]

Figure 3.3(a) shows the influence lines for the moment at midspan (ps-m) and the support reaction (ps-r) for a simply supported girder. Figure 3.3(b) is for a 2-span continuous girder, and shows the midspan moment (ps2tr-m), support reaction (p2tr-r), and intermediate support (ps2tr-a)

Using the data from Figure 3.2 and applying it to the influence lines from Figure 3.3, variable amplitude loading histories were developed, as shown in Figure 3.4:

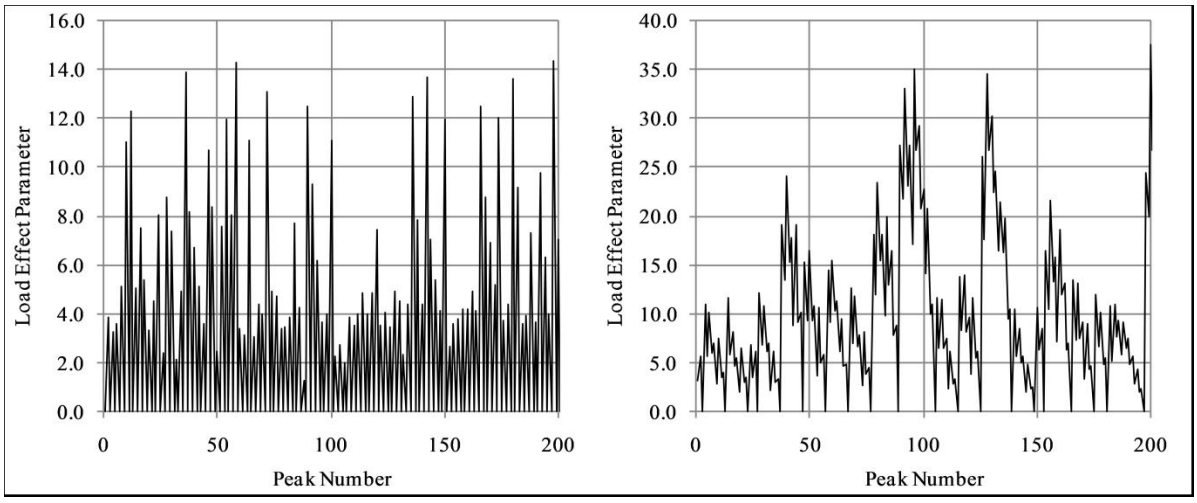

a) ps-m-40 *b) ps-r-15*

Figure 3.4: Variable amplitude loading sample histories [Ghahremani, 2010]

The history on the left, ps-m-40, is significantly more narrow-banded. As it is the stress at the midspan of a simply supported girder, each truck passage generally results in only one large load spike. Comparing this to the history on the right, we can see that the ps-r-15 history contains many more intermediate peaks, as each wheel of the truck causes a local maximum and minimum stress as it moves over the support.

In addition to considering different types of loading histories, SBFM can also consider treatment strategies. There are several different types of post-weld treatments, which can increase the fatigue life by introducing residual compressive stresses, in this thesis needle peening will be modelled.

Running MCS on SBFM, using 50,000 runs as determined by Figure 3.1, we get the S-N curves shown in Figure 3.5.

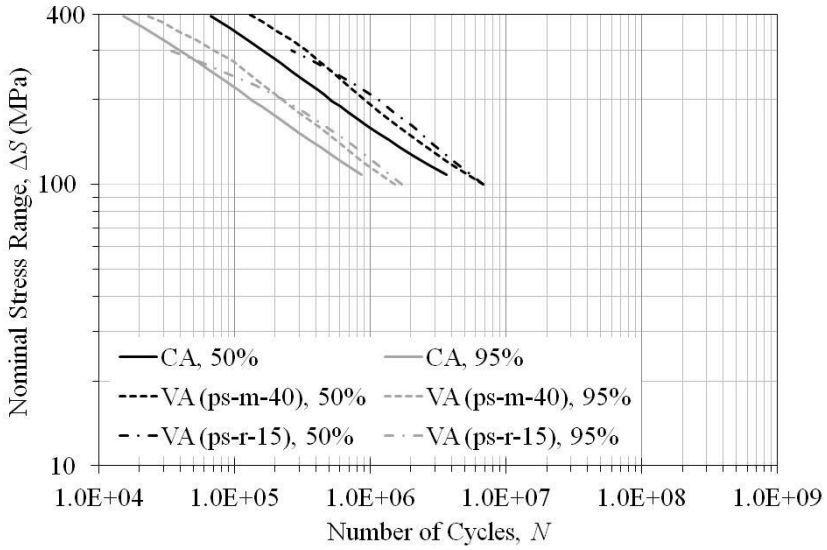

Figure 3.5: MCS on SBFM S-N curves

The dark lines are the 50% survival probabilities, and the grey lines are 95%. There are some differences observed at high stress ranges between the different loading histories, with both VA histories showing longer lives than the more conservative CA. The curves end at a stress range of around 100 MPa, this is due to the issue of infinite lives, which will be discussed later.

3.2 M-DRM

While the SBFM model employing MCS described in the previous section is highly accurate and allows the effects of many parameters on the fatigue behaviour of the weld to be assessed in a probabilistic

framework, it has the significant disadvantage of being highly computationally costly and slow. One possibility for addressing this shortcoming is to perform the analysis instead using the more computationally efficient Multiplicative Dimension Reduction Method (M-DRM).

As there are 17 input variables, a total of 86 runs (5·17+1) of the SBFM model are required to perform the SBFM analysis for a given stress range. This is significantly less than the 50,000 runs required for MCS analysis.

M-DRM was performed using SBFM, with the results compared to MCS in Figure 3.6:

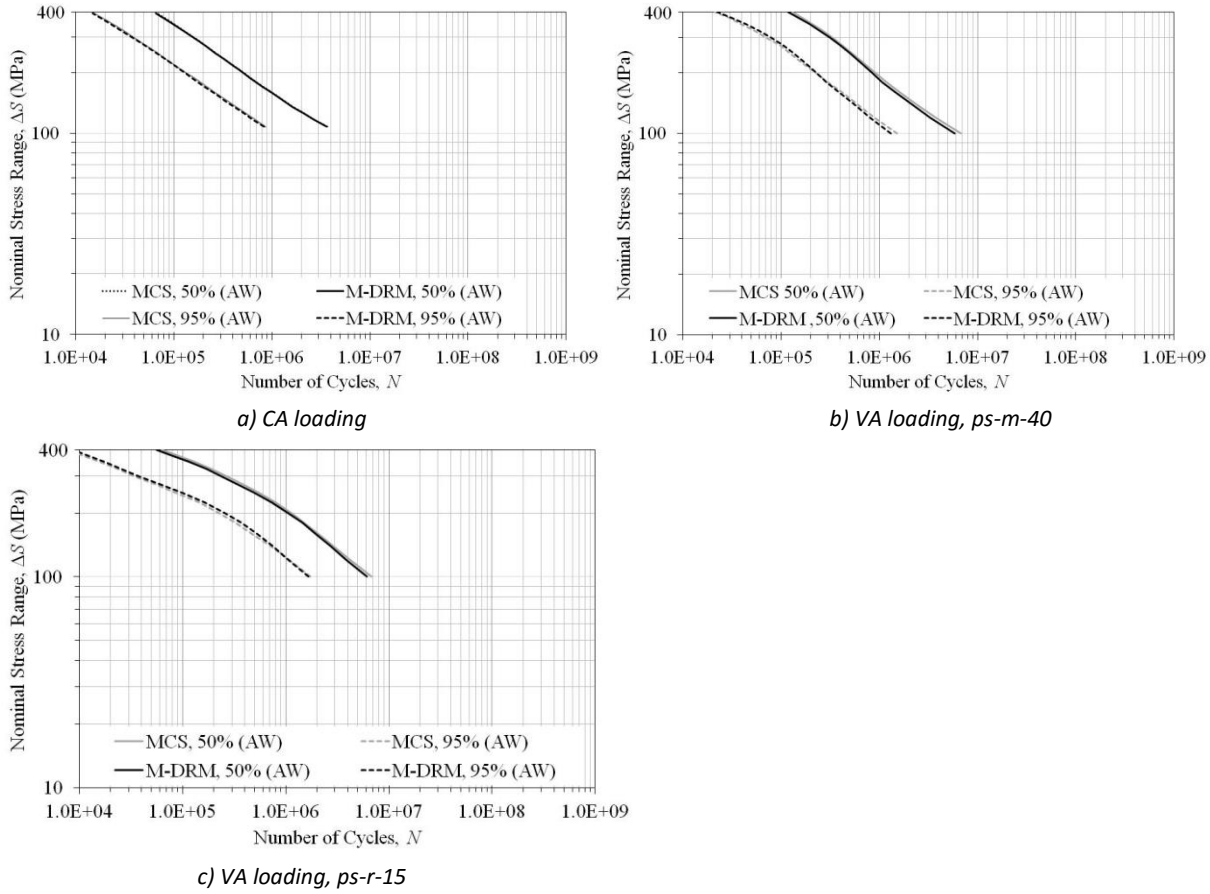

a) CA loading

b) VA loading, ps-m-40

c) VA loading, ps-r-15

Figure 3.6: MCS vs M-DRM

As shown, M-DRM fits very closely to MCS, with differences in the curves barely noticeable, at a fraction of the computational time. However, these are still not full S-N curves, similar to the MCS, the issue of infinite lives continues for the M-DRM calculations below about 100 MPa. The behaviour at lower stress levels and higher number of cycles is unknown.

3.3 Infinite lives

In welds, it is possible for testing or fracture mechanics analysis to determine that the fatigue life is effectively infinite, if the local applied stress range is sufficiently small or the fatigue resistance of the weld is particularly high. In a probabilistic SBFM analysis, the end result may be a histogram such as the one shown in Figure 3.7, which exhibits a very long tail to the right of the mean, which may eventually be truncated at the number of cycles at which the analysis is stopped.

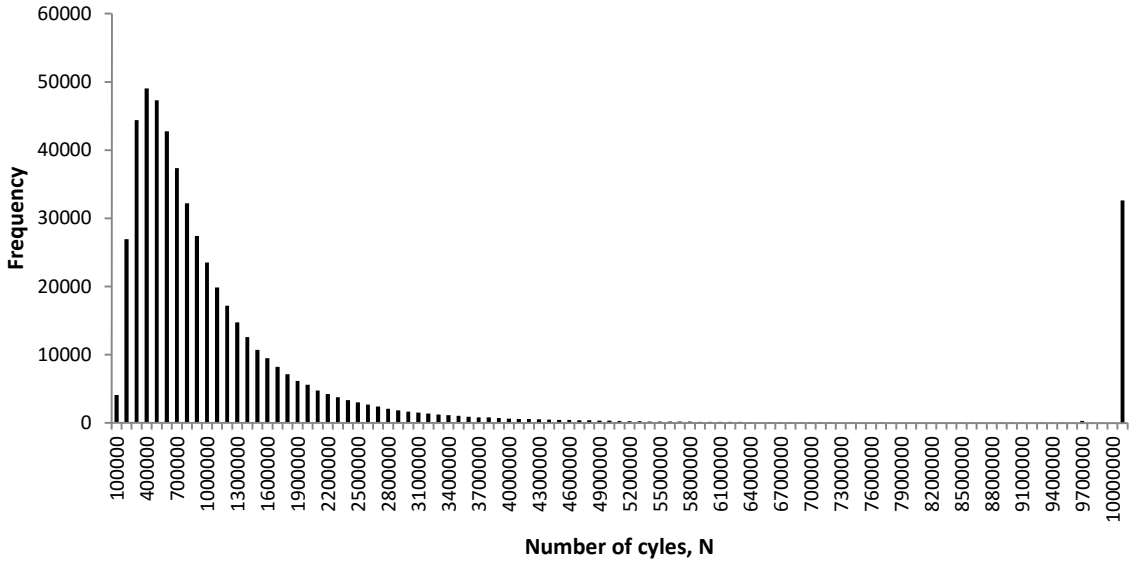

Figure 3.7: MCS SBFM Histogram

In Figure 3.7, the distribution of number of cycles to failure is centered around 500,000 cycles to failure, and gradually decreases to zero. However, there is a significant spike at the fatigue life where the analysis is stopped. The analysis could continue, but the significant extra computational time would not be worth the extra information. The percentage of infinite lives rises as the stress range decreases.

This trend makes it difficult to calculate properties of the statistical distribution of the fatigue life, since parameters such as the mean and standard deviation cannot be calculated in the normal way if the set of analysis results includes infinite lives.

One solution to this problem would be to neglect the infinite results, and simply take the average of the rest. At lower stress ranges the average of the finite lives would still be higher, and so this would capture that increase. However, at lower stress ranges more than half of the lives can be infinite, and so neglecting

these can result in a significant error of estimation. An additional problem is that there are some results which may be very high, for example between one and ten billion, which are not infinite but can still skew the data significantly when included in average and standard deviation calculations.

A better solution is to sort the results from least to greatest, and using the middle or "median" value, as opposed to the average. At higher stress ranges, where no infinite lives occur, the average may in fact be equal to the median. The resulting point corresponds with a 50% survival probability. Points for other survival probabilities can be obtained in a similar way – i.e. by ranking the results and selecting the fatigue life below which a certain percentage of the trials result in "survival" of the weld.

Figure 3.8 shows survival probability curves obtained by MCS, which have been extended to lower stress levels where trials with infinite fatigue lives become significant in number. Three loading histories are compared: CA loading at a stress ratio of R = 0.1 and VA loading under the two highway bridge loading histories discussed earlier. In this figure, results for as-welded (AW) and needle peened (NP) welds are now also compared. Modelling this weld retrofitting treatment in SBFM is done by simply changing the residual stress distribution along the crack path. The model for the residual stress distributions for both cases (AW and NP) are shown in Figure 2.16. These mean stress distributions along the crack path are multiplied by the statistical parameters $VAR(\sigma_{weld})$ and $VAR(\sigma_{pwt})$ to account for uncertainty in the residual stresses due to the welding process and due to post-weld treatment by needle peening.

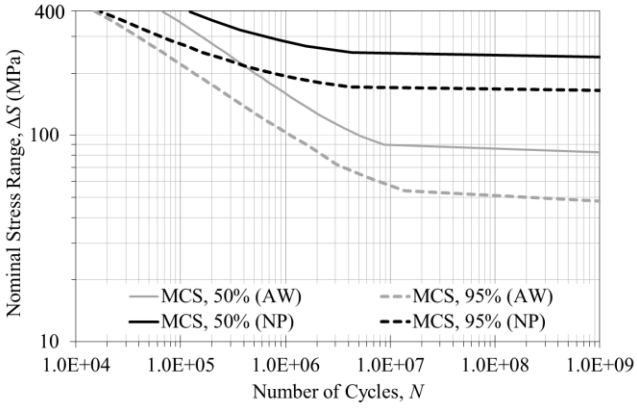

a) Constant Amplitude (CA) Loading

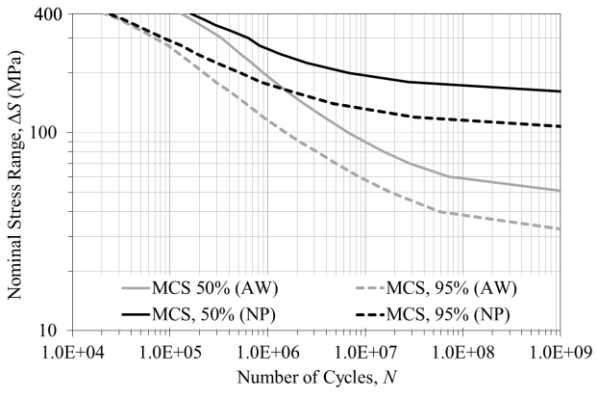

b) Variable Amplitude (VA) Loading, ps-m-40

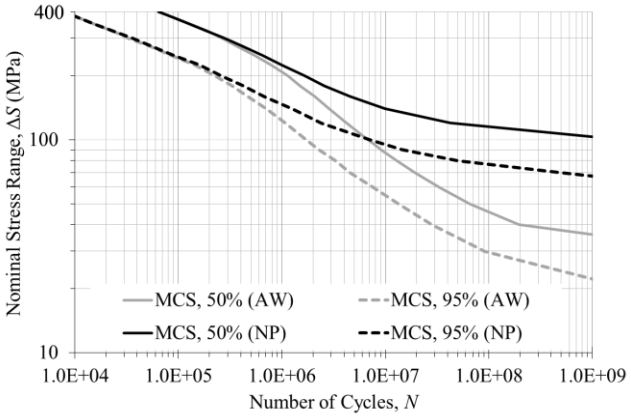

c) Variable Amplitude (VA) Loading, ps-r-15

Figure 3.8: MCS S-N curves

The computational time to plot these graphs was approximately 2 full days per graph, depending on the loading history, with the VA loading histories requiring longer analysis times.

As the M-DRM input grid points (see Figure 2.10 in Chapter 2) vary by as much as several times the standard deviation around the mean, the problem of handling analysis trials that result in infinite lives becomes significant at much higher stress ranges when performing M-DRM analysis than for it does MCS. However, once the problem occurs it is not as easily handled, as every grid point is needed to determine the statistical moments of the fatigue life distribution at a given stress range.

Figure 3.9 presents a graph that shows the effect of varying the stress intensity factor range threshold, ΔK_{th}, vs. the number of cycles to failure, N, for two nominal stress ranges, ΔS: 80 MPa and 90 MPa. The dark vertical lines are the M-DRM input grid points for the statistical variable ΔK_{th}. For ΔS = 90 MPa all grid points result in finite life estimates, but at ΔS = 80 MPa, the last grid point returns an infinite value. This means that the M-DRM analysis cannot be performed accurately. Since it is the lower tail of the fatigue life distribution that we are most interested in, one possible practical solution would be to make an estimation of the fatigue life for that grid point by linear extrapolation using the finite fatigue lives obtained for the four known points, as shown in Figure 3, accepting that this assumption will not be accurate for the upper tail.

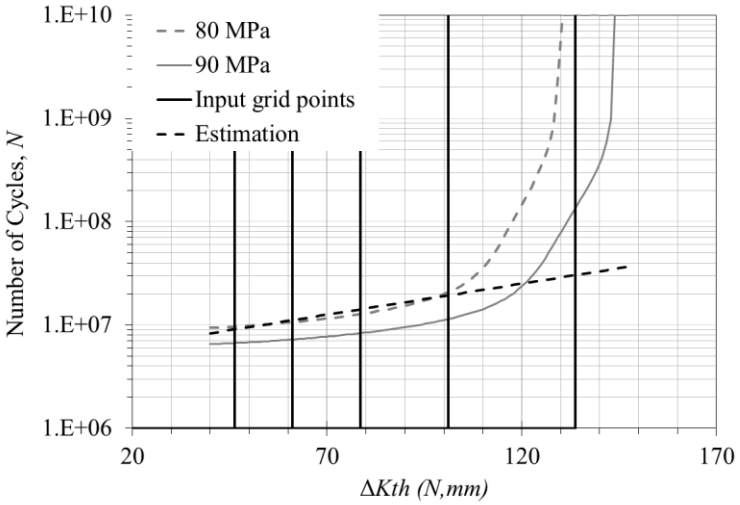

Figure 3.9: Infinite life in variable ΔK_{th}

This approach was investigated in this study and it was found to be effective in lowering the minimum stress level that could be analyzed using M-DRM, as illustrated in Figure 3.10.

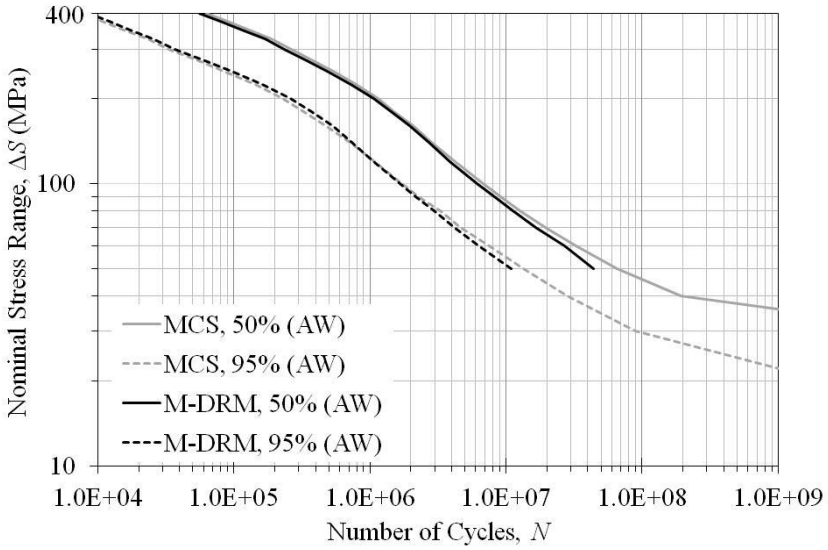

Figure 3.10: Dealing with infinite lives in M-DRM (ps-r-15 loading)

However, eventually so many of the grid points yield infinite lives that the error resulting from this approximation becomes too great, and so another approach is required for performing analyses at lower stress ranges.

The most successful approach investigated in the current study is summarized in the following paragraphs. Simply stated, instead of using the SBFM code to calculate the number of cycles to failure, *N*,

it can be modified to calculate the threshold stress range below which there is no crack propagation. This is done by gradually increasing the stress range until $\Delta K_{eff} = \Delta K_{th}$. The output is the limiting or threshold stress range for a given combination of input parameters. This threshold stress range will vary with variations in the input parameters, such as the initial defect depth, a, threshold stress intensity factor range, ΔK_{th}, etc. M-DRM can then be performed using the modified SBFM model, and statistical parameters of the threshold stress range can be calculated and plotted. This threshold stress range would represent the lower bound of an S-N plot, which the finite life curve will never cross.

Figure 3.11 shows the resulting S-N curve drawn using M-DRM. At high stress ranges, M-DRM analysis results in finite fatigue life predictions for all of the analyzed grid points, and it is a straight forward task to use the results to plot a 50% survival probability curve (solid black) and a 95% curve (dashed line). The calculated curves continue down to lower and lower stress ranges until multiple M-DRM grid points result in infinite life predictions and results are no longer accurate. M-DRM is then performed using the modified SBFM code, and 50% and 95% survival probability lines are plotted based on the distribution of the threshold stress range. We now have lines describing the finite and the infinite life regions of the S-N plot. To complete the S-N plot, these lines can be simply connected.

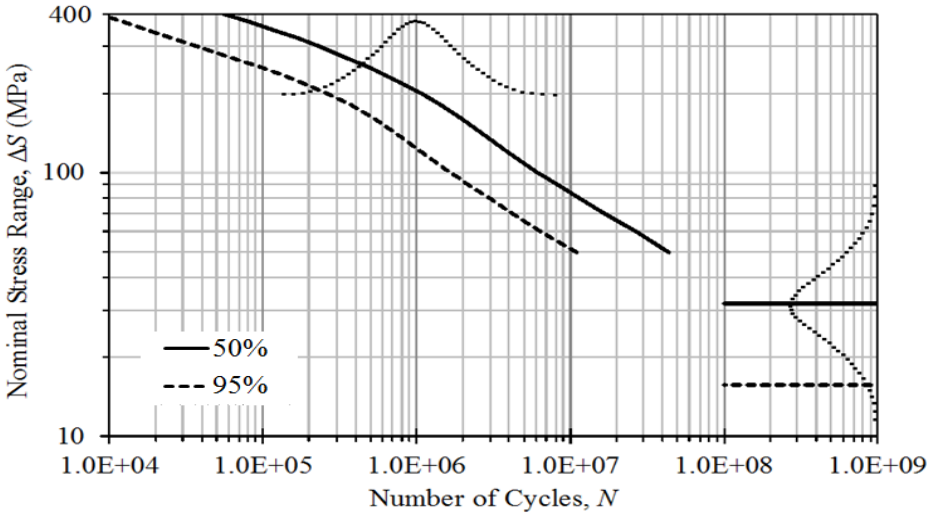

Figure 3.11: M-DRM finite and infinite life analysis

3.4 Sensitivity analysis using M-DRM

Using Equations (2.20) and (2.21) from Section 2.2.2, sensitivity analysis of the input variables can be performed with M-DRM. The results of such an analysis are shown in Figure 3.12. The sensitivity of the input variables is on the vertical axis, and the applied stress range is on the horizontal axis. The resulting sensitivities in this figure are for an as-received weld.

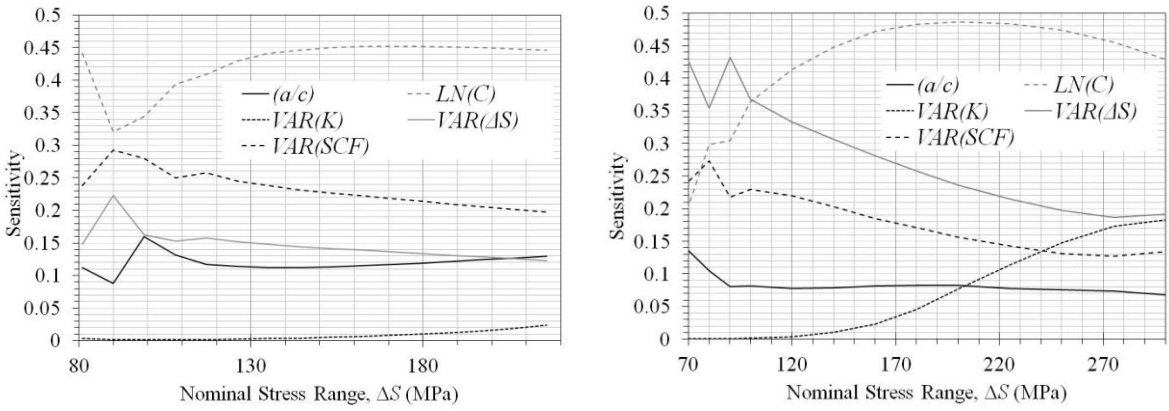

a) CA *b) VA (ps-m-40)*

Figure 3.12: M-DRM sensitivity analysis for an as-received weld

The higher the sensitivity for a given parameter, the greater the influence variations in the parameter will have on the predicted fatigue life, based on a finite life analysis. As shown in this figure, the Paris Constant *C* has the largest sensitivity, at almost 0.5, both under CA and VA loading. The *VAR*(*SCF*) parameter yields a high sensitivity for both loading types. The parameter describing the uncertainty in the applied stress range, *VAR*(Δ*S*), is higher under VA loading. The sensitivities of some of the 17 statistical variables are negligible, and so not shown. The reason we start to see significant fluctuations in the sensitivities at the lower stress ranges is due to the infinite life predictions for certain grid points. These start at around Δ*S* = 135 MPa, and so the problem does not become severe until very low stress ranges, when close to half the variables start to experience infinite lives in their input points.

3.5 Comparison of MCS and M-DRM analysis results

A comparison between M-DRM and MCS is shown in Figure 3.13 for the three different loading cases, and for both as-welded (AW) and needle peened (NP) welds.

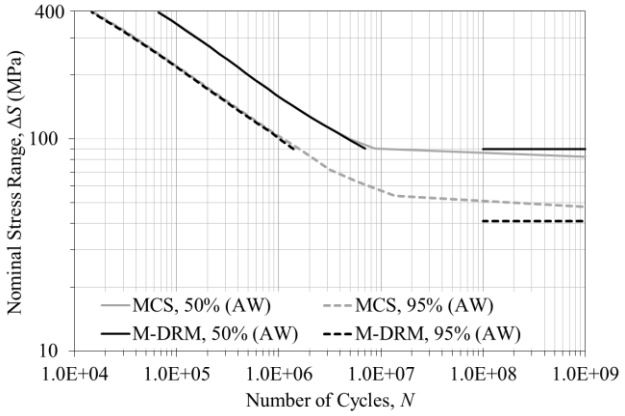

a) As-welded, constant amplitude (CA) loading.

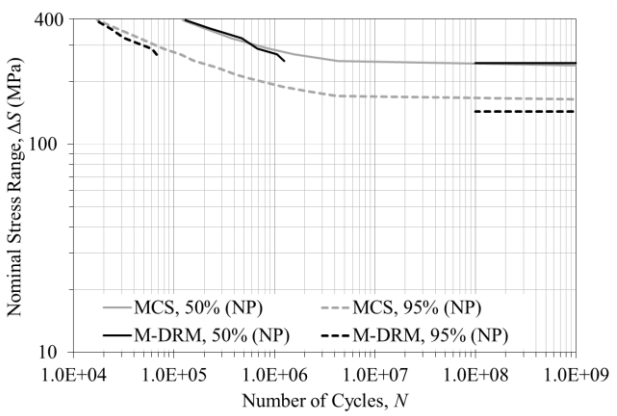

b) Needle peened, constant amplitude (CA) loading.

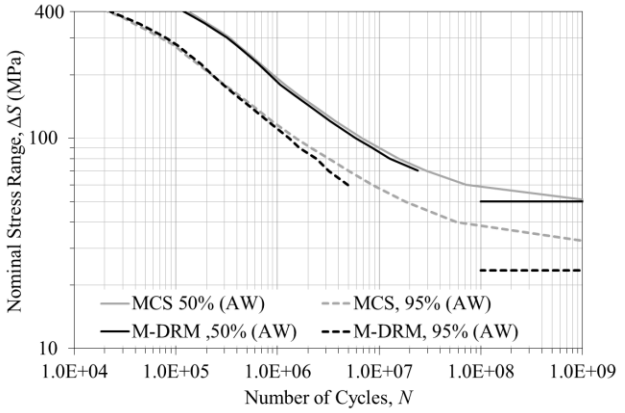

c) As-welded, variable amplitude (VA) ps-m-40 loading

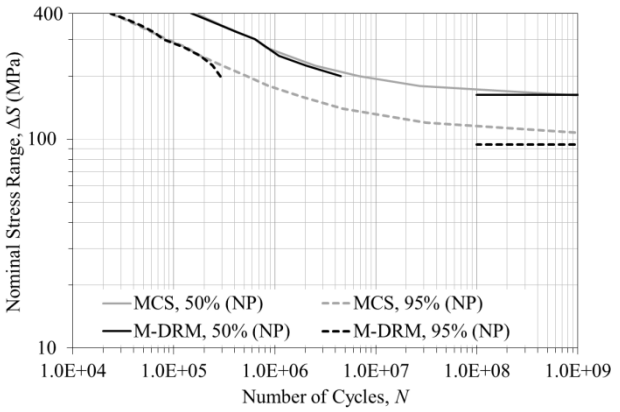

d) Needle peened, variable amplitude (CA) ps-m-40 loading.

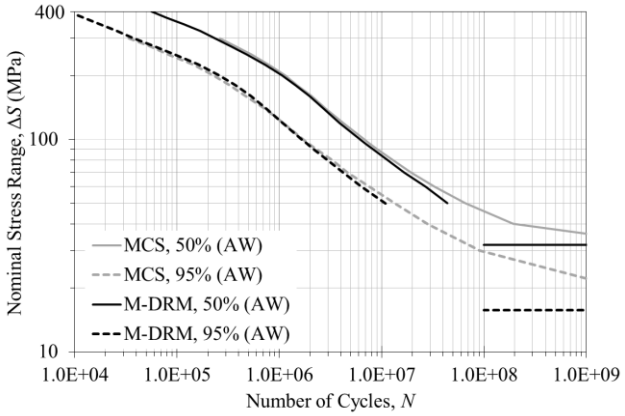

e) As-welded, variable amplitude (VA) ps-r-15 loading

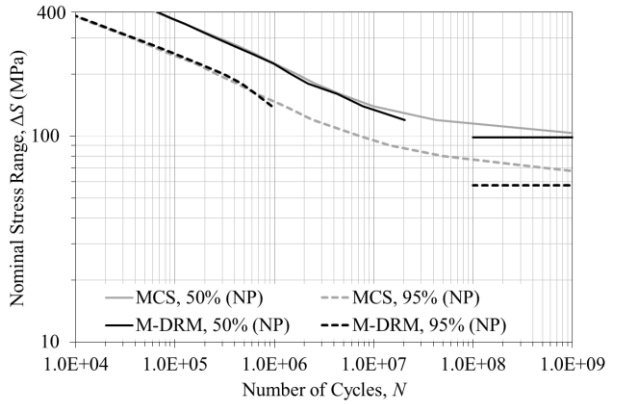

f) Needle peened, variable amplitude (CA) ps-r-15 loading.

Figure 3.13: M-DRM vs MCS results

Taking a closer look at the results compared in Figure 3.13, a number of observations can be made. At high stress ranges, M-DRM was found to be accurate in predicting the MCS results within 1%. As the M-

DRM starts to result in infinite life predictions, the accuracy decreases slightly, but is still well within 5%. Eventually there are infinite life predictions at too many grid points, at which point the finite life analysis is halted. The infinite life analysis is then performed to determine the threshold stress range.

The computational benefits of M-DRM were very obvious when performing these comparisons. The time to generate a single S-N curve using MCS was approximately 2 full days, depending on the complexity of the loading history, whereas the M-DRM curves could be plotted in under an hour.

There are a couple conclusions that can be drawn from these plots. The first concerns the effect of needle peening. This can also be seen in Figure 3.8, where the as-welded and needle peened curves are superimposed on the same graph. At high stress ranges there is little to no treatment benefit, but at low stress ranges needle peening can have a significant effect in increasing the life of a weld. This is due to the compressive residual stresses that needle peening introduces. For higher stress ranges, the applied tensile stresses are greater than the compressive residual stress due to needle peening. The treatment stress is therefore insufficient to arrest crack growth. At lower applied stress ranges, the tensile stresses generated are not enough to overcome the compressive residual stresses, and so the crack does not grow. A second conclusion concerns the effect of variable amplitude loading. In general, the effect of the loading history type is less at the higher stress ranges. At the lower stress ranges, the CA loading analysis results in infinite lives at higher stress levels. Under the VA loading histories, even though the equivalent stress range is low, there are occasional overload cycles in the loading history that are large enough to ensure that fatigue crack growth still occurs. As the fatigue crack grows, the smaller cycles also start to cause fatigue damage, and eventually fatigue failure may still result.

Thirdly, the type of VA loading does make a difference. Comparing the two investigated VA histories, the ps-r-15 history has a lower threshold stress range. This result can be explained in part by the greater difference between the peak stress range and the equivalent stress range for this history.

In summary, MCS on SBFM can be used to plot S-N curves, with low stress levels plotted using median as opposed to average. M-DRM can accurately reproduce these curves with a fraction of the computational time, plotting at low stresses by extrapolating for infinite grid points and performing M-DRM on threshold stress values as opposed to number of cycles to failure. However, both of these methods are still complicated, and at a minimum require a complex model such as SBFM, and so are unsuitable for use in BMSs. As a result, in the next chapter, the much simpler Markov chain models will be explored.

4.0 Modelling fatigue deterioration using Markov chains

4.1 Introduction

As discussed in Section 2.3, Markov chains can be a useful tool for predicting deterioration of structures in large infrastructure networks due to their relative simplicity and ease of use. They are commonly used in bridge management systems (BMSs). They can be applied to complex structures by dividing the structure (e.g. bridge) into elements, and then dividing each element into discrete condition states (CSs), which are typically defined by observable parameters such as crack size or percentage of section loss. A transition probability matrix (TPM) is defined, which governs the movement between CSs, in order to calculate probabilities of being in each CS vs. time. The initial conditions are assumed or calculated. CSs can also be altered to model management actions such as repair and replacement.

This chapter focuses on the calibration of Markov chains to model fatigue deterioration. Calibrations will be performed using three different data types: previously established (design) S-N curves, failure data, and crack growth output obtained from a calibrated probabilistic SBFM model. The results of these calibrations will then be compared. Following this, it will be demonstrated how the calibrated Markov chain models can be used to model fatigue management actions for bridge welds (e.g. inspection, treatment, repair, and replacement) and to model the deterioration of correlated elements due to multiple mechanisms, such as corrosion and fatigue. Lastly, the ability of the simple Markov models to predict optimal fatigue management strategies will be critically assessed.

4.2 Calibration

As shown in Table 2.4 from Section 2.3.1, the number of CSs used in common BMSs around the world is not set, but changes from one proprietary program to the next. Therefore in an effort to capture the range of Markov chain sizes commonly used in existing BMSs, two fixed Markov chain sizes are investigated in this thesis, namely: five and ten condition states. The results of this investigation are therefore expected to be relevant to a wide range of BMSs. The results can also be used to determine if the number of CSs in a Markov chain has an effect on its ability to model the fatigue deterioration and management of welds. The benefit of using two Markov chains with the number of CSs divisible by a common integer is that it is easier to compare results for individual CSs between the two models.

4.2.1 Calibration using design S-N curves

One possible way of calibrating a Markov chain model to predict fatigue deterioration is to use the design or "S-N" curves in existing standards. While these curves don't provide any information about the rate of fatigue damage accumulation (i.e. the rate of transitioning through the intermediate CSs), they can be used to determine the statistics of the time required to arrive at the failure CS. The benefit of this approach is that the design S-N curves have been established using very large quantities of test data.

Figure 4.1, taken from S16-14 [CSA, 2014], shows the relationship between the stress range, *S*, and the number of stress cycles to failure, *N*, for detail categories A to E1. These S-N curves represent the 97.7% survival probability for the various detail categories. Each curve has a Constant Amplitude Fatigue Limit (CAFL – dashed line), to describe a stress level below which the fatigue life will effectively be infinite. Below the CAFL, the S-N curve slope becomes flatter (the slope factor, *m*, increases from 3 to 5). The S-N curve below the CAFL is used for fatigue design under variable amplitude (VA) loading.

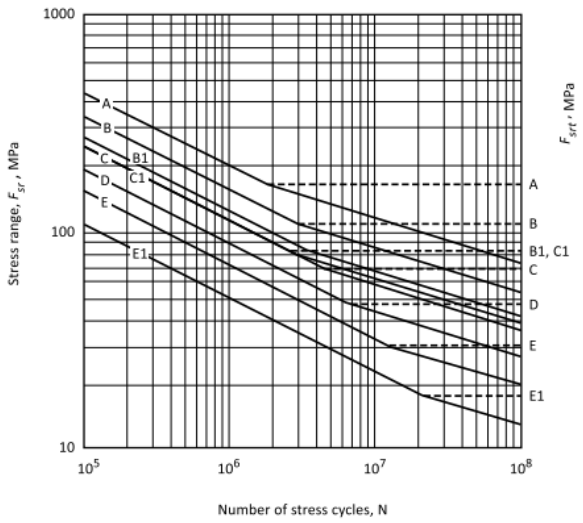

Figure 4.1: S-N plot [S16-14]

The CAFL (F_{srt}) for each detail category is given in Table 4.1.

Table 4.1: S-N curve constants [S16-14]

Detail category	Fatigue life constant, γ	Constant amplitude threshold stress range, F_{srt}, MPa
A	8190×10^9	165
B	3930×10^9	110
B1	2000×10^9	83
C	1440×10^9	69
C1	1440×10^9	83
D	721×10^9	48
E	361×10^9	31
E1	128×10^9	18
M164	561×10^9	214
M253	1030×10^9	262

For each detail category, the number of cycles associated with the CAFL (or the point on the S-N curve at which the slope changes) can be calculated using Equation (4.1):

$$N = \frac{\gamma}{F_{srt}^{\ 3}} \tag{4.1}$$

Design S-N curves such as these are generally obtained by calibration using fatigue life data obtained from many laboratory tests conducted at various stress ranges on a given fatigue detail. An internationally recognized procedure for performing this calibration can be found in [Hobbacher, 2009]. In order to shift these curves so that they can be used to represent other survival probabilities, normally one must collect a statistically significant quantity of fatigue life data for the detail category of interest and essentially repeat the calibration performed by the code writers for the new survival probability. Thankfully, for the North American detail categories such as those found in [CSA, 2014], a set of correction factors, R_R, can be found in [AASHTO, 2011], for shifting the curves so that they can be used for other important survival probabilities. These factors are provided in Table 4.2, where “minimum” refers to 97.7% and “mean” refers to 50%.

Table 4.2: R_R factors [AASHTO. 2011]

Detail Category[a]	R_R		
	Evaluation Life	Minimum Life	Mean Life
A	1.7	1.0	2.8
B	1.4	1.0	2.0
B′	1.5	1.0	2.4
C	1.2	1.0	1.3
C′	1.2	1.0	1.3
D	1.3	1.0	1.6
E	1.3	1.0	1.6
E′	1.6	1.0	2.5

Using the CAFL point from the S-N curve to get the 97.7% survival probability, and the R_R value to get the 50% survival probability, the following equation can be used:

$$N_{i,50\%} = N_{i,97.7\%} \cdot R_{R,i} \tag{4.2}$$

Where i is the detail category, $N_{i,97.7\%}$ is the number of cycles to 97.7% probability of failure, calculated from Equation (4.1) and Table 4.1 for detail category i, and $R_{R,i}$ is taken from Table 4.2. The result from this equation is shown in Table 4.3.

Table 4.3: Number of cycles at CAFL for two survival probabilities.

Detail category	**Stress (MPa)**	**N (cycles) (97.7%)**	**N (cycles) (50%)**
A	165	1.82E+06	5.10E+06
B	110	2.95E+06	5.91E+06
B1	83	3.50E+06	8.39E+06
C	69	4.38E+06	5.70E+06
C1	83	2.52E+06	3.27E+06
D	48	6.52E+06	1.04E+07
E	31	1.21E+07	1.94E+07
E1	18	2.19E+07	5.49E+07

In order to perform the Markov chain calibration for a given detail category, the TPM is initially set up with all of the transition probabilities set to the same arbitrary number. The initial CS vector is set up assuming that there is a 100% chance of being in CS1 at year zero. A simulation is then performed to obtain the probability of failure (i.e. being in the highest CS) versus the number of years of service (with a constant number of cycles per year assumed). Based on the analysis, the number of cycles associated with the 97.7% and 50% survival probabilities can be determined and compared with the similar values at a given stress level (e.g. the CAFL) for the detail category of interest, based on Table 4.3. The transition probabilities are then changed until the number of cycles corresponding with 97.7% and 50% survival probability match the values in Table 4.3. For the current study, this was first done by minimizing the sum of difference of squares between the number of cycles to failure calculated by the Markov chain and the target values from Table 4.3. Since the design S-N curve provides no information about the probability of being in any of the intermediate CSs, the simplest assumption is that the transition probabilities are the same for all CSs. Thus, only one number (the transition probability for all CSs) is varied in the calibration. The result for Detail Category 'D' is presented in Figure 4.2.

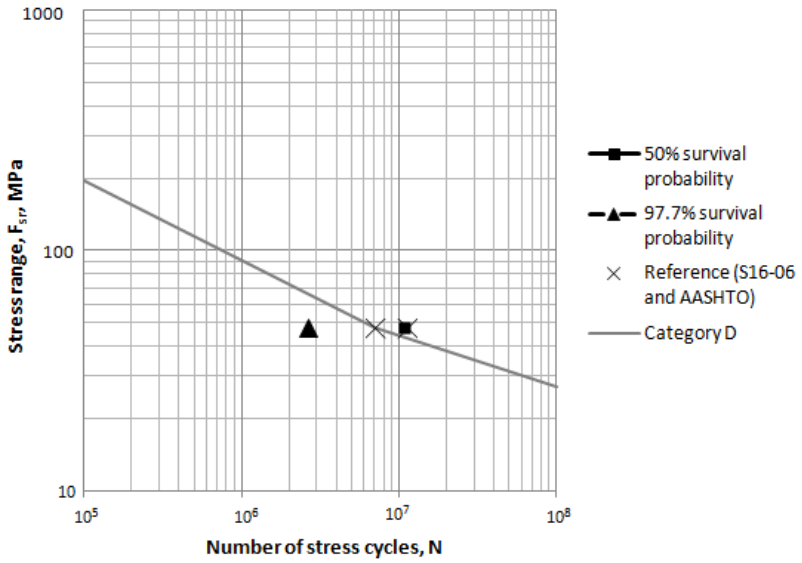

Figure 4.2: S-N plot, Category D calibration

The grey line is the S-N curve taken from [CSA, 2014]. The two 'X's on the plot are the 50% and 97.7% points according to Table 4.3. The solid markers are the result from the Markov chain calibration, the triangle is 97.7% and the square is 50% survival probability.

As seen in Figure 4.2, the estimation of *N* for the 50% survival probability is very accurate. However, the estimation for 97.7% is well below the design S-N curve. This is because the 50% value is much larger, around $1 \cdot 10^7$, and so to minimize the total sum of difference of squares, the solver in Excel will prioritize that difference over the smaller 97.7% value, which is around $7 \cdot 10^6$. Changing the optimizing function to be the relative difference of squares, we get the result shown in Figure 4.3.

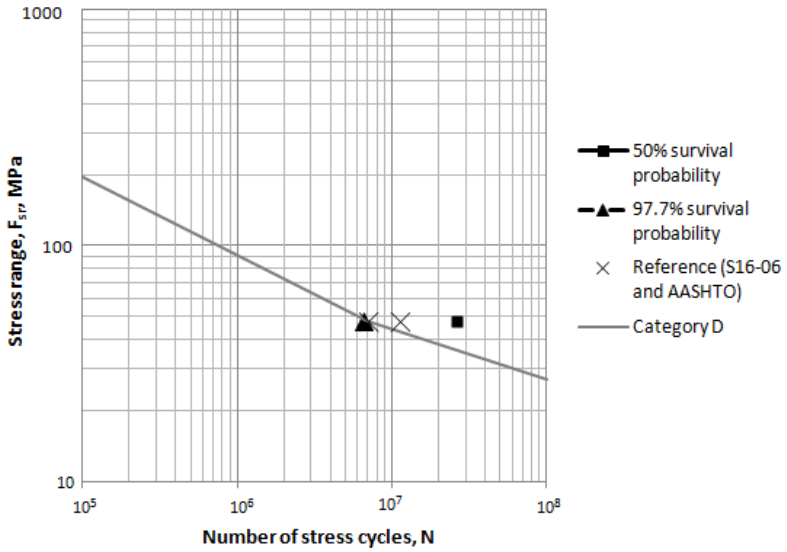

Figure 4.3: S-N plot, Category D calibration

We now see the reverse problem, where the 97.7% estimation of *N* is accurate, but the 50% estimation is too high. Averaging the transition probabilities obtained using the two methods described earlier gives us a result that balances the importance of both points, as shown in Figure 4.4.

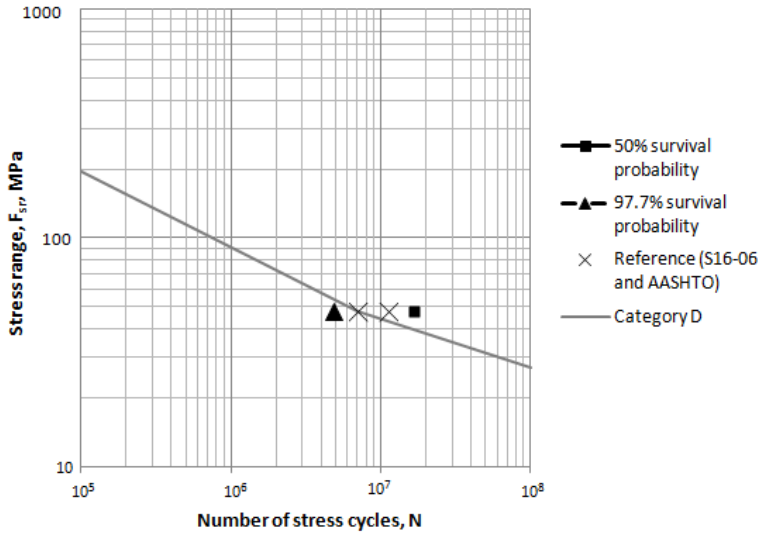

Figure 4.4: S-N plot, Category D calibration

Repeating this process for all of the detail categories and for both the five and ten CS Markov chain models, we get the results presented in Table 4.4. Note that the transition probabilities for each CS are the same, since a uniform Markov chain is assumed, so only one value is reported in the table.

Table 4.4: Transition probability calibration using S-N plots

Category:	**5CS**	**10CS**	**SR**	**DSL**
A	0.0468	0.1710	165	9.12E+06
B	0.0616	0.2144	110	1.48E+07
B1	0.0746	0.2640	83	1.75E+07
C	0.0804	0.2636	69	2.19E+07
C1	0.0815	0.2594	83	1.26E+07
D	0.0690	0.2295	48	3.26E+07
E	0.0697	0.2355	31	6.06E+07
E1	0.0565	0.2096	18	1.10E+08

In Table 4.4, SR is the stress range for which the calibration was performed (taken as equal to the CAFL for all detail categories), and DSL is the design service life. For this calibration exercise, good results were achieved by assuming a 100 year service life with the number of cycles per year set so that the number of cycles at the end of the DSL would be equal to the number of cycles, *N*, associated with the CAFL for the 97.7% survival probability curve, multiplied by five.

In order to draw the rest of the S-N curve, the relationships between the transition probabilities and SR and DSL are required. Equation (4.3) [Walbridge et al, 2012] shows the relationship between the transition probabilities and the number of cycles to failure:

$$q_i = 1-(1-q_0)^{N_i/N_0} \tag{4.3}$$

where q_i is the new transition probability associated with a certain number of cycles N_i, q_0 is the base transition probability associated with a base number of cycles N_0. The relationship between transition probabilities and stress range is shown in Equation (4.4) [Lassen, 1991]:

$$q_i = \frac{1}{(\Delta S_0 / \Delta S_i)^m \cdot (1+(1-q_0)/q_0)} \tag{4.4}$$

where q_i again is the new transition probability associated with a certain stress range ΔS_i, q_0 is the base transition probability associated with a base stress range ΔS_0, and m is the slope of the S-N curve. Once a base transition probability is calibrated for a set stress range and design service life, these two equations can be used to translate the transition probabilities to any stress range or design service life, and essentially draw an S-N curve for a given survival probability using the calibrated Markov chain model. Using a slope m = 3 for stress ranges above the CAFL and 5 for stress ranges below the CAFL, the S-N curve Detail Category 'D' is illustrated in Figure 4.5 for the 97.7% and 50% survival probabilities.

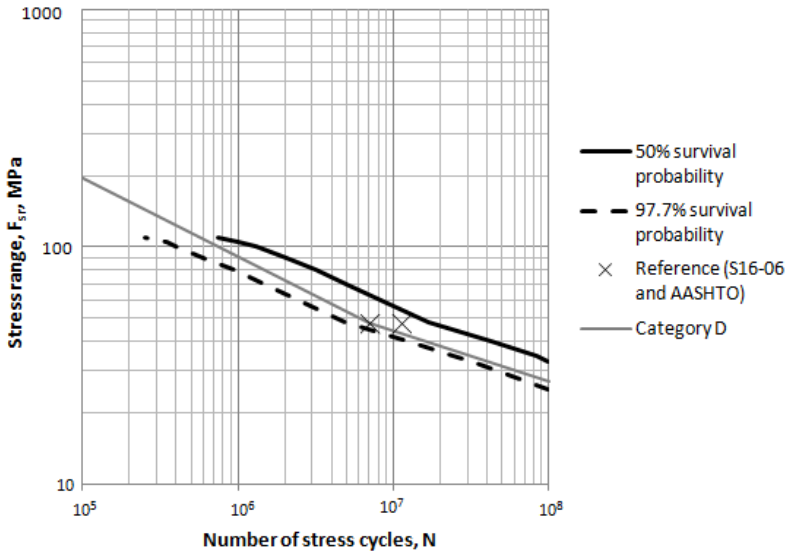

Figure 4.5: S-N plot using calibrated Markov model, Detail Category 'D'

The slopes of the 97.7% line, the dashed linetype, follow very closely, including the change in slope at the CAFL. The only difference is the offset that occurred when calibrating. The lack of linearity of the curve obtained using the Markov model is due to the choice of the number of cycles per year, which leads to small errors as the transition probabilities approach zero or one. Repeating this for all detail categories, we get a set of S-N curves for a given survival probability, as shown in Figure 4.6. Both the 5CS and 10CS graphs show similar results, which model closely the original S-N curves.

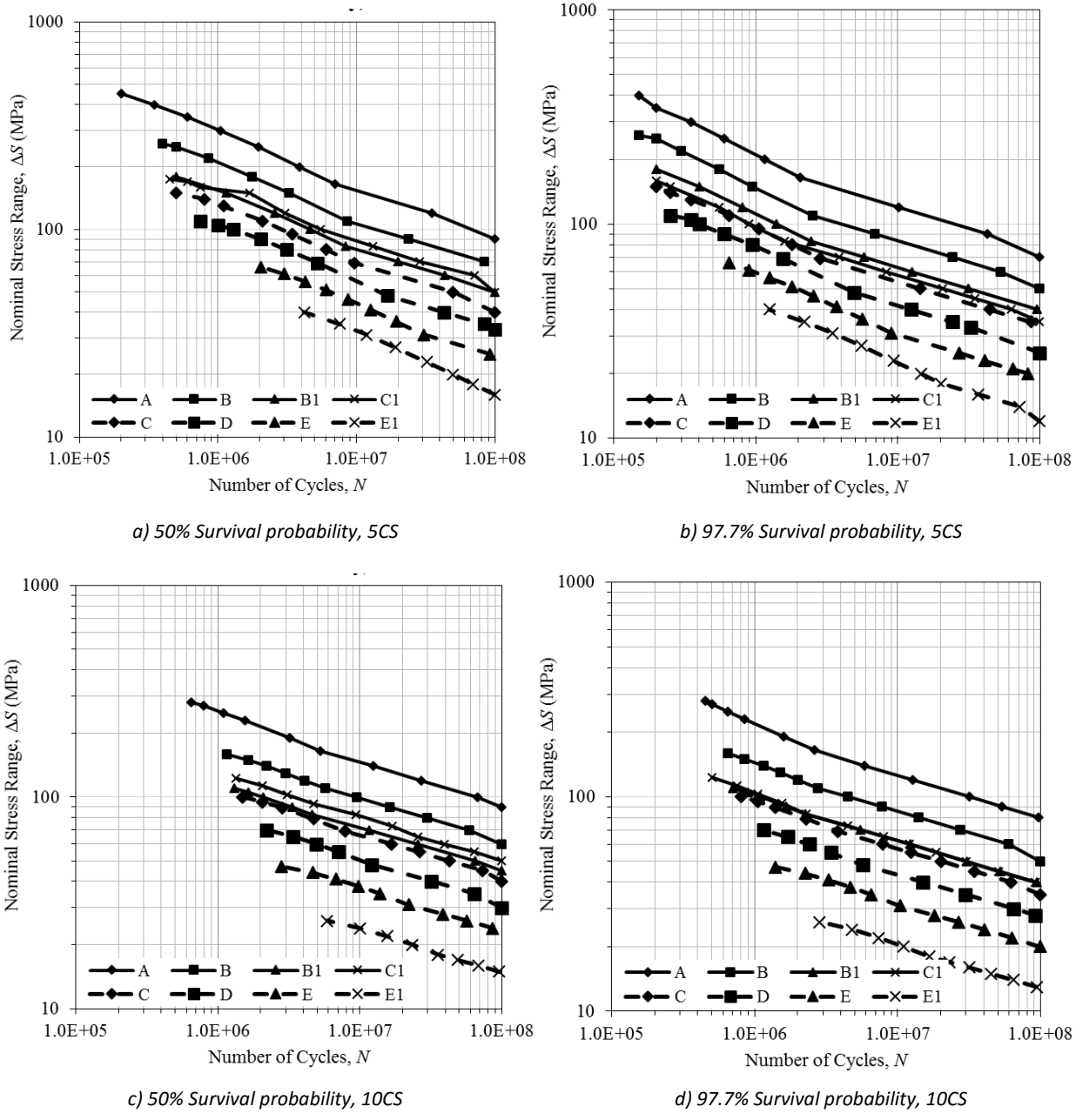

a) 50% Survival probability, 5CS

b) 97.7% Survival probability, 5CS

c) 50% Survival probability, 10CS

d) 97.7% Survival probability, 10CS

Figure 4.6: S-N plots using calibrated Markov chain model, 50% and 97.7% survival probability, 5CS and 10CSmodels

This method of calibration relies solely on 2 points corresponding with the 97.7% and 50% survival probabilities, and those differ by a single factor. While the approach is relatively simple, the CSs in the resulting model have no physical meaning (i.e. they are not associated with a measureable parameter). It should also be recalled that in calibrating the Markov chain, it was simplistically assumed that the initial weld was perfect, or that there was a 100% probability of it starting in CS1.

4.2.2 Calibration using SBFM failure data

Using a similar approach to the one described in the previous section, a Markov chain model can be calibrated using a specific set of failure data, such as fatigue test results from one test series that are applicable to a very specific specimen size and geometry. To demonstrate this, the probabilistic SBFM model described in the previous chapter was used to generate an artificial set of failure data. Recall that this model and the input parameters used in Chapter 3 were calibrated in [Walbridge et al, 2012] using test data applicable to transverse stiffener welds in mild steel specimens, so the distribution of the number of cycles to failure obtained using this model is very close to that of the real data set. The result of this calibration is presented in Table 4.5 for SR = 69 MPa (CAFL for Detail Category 'C'). It should be noted that these are illustrative results for an as-received (i.e. untreated) weld.

Table 4.5: SBFM failure data TPM calibration

Category:	**5CS**	**10CS**	**SR**	**DSL**
C	0.037	0.091	69	2.19E+07

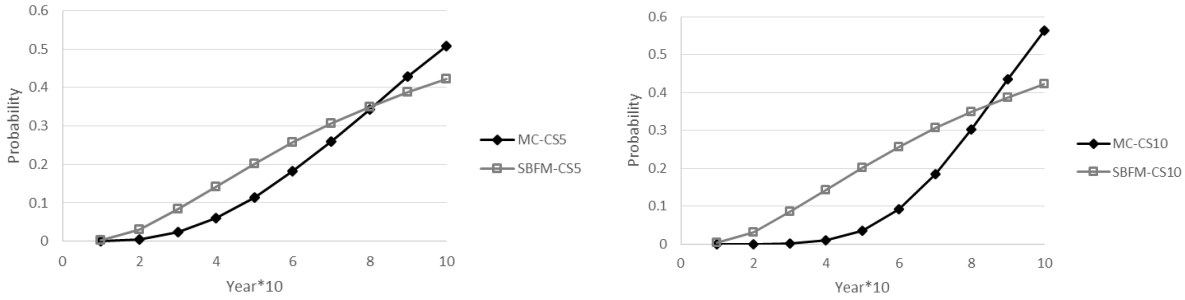

a) 5CS: Probability of Failure *b) 10CS: Probability of Failure*

Figure 4.7: Comparison of failure probabilities using probabilistic SBFM and calibrated Markov chain models

A comparison of the failure probabilities versus time obtained using the probabilistic SBFM and the calibrated Markov chain models is presented in Figure 4.7. Looking at this figure, it can be seen that the 5CS and 10CS Markov chain curves follow the general trend of the corresponding probabilistic SBFM curve, but start slower and catch up near the end. This trend is sharper for the 10CS model (Figure 4.7b), due to the nature of larger Markov chains. Specifically, it takes a minimum of 10 years for the probability of failure to become non-zero with the 10CS model, as it is assumed that the weld is perfect to begin with, and deterioration can only occur in jumps of one CS per year. This causes a very slow start, and so to compensate the optimization process increases the slope later.

The Markov chains produced here are again uniform Markov chains, with a single transition probability for all CSs. As in the previous section, it was assumed that the initial condition is 100% in CS1, as again the CSs have no physical meaning and this is the simplest a priori assumption.

4.2.3 Calibration using SBFM crack growth data

The SBFM analysis used in the previous section divided the output into two states, either failed or not, with failure defined by having a crack larger than some critical crack size (half of the plate thickness or $T/2$ is the critical crack size assumed in this study). This approach can be refined considerably by dividing the output into further categories (based on the crack depth, a) and defining them as condition states. A Markov chain can then be calibrated to this data, and instead of a uniform Markov chain, where each transition probability is the same and has no physical meaning, each transition probability can be calibrated separately, in order to optimize the ability of the model to predict the evolution of the crack depth, rather than simply the time to failure. To demonstrate this, CS definitions were established for the 5CS and 10CS Markov chain models, as defined in Table 4.6.

Table 4.6: Condition state definitions based on crack length, a

Condition State	**5CS upper limit (mm)**	**10CS upper limit (mm)**
1	0.25	0.1
2	1.0	0.15
3	2.5	0.25
4	T/2	0.5
5	failure	1.0
6	-	1.625
7	-	2.5
8	-	3.75
9	-	T/2
10	-	Failure

The probabilistic SBFM model can then be run to obtain statistics of being in each CS at the end of a given analysis period. These results are presented graphically in Figure 4.8.

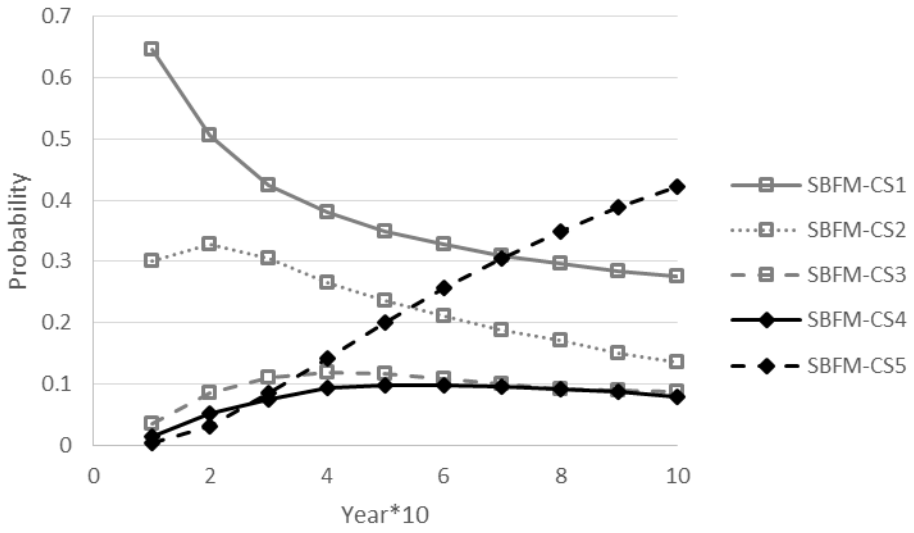

Figure 4.8: SBFM output for as-received transverse stiffener weld (SR = 69 MPa, 219,000 cycles per year)

In Figure 4.8 we can see the movement between CSs. In the beginning, based on the initial crack depth distribution, the weld has the highest probability of being in CS1, followed by CS2. As the weld deteriorates, the probability of residing in CS1 decreases, and the probabilities associated with the other CSs increase. First the CS2 probability rises slightly, then CS3 and CS4 rise slightly. Near the middle of the lifespan the majority of the probability still resides in CS1, but the others have increased, particularly CS5. Near Year 70 is when the majority of the probability resides in the failure CS for the first time, and that trend continues until just above 40% of the welds have failed after 100 years. Note that this is for a transverse stiffener weld with a stress range of 69MPa and 219,000 cycles per year assumed. A high stress range and number of cycles was chosen to get probabilities of failure that could be compared. In actual welds, the probability of failure is expected to be very low.

All previous Markov chain models assumed that the weld started at CS1. However, for this analysis more detailed initial conditions can be determined, since we know the statistical distribution of the initial crack depth, a_i. Recalling back to Table 3.1, the mean and standard deviation of a_i is 0.15 and 0.045 respectively, with a log-normal distribution.

Given the vector of initial probabilities of being in each CS, the transitions probabilities in the TPM associated with each CS can be calibrated in order to minimize the error in the estimated probability of being in each CS (e.g. the sum of the differences between the probabilistic SBFM and Markov chain predictions) after various periods of time within the service (e.g. every 10 years). This was done using the

5CS and 10CS Markov models for the as-received transverse stiffener weld at SR = 69 MPa and 219,000 cycles per year. The results are summarized in Tables 4.7 and 4.8, and compared to the previous TPM calibrated.

Table 4.7: 5CS calibration results for as-received transverse stiffener weld (SR = 69 MPa, 219,000 cycles per year)

Condition State	**Initial Probabilities**	**TPM (crack growth data)**	**TPM (SBFM failure data)**	**TPM (S-N Det. Cat. 'C')**
1	0.697	0.012	0.037	0.080
2	0.302	0.027	0.037	0.080
3	0.001	0.062	0.037	0.080
4	0.000	0.070	0.037	0.080

Table 4.8: 10CS calibration results for as-received transverse stiffener weld (SR = 69 MPa, 219,000 cycles per year)

Condition State	**Initial Probabilities**	**TPM (crack growth data)**	**TPM (SBFM failure data)**	**TPM (S-N Det. Cat. 'C')**
1	0.049	1E-5	0.091	0.264
2	0.234	0.007	0.091	0.264
3	0.362	0.019	0.091	0.264
4	0.234	0.036	0.091	0.264
5	0.121	0.058	0.091	0.264
6	0.000	0.108	0.091	0.264
7	0.000	0.162	0.091	0.264
8	0.000	0.238	0.091	0.264
9	0.000	0.112	0.091	0.264

Looking at the results in Tables 4.7 and 4.8, it is difficult to directly compare the SBFM crack growth data calibration to the others, as this calibration uses different initial CS probabilities. When comparing the 5CS and 10CS results, the 10CS TPM has a higher transition probability in all cases. This is due to the fact that to reach failure the weld must pass through more CSs for the 10CS model.

The results of the calibration to crack growth data of the 5CS and 10CS Markov models are shown in Figures 4.9 and 4.10.

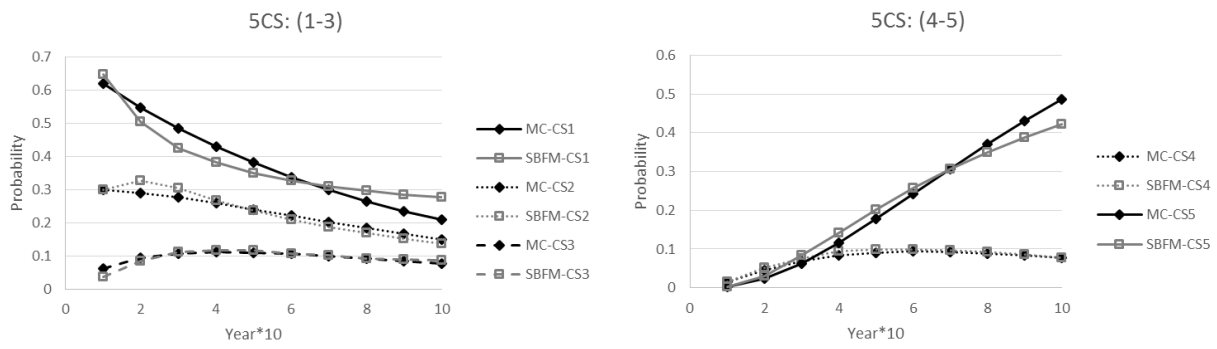

Figure 4.9: Comparison of CS probabilities using probabilistic SBFM and calibrated 5CS Markov chain models

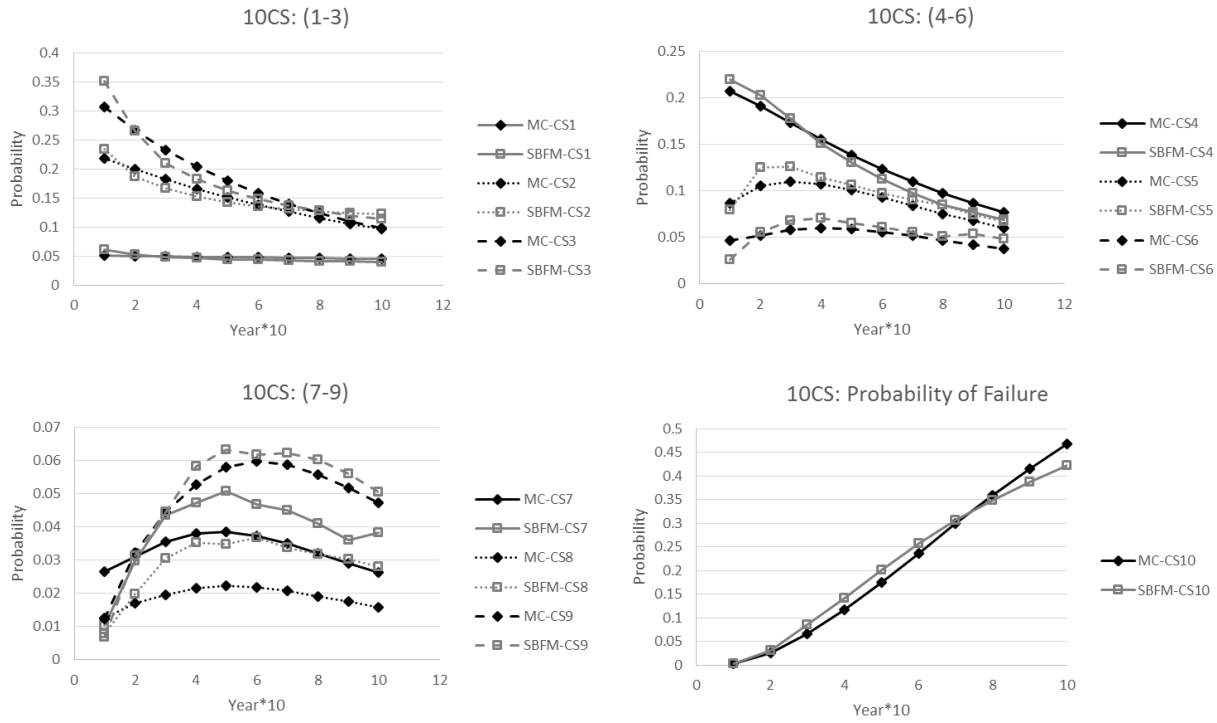

Figure 4.10: 10CS Comparison of CS probabilities using probabilistic SBFM and calibrated 10CS Markov chain models

The dark lines with diamond markers in Figures 4.9 and 4.10 are the results obtained using the Markov chain models, and the grey lines with square markers are the results obtained using the probabilistic SBFM model. Each linetype, whether solid, dashed, or dotted, corresponds to a different CS. As shown, this method results in a very close estimation for most CSs. The estimation of CS7 and CS8 in Figure 4.10 does not appear to be a good fit, but it is important to look at the vertical scale, which only goes up to probability of 7%. The error is one percentage point. It is interesting to compare the probability of failure, or of being in CS5 for the 5CS model and CS10 for the 10CS model, to the previous method,

which was calibrated by only minimizing the difference in the probability of failure (Figure 4.7). Comparing the results, it can be seen that a closer fit is achieved by minimizing the difference in all the condition states using the last method described.

There have been three methods presented for calibrating a Markov chain to fatigue data. The first involves using two points on the S-N graphs, the 50% and 97.7% survival probability points. The last two methods involve data from SBFM, one from failure data, and one from crack growth data divided into condition states. It is difficult to compare these methods against each other, as the one calibrated to S-N curves will perform better on an S-N plot than one calibrated to SBFM failure data, and vice versa. Graphing these can still be useful, but not as the only method of comparison. Therefore a different method is required for a non-biased comparison.

4.3 Life cycle cost analysis (LCCA) using Markov chain models

The end goal is to use the Markov chains to calculate life cycle costs of maintenance strategies in order make the optimal choice. This section will present a framework to calculate these life cycle costs, including a discussion on sample maintenance actions and costs, and how these can be combined to form maintenance strategies. This process will then be used to compare the three different methods of calibration developed in the previous chapter as an unbiased method of comparison. Inspiration for the LCCA process is drawn from [Walbridge et al., 2012], which also uses fatigue Markov chains to model life cycle costs. The paper used four maintenance strategies, as follows:

S0: base case, no inspection (MPI), repair (gouging and rewelding), or needle peening
S1: needle peening after 20 years of service loading
S2: inspection, repair (if needed), and needle peening after 20 years of service loading
S3: inspection, repair, and needle peening as needed after every 20 years of service loading

Needle peening is a preventative treatment which increases the life of the weld as discussed in Section 2.5. Inspection is the process of determining if there are cracks in the weld using detection techniques such as Magnetic Particle Inspection (MPI), and repair is performing gouging and rewelding to remove the crack. Inspection and repair are modelled separately as inspection is a set cost, whereas repair cost is dependant on how many are performed.

[Walbridge et al., 2012] used seven loading conditions, varying the applied stress range (SR) and design service life (DSL), shown in Table 4.9.

Table 4.9: Loading case properties

Loading Case:	Stress Range (MPa)	Design Service Life (cycles/year)
LC1	84	10^4
LC2	120	10^4
LC3	43	10^5
LC4	60	10^5
LC5	84	10^5
LC6	30	10^6
LC7	43	10^6

The loading conditions were chosen to cover a wide range of possible highway bridge loading histories.

A large part of comparing maintenance strategies is the ratios between inspection, treatment, repair and replacement costs. These amounts vary widely based on materials, access, equipment, labour, and traffic, among many other factors, and so it is difficult to choose values that will be applicable to all scenarios. In general, the cost will increase in the order listed above, from inspection to replacement, and so in an effort to minimize the number of variables it was assumed that the costs increased by a factor from one to the other. A user can look at their own costs, determine what their factor between respective categories is, and interpolate between the results presented to determine what the optimal maintenance strategy for their bridge is.

The three chosen cost factors and the appropriate costs are shown in Table 4.10:

Table 4.10: Cost factors

Cost Factor	1	3	10
Inspection	$1	$1	$1
Treatment	$1	$3	$10
Repair	$1	$9	$100
Replacement	$1	$27	$1000

The calibrated transition probabilities are used to set up a Markov chain, and probabilities of being in each condition state are modelled for 100 iterations to represent a 100 year life. The transition

probabilities are modified using Equations (4.3) and (4.4) to account for different stress ranges and design service lives according to the different loading cases.

Each year the previous probabilities are multiplied by the TPM to obtain the new probabilities of residing in each CS. In addition to this, there are three calculations that can occur in every year.

Replacement

The first calculation, which occurs in each year, is replacement. This is when an element fails and replacement is required. The cost is calculated by multiplying the probability of being in the last CS, or failure, by the replacement cost. Thus only a fraction of the total replacement cost is applied each year. This is then assumed to be replaced by a like-new piece with the same initial probabilities of defects. To achieve this, the probability of failure is multiplied by the initial conditions, and returned to CS1, CS2, etc.

Repair

The second calculation is inspection and repair, which occurs when specified by the maintenance strategy (eg for maintenance strategy [S0; S1; S2; and S3], repair occurs [never; never; at year 20; and at year 20, 40, 60, and 80], respectively). Repair is assumed to be grinding and re-welding the weld at the location of a detected crack, and is then treated as an original weld with the same vector of initial conditions. Repair can only occur with an inspection which detects a crack. There are many types of inspection techniques for welds, for this thesis inspection will be modelled with probabilities associated with Magnetic Particle Inspection (MPI). According to [Lassen, 1991], the probability of detection, P_D, can be defined using Equation (4.5).

$$P_D = P_0 \cdot (1 - EXP(-\gamma \cdot (a - a_0))) \tag{4.5}$$

Where P_0 is the probability of detection for a large crack, a_0 is the smallest detectable crack size, and a is the current crack size. For a given CS, the value for a is the average between the maximum and minimum crack sizes. Values of $P_0 = 0.9$, $a_0 = 1$ mm, and $\gamma = 1$ are suggested for magnetic particle inspection [Lassen, 1991].

The following example will demonstrate how repair is modelled. Table 4.11 shows the initial conditions of a sample weld, and after 20 years of deterioration the probabilities of residing in each CS are evenly distributed at 0.2.

Table 4.11: Markov Chain repair example

	CS1	**CS2**	**CS3**	**CS4**	**CS5**
Initial Conditions	0.8	0.2	0	0	0
…					
Year 20	0.2	0.2	0.2	0.2	0.2

Calculating the changes due to inspection and repair for CS1 and CS2 has no effect, as the probability of detection is 0. Inspection and repair performed on CS three is 47.5% effective using Equation (4.5) and CS definitions from Table 4.6, and so the probability of a weld remaining in CS3 is $0.2 – (0.2 \cdot 0.475) = 0.105$. The remaining probability, 0.095, is divided between CS1 and CS2 as per the initial conditions, 80% and 20% respectively, and added to those probabilities. The resultant probabilities of all CSs after considering the effect of inspection and repair of CS3 is shown in Table 4.12.

Table 4.12: Markov chain repair example

CS	**1**	**2**	**3**	**4**	**5**
Probability	0.276	0.219	0.105	0.2	0.2

Note that the sum of all CSs still adds to one. We can repeat this process for CS4 and CS5, with probabilities of detection of 0.899 and 0.9 respectively according to Equation (4.5), and we get the final CS probabilities in Table 4.13.

Table 4.13: Markov chain repair example

CS	**1**	**2**	**3**	**4**	**5**
Probability	0.564	0.291	0.105	0.0202	0.020

These are the CS probabilities which are used for further calculations. To calculate the probabilities associated with year 21, this vector is multiplied by the transition probability matrix.

The costs associated with repair are the sum of all probabilities moved multiplied by the inspection and repair cost specified according to Table 4.10. The sum of all probabilities moved is the sum of products of the probability of detection multiplied by the probability in each CS, as described in Equation (4.6):

$$Cost_{\text{Repair}} = (\text{Inspection+Repair}) \cdot \sum_{i=1}^{5} PD_{CSi} \cdot P_i \qquad (4.6)$$

Where PD_{CSi} is the probability of detection of CS i, and P_i is the probability of residing in CS i.

For the example above, using an inspection cost of \$1 and a repair cost of \$9, the cost associated with repair would be $(0.475 \cdot 0.2) + (0.899 \cdot 0.2) + (0.9 \cdot 0.2) = 0.455 \cdot (1 + 9) = \$4.55$. This cost is clearly not to be taken on its own, but rather used as comparison to other strategies.

Treatment

The third possible calculation is treatment. For this paper treatment is assumed to be needle peening, as outlined in Section 2.5. Needle peening introduces compressive residual stresses into the weld toe area, which can reduce or completely stop crack growth. The data for treatment is taken from [Walbridge et al, 2012], in which a transition probability matrix is developed from treated weld specimens. These specimens were tested in laboratory settings to failure, and the number of cycles reported. The TPM for treated welds is shown in Table 4.14:

Table 4.14: TPM for treated welds

Condition State	**5CS**	**10CS**
1	1E-12	2.91E-06
2	3.43E-03	5.34E-05
3	Same	1.19E-06
4	Same	7.24E-04
5		5.85E-02
6		Same
7		Same
8		Same
9		Same
m:	5.125	3.352

The smaller crack sizes are affected by needle peening, and so have a different transition probability. However, needle peening only acts up to a certain depth, 1 mm, and so any probability beyond that remains unchanged from the untreated TPM. Remembering Table 4.6, the 1 mm depth corresponds to the end of CS2 for 5CS and CS5 for 10CS.

During years in which treatment is specified, the transition probability matrix used is changed from the untreated weld to the treated weld, and a one-time cost of treatment is applied according to Table 4.10. This change is constant for all years after the treatment year.

Using the maintenance actions described above with the costs described in Table 4.10, a cost per year of maintaining the bridge can be calculated. This is then converted to a Net Present Value, using Equation (4.7).

$$NPV(i,N) = \sum_{t=0}^{N} \frac{R_t}{(1+i)^t} \tag{4.7}$$

Where *NPV(i,N)* is the net present value of *N* years at discount rate of *i*, and R_t is the total cost for year *t*. These calculations are then summed for all years.

Using the loading cases and maintenance strategies described above, which use different combinations of replacement, repair and treatment, Figure 4.11 is developed, as presented in [Walbridge et al., 2012]

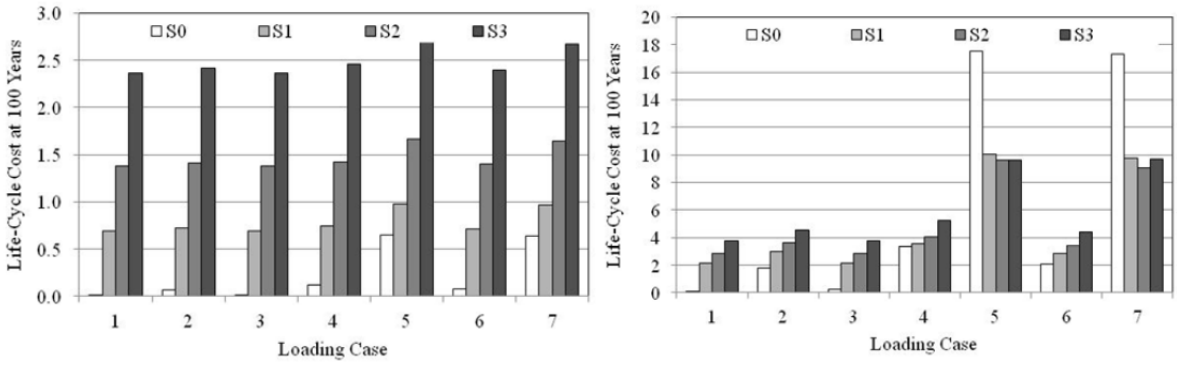

a) Cost factor = 1

b) Cost factor = 3

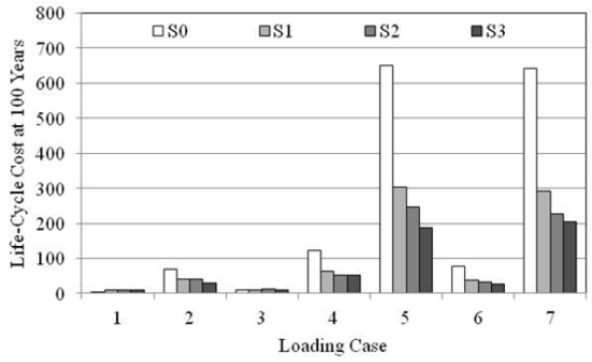

c) Cost factor = 10

Figure 4.11: Life cycle cost comparison [Walbridge et al, 2012]

These figures can be used to determine what the optimal maintenance strategy is, the most cost-effective way to spend limited maintenance budget funds. The vertical scale is the life cycle cost after 100 years. The horizontal scale is divided into the seven loading histories, shown in Table 4.9, and then divided further into the four maintenance strategies. The three figures are different ratios for the costs of inspection, treatment, repair and replacement, the cost factors being 1, 3, and 10.

As shown in Figure 4.11(a), when the costs of repair and treatment are low, the cost increases drastically for maintenance strategies which involve more repair and treatment, and the cost of doing nothing is almost zero. As the cost factor rises to 3, for most of the loading cases the trend is still the same, with the cost of doing nothing the cheapest and the strategies involving more repair and treatment more expensive. However, for loading cases with higher stress ranges and design service lives this trend is almost reversed, with the cost of doing nothing now the highest, and the costs of the remaining three options, which all include treatment, being about equal. As the cost factor rises to 10, the cost of doing nothing increases significantly, and becomes the most expensive option in most cases, with the maintenance strategies decreasing in cost from there. This is due to the higher cost of replacement, it becomes cost effective to spend some money on treatment and inspection in order to reduce the probability of failure and costly replacement.

4.4 Comparison of Markov models calibrated using different approaches

There have been three calibration methods discussed in this chapter, calibration using S-N curves, using SBFM failure data, and using SBFM crack growth data. There have been four methods for graphing and comparing calibration methods discussed in this chapter; the S-N curves, probability of failure according to SBFM, probabilities of being in each CS according to SBFM, and LCCA. Two of those, probability of

failure according to SBFM and probability of being in each CS according to SBFM, can be represented by one series of graphs. This section will now compare the methods of calibration using the graphing methods developed.

4.4.1 5 Condition state model

The following series of figures (Figures 4.12, 4.13, 4.14) compare the three different calibration methods, using the three graphing and comparing methods, for the five condition state model. Note that these are all for detail category C.

Calibration to S-N curves

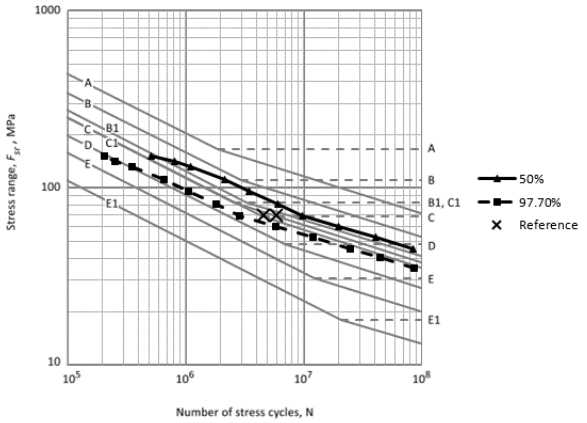

a) S-N curves

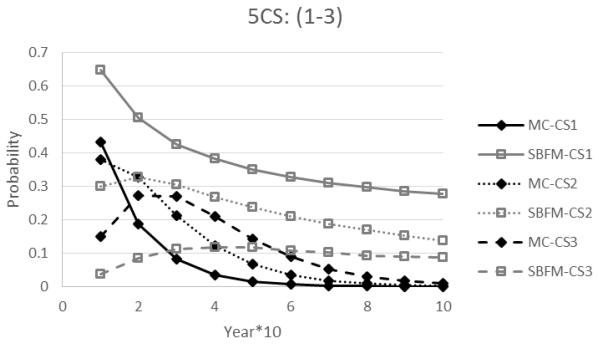

b) SBFM probabilities of condition states (CS1-CS3)

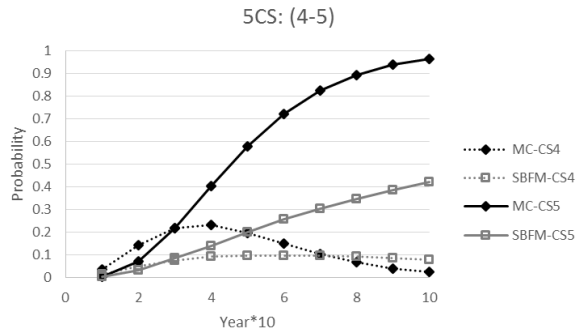

c) SBFM probabilities of condition states (CS4-CS5)

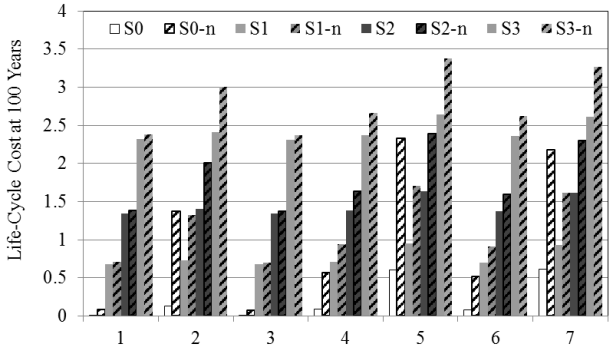

d) LCCA, cost factor = 1

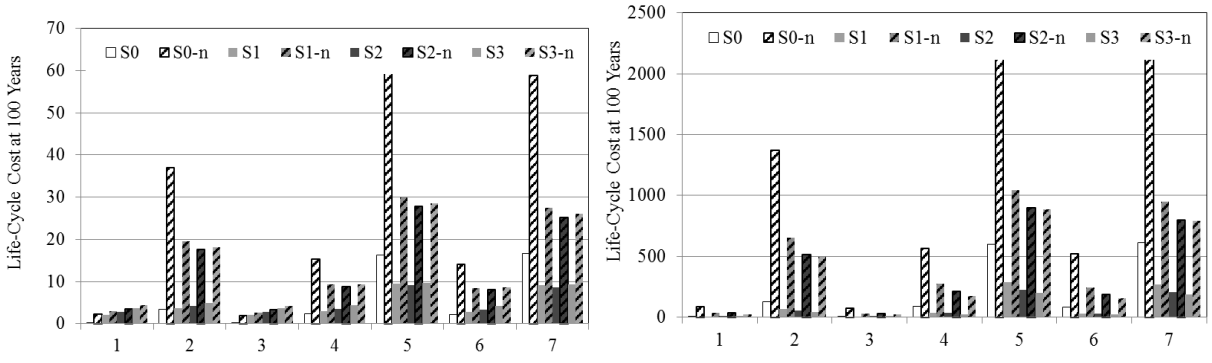

e) LCCA, cost factor = 3 *f) LCCA, cost factor = 10*

Figure 4.12: 5CS Calibration comparison using design S-N curves

According to Figure 4.12(a), S-N curve fit is good, however, this was expected, as this method was calibrated to the S-N curve. The fit to the other two methods, Figures 4.12(b) and 4.12(c), using Monte Carlo SBFM, is poor. Recall that a perfect fit would be no difference between the black and grey lines of a single linetype, any deviation from this is a worse fit. CS1 rapidly decreases to almost zero by year 50 compared to 35% for SBFM results, and shows an almost 100% chance of failure at the end of the life, compared to 40% for SBFM. The CSs in between are also not accurate. For the final method, comparing LCCA at 100 years, there are also significant differences, shown in Figure 4.12(d), 4.12(e), and 4.12(f). These graphs are set up in a similar manner to Figure 4.11, with the original values graphed in the same shades. The new values are graphed right beside the columns they are being compared to, and are hatched with a solid diagonal black pattern, and labelled with a "-n" for new. For the cost factor of 1 graph, most of the costs are similar, however, some are significantly off, which is more dangerous. If all costs are off by a similar amount, then the optimal maintenance strategy, the one with the lowest relative cost, is still the same, and therefore the analysis is still legitimate. However, for some of them, loading case 2, 5, and 7 in particular, the optimal maintenance strategy has changed. The relative cost of S0 has risen above the cost of S1, and so changes what the engineer would choose as the most cost-effective maintenance strategy. For the graph with the cost factor of 3, not only are the values significantly different, often by a factor of two or three, but the order has also changed, which means a different optimal maintenance strategy. In particular loading cases 2, 4 and 6 have had their relative costs reversed. For the load factor of 10, the costs have increased significantly, by a factor of up to 10, so much that it is difficult to tell how the trend has changed. What has changed is the relative costs between loading cases; originally loading case 2 and 4 were approximately equal, but this method predicts that loading case 2 is now twice as expensive as loading case 4.

Despite the benefits of simpler analysis and ease of computation, as SBFM is not even required, the calibration of the transition probability matrix to S-N curves performs poorly on the other graphs.

Calibration using SBFM failure data

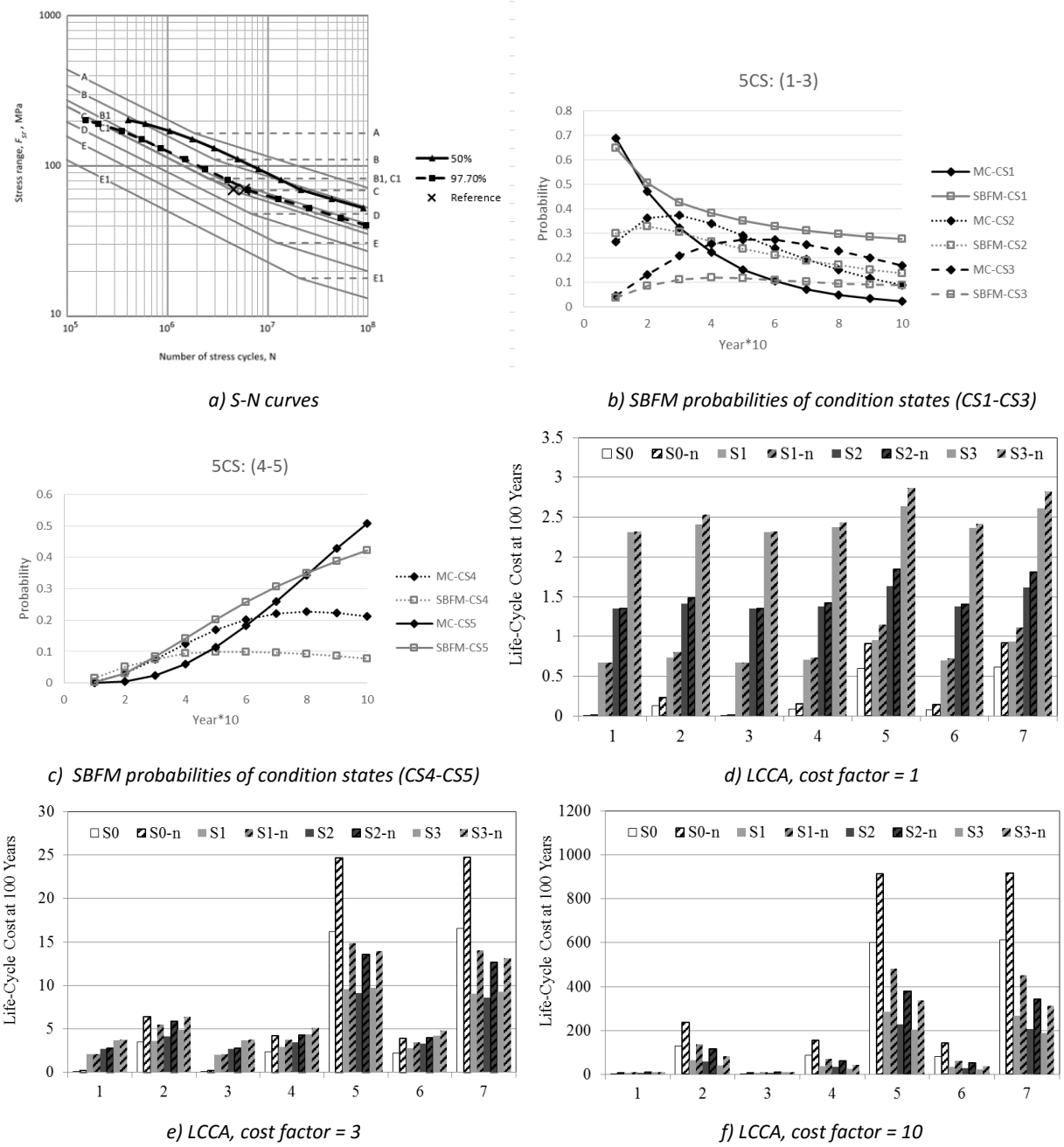

a) S-N curves

b) SBFM probabilities of condition states (CS1-CS3)

c) SBFM probabilities of condition states (CS4-CS5)

d) LCCA, cost factor = 1

e) LCCA, cost factor = 3

f) LCCA, cost factor = 10

Figure 4.13: 5CS Calibration comparison using SBFM failure data

As shown in Figure 4.13(a), the S-N plot is not perfect, the 97.7% line is very close, but the 50% line is significantly off. Note however that the distance between the two lines is about the same as the previous method, therefore the error from calibration to design S-N curves is a property of Markov chains, as opposed to an error in calibration. The graphs comparing to SBFM condition states, Figures 4.13(b) and 4.13(c), are much closer than the previous method, but this is expected as this was calibrated to SBFM failure data. They are still not a great fit however, particularity for CS1, which is supposed to be at around 30% at the end of the life, but this model shows about 0%. The next graphs, Figures 4.13(d) through 4.13(f), comparing life cycle costs, are again better than the calibration to S-N curves. The graph for a cost factor of 1 is much closer, particularly with respect to relative amounts. Both the original graph and the new one show the same optimal maintenance strategy, and the values are similar. However, in the graph for the cost factor of 3, we see the problem previously mentioned, where the new model has a different optimal choice, particularly for load cases 2, 4, and 6. The relative values for maintenance strategies S1, S2 and S3 appear to be similar; it is only S0 which rises at a rate not relative to the others. For the last graph, the relative rates are the same again, with both methods predicting the same optimal strategy, and the relative rates between loading cases is about the same.

Adding complexity to the Markov chain calibration has improved the results, however they are still not acceptably close. It is unclear if the benefit gained from increased accuracy of prediction is worth the extra computational time and effort required.

Calibration using SBFM crack growth data

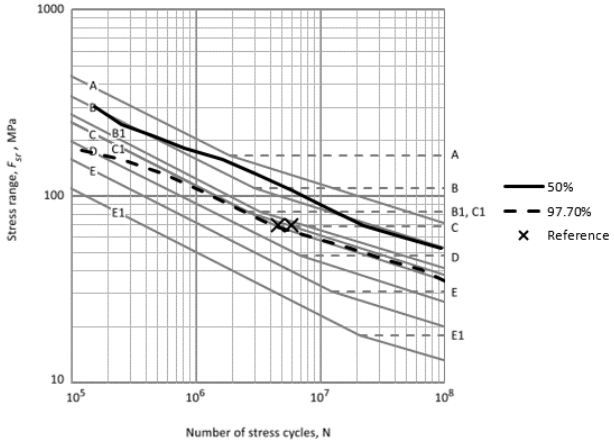

a) S-N curves

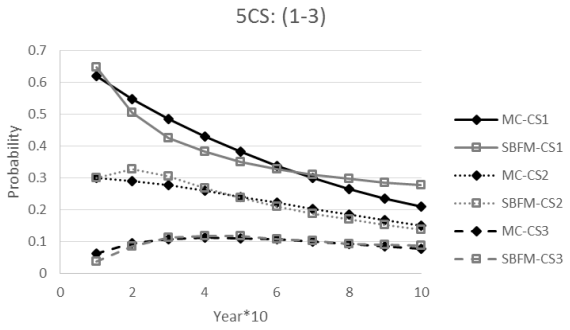

b) SBFM probabilities of condition states (CS1-CS3)

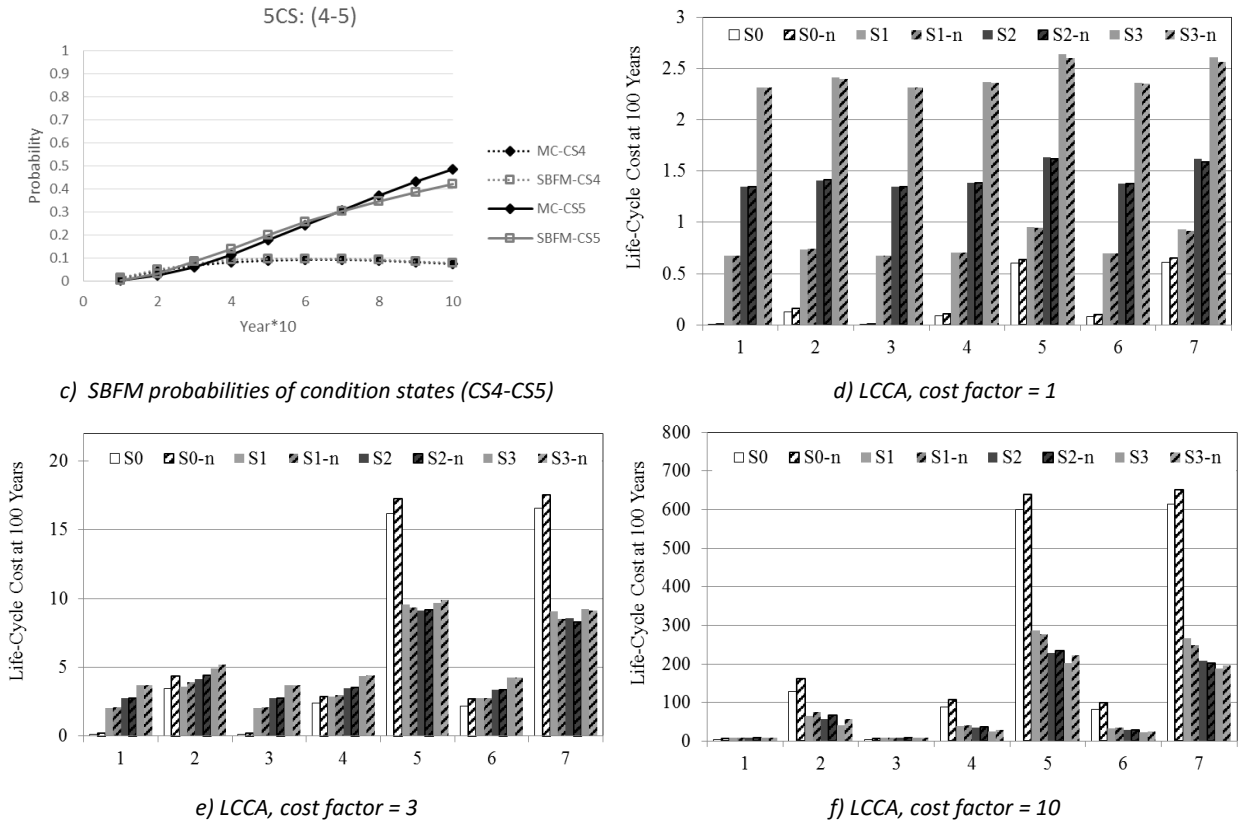

c) SBFM probabilities of condition states (CS4-CS5)

d) LCCA, cost factor = 1

e) LCCA, cost factor = 3

f) LCCA, cost factor = 10

Figure 4.14: 5CS Calibration comparison using SBFM crack growth data

A note on Figure 4.14(a), this method of calibration allows for the S-N curve to be drawn at much higher stress levels due to the non-uniform TPM, as some of them can still predict after others have reached 1.0. The slight deviation at high stress levels shown in the graph is due to the fact that above 150 MPa half of the transition probabilities have reached 1.0 and are no longer predicting correctly. Aside from that, the 97.7% line on the S-N curve is very accurate, staying on the line until very high stress ranges. However, the 50% line is off, with an even wider spread than before. The SBFM conditions state curves, shown in Figures 4.14(b) and 4.14(c), are very accurate, with very little difference. This was expected, as that was the method of calibration performed. It is interesting to note that calibrating all condition states results in a more accurate fit of the failure CS than simply calibrating to the failure CS, as performed in the previous method. The final method of comparison, the life cycle cost, is also a very accurate fit. The relative amounts are the same, so both methods predict the same optimal strategy, and the absolute values are very similar. Note that to compare these graphs, the initial conditions for the Markov chain were changed to match that of the [Walbridge et al, 2012] paper, [0.968, 0.032, 0, 0, 0].

The calibration to SBFM crack growth data performs the best on two of the three comparison methods, for the SBFM CS results and for the LCCA. For the final method, S-N curves, this method has a very accurate 97.7% line, and can predict to very high stress ranges, but the gap between the 97.7% and 50% curve lines is slightly larger than the other two methods. Therefore increasing the complexity of the Markov chain calibration results in a significantly more accurate model, and is worth the extra computational effort. This is partially due to the calibration to complex SBFM as opposed to simple S-N curves, and also due to the use of transition probability matrices with different values as opposed to one uniform value. This allows for more precise measurements of early CSs, which in turn results in more precise measurements of failure CSs.

4.4.2 10 Condition state Markov chain

This next section performs the same analysis as above, but instead using ten condition states as opposed to five. It can then be determined if the increasing complexity of the Markov chain has any effect on the accuracy of the model.

Calibration using design S-N curves

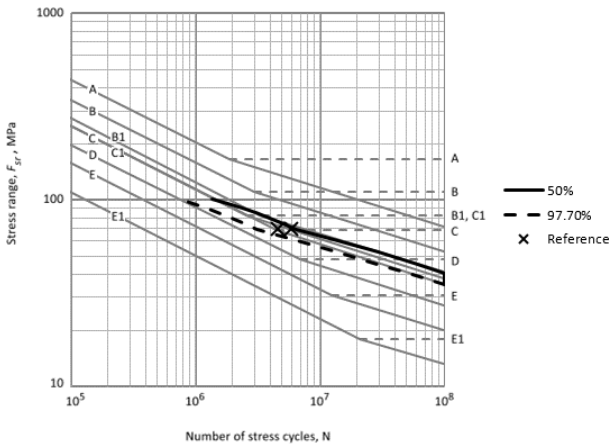

a) S-N curves

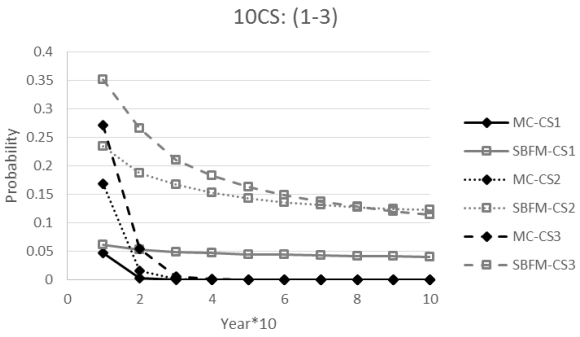

b) SBFM probabilities of condition states (CS1-CS3)

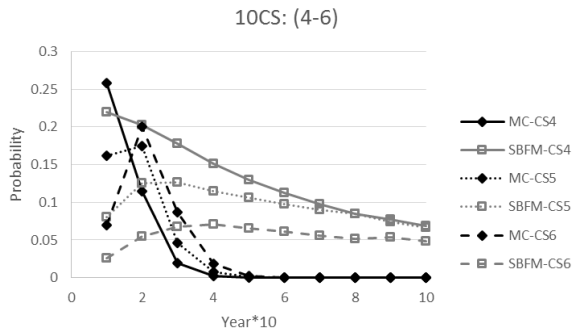

c) SBFM probabilities of condition states (CS4-CS6)

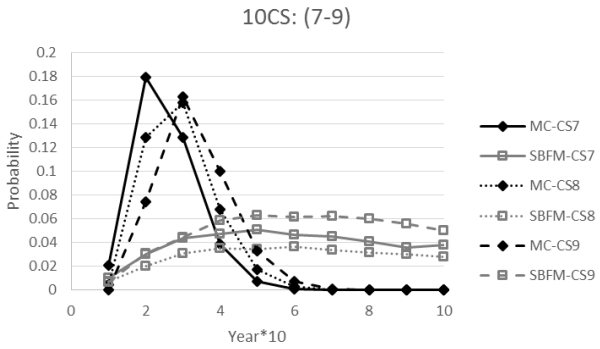

d) SBFM probabilities of condition states (CS7-CS9)

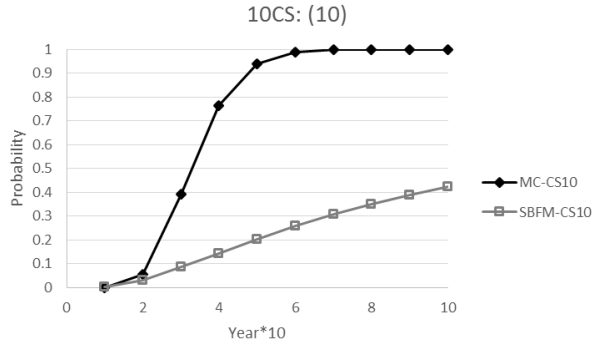

e) SBFM probabilities of condition states (CS10)

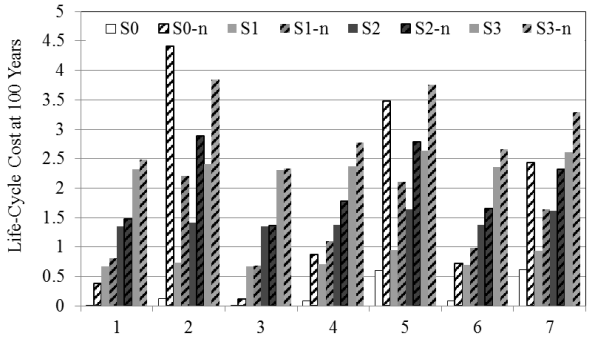

f) LCCA, cost factor = 1

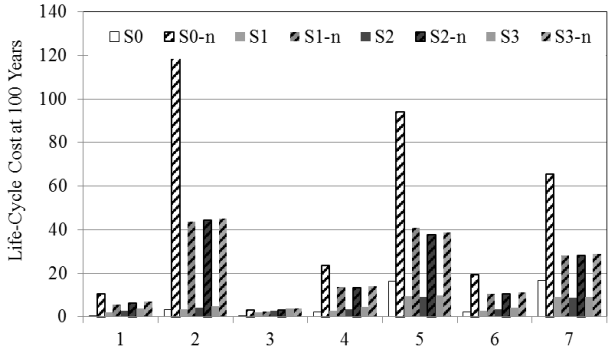

g) LCCA, cost factor = 3

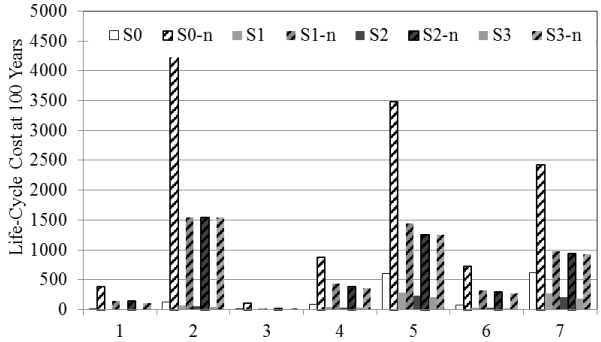

h LCCA, cost factor = 10

Figure 4.15: 10CS Calibration comparison using design S-N curves

As expected, and similar to the five condition state model, the S-N curve fit, shown in Figure 4.15(a), is good, although does not go to very high stress ranges. However, the fit to SBFM condition states, shown in Figures 4.15(b) through 4.15(e), is very poor; all of the CSs peak very early before moving to the next one. The failure CSs reaches above 90% probability by year 50, and stays at near 100% from then on,

compared to about 40% failure at the end of the life as predicted by SBFM. The third comparison method, total life cycle cost at 100 years shown in Figures 4.15(f) through 4.15(h), is also very poor. The graph of a cost factor of 1 has significant variation between the original values and the new values. For loading case 2, 5, and 7, the optimal maintenance strategy suggested is different. For loading case 2, the lowest cost suggested by the original method, S0, is actually the most expensive as shown by the new method. The next cost factor, 3, also has significant variation, so much that it is difficult to tell how much variation. The vertical axis scale has changed from a maximum of $20 in the original graph to $120 here. The last cost factor, 10, is such a bad fit that the original values are barely visible, with the vertical axis changing from $800 to $5000.

Similarly to the 5CS, the calibration of the transition probability matrix to S-N curves performs poorly on the other graphs, and therefore is not a very viable option.

Calibration using SBFM failure data

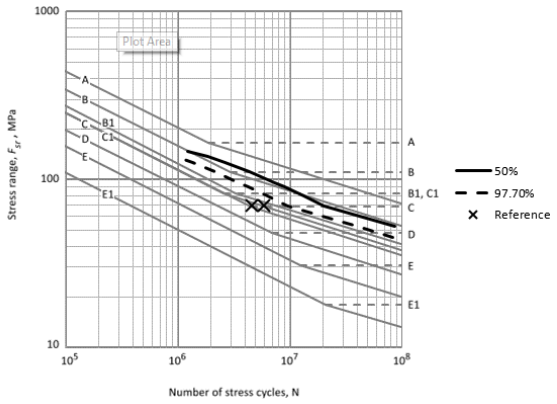

a) S-N curves

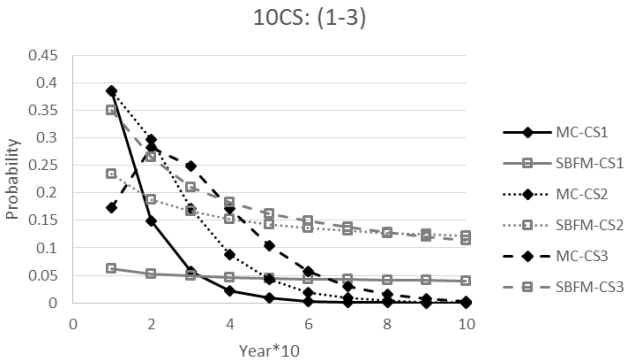

b) SBFM probabilities of condition states (CS1-CS3)

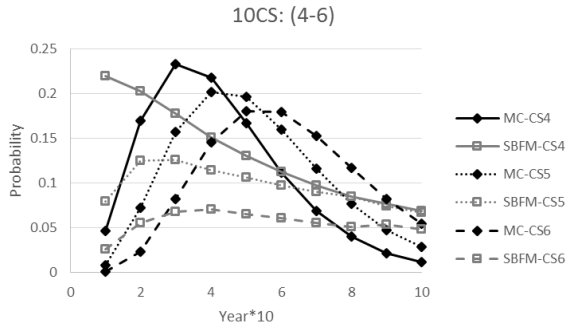

c) SBFM probabilities of condition states (CS4-CS6)

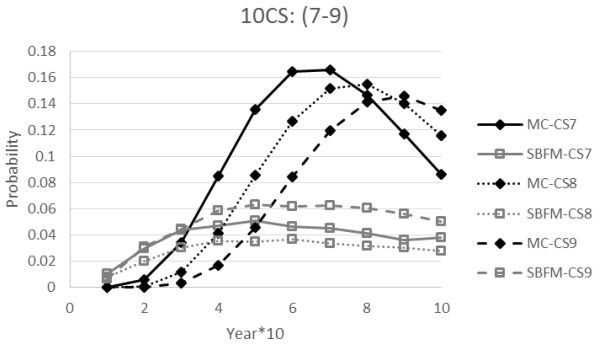

d) SBFM probabilities of condition states (CS7-CS9)

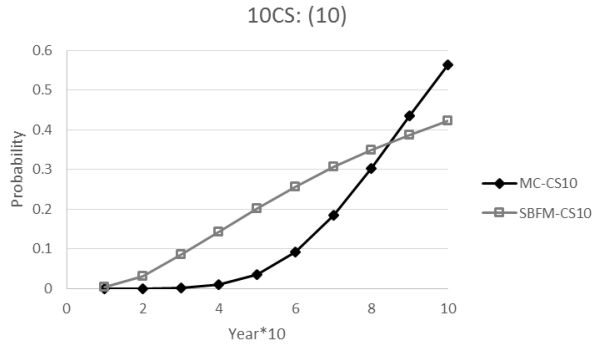

e) SBFM probabilities of condition states (CS10)

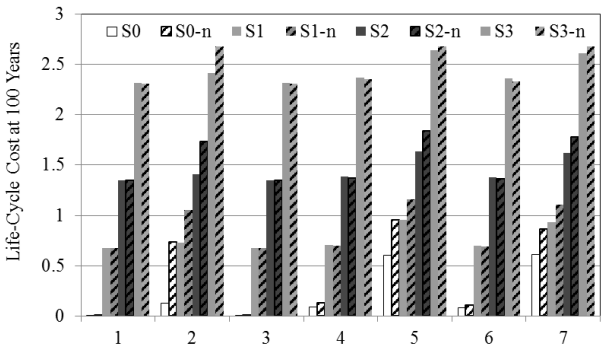

f) LCCA, cost factor = 1

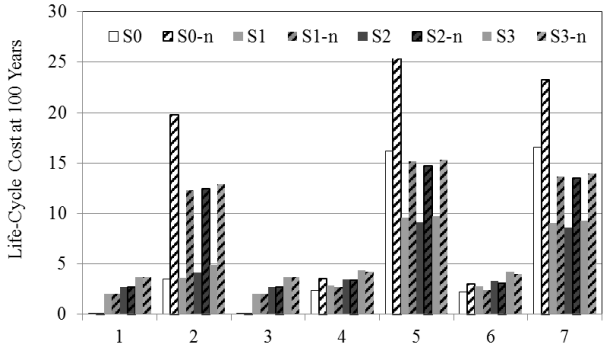

g) LCCA, cost factor = 3

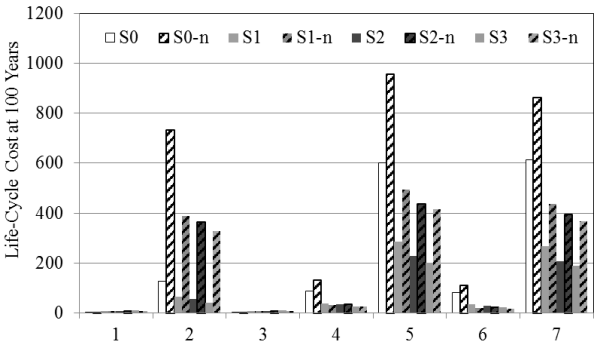

h LCCA, cost factor = 10

Figure 4.16: 10CS Calibration comparison using SBFM failure data

The S-N plot, shown in Figure 4.16(a), is not very accurate, with both the 97.7% and the 50% lines off from the reference marks. However, the gap between the two is much closer than the previous method. The SBFM conditions state graphs are also not very accurate, with a very obvious peak that shifts through the CSs until it all collects in the failure CS. None of the early CSs have the same shape, until CS10. The final method of comparison, life cycle cost comparison, show a closer fit than the previous method. The cost ratio of 1 predicts the same optimal maintenance strategy as the original method, although the relative cost of S0 has risen significantly more than the others. The graph of the cost ratio of 3, however, shows a different optimal maintenance strategy than the original, particularly for loading cases 2, 4 and 6, but for the other loading cases the costs seem to change by the same relative amount. The total costs are also still significantly off. For the final loading factor of 10, the fit is still not very close, however, the relative change in costs are constant, and both methods predict the same optimal maintenance strategy.

Despite the increased complexity over the calibration of the S-N curve by using SBFM, there is little improvement in the results, particularly for the comparison against SBFM. The life cycle cost comparison is better, with results not as significantly different as the previous method, although the S-N curve fit is worse.

Calibration using SBFM crack growth data

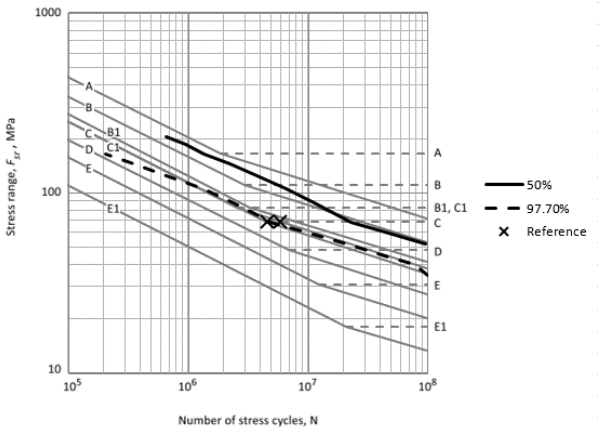

a) S-N curves

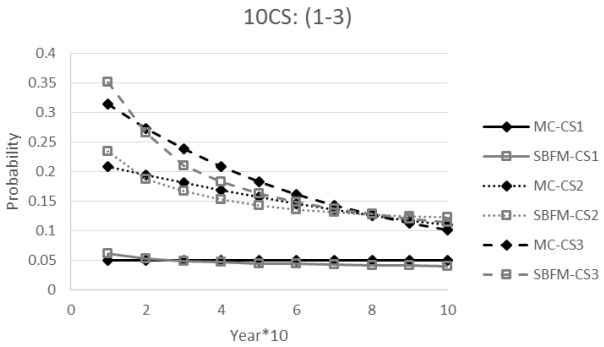

b) SBFM probabilities of condition states (CS1-CS3)

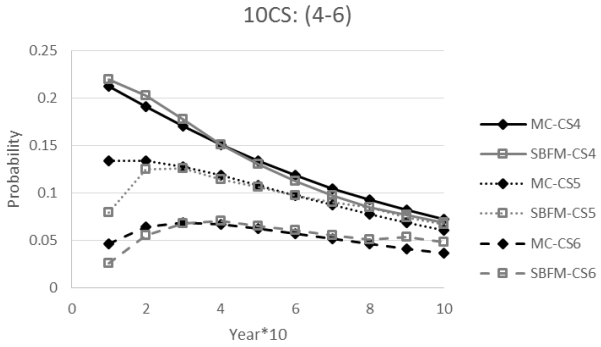

c) SBFM probabilities of condition states (CS4-CS6)

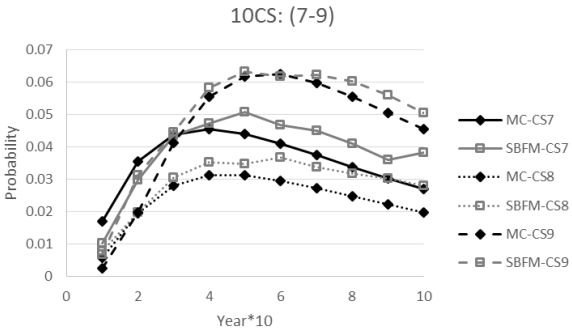

d) SBFM probabilities of condition states (CS7-CS9)

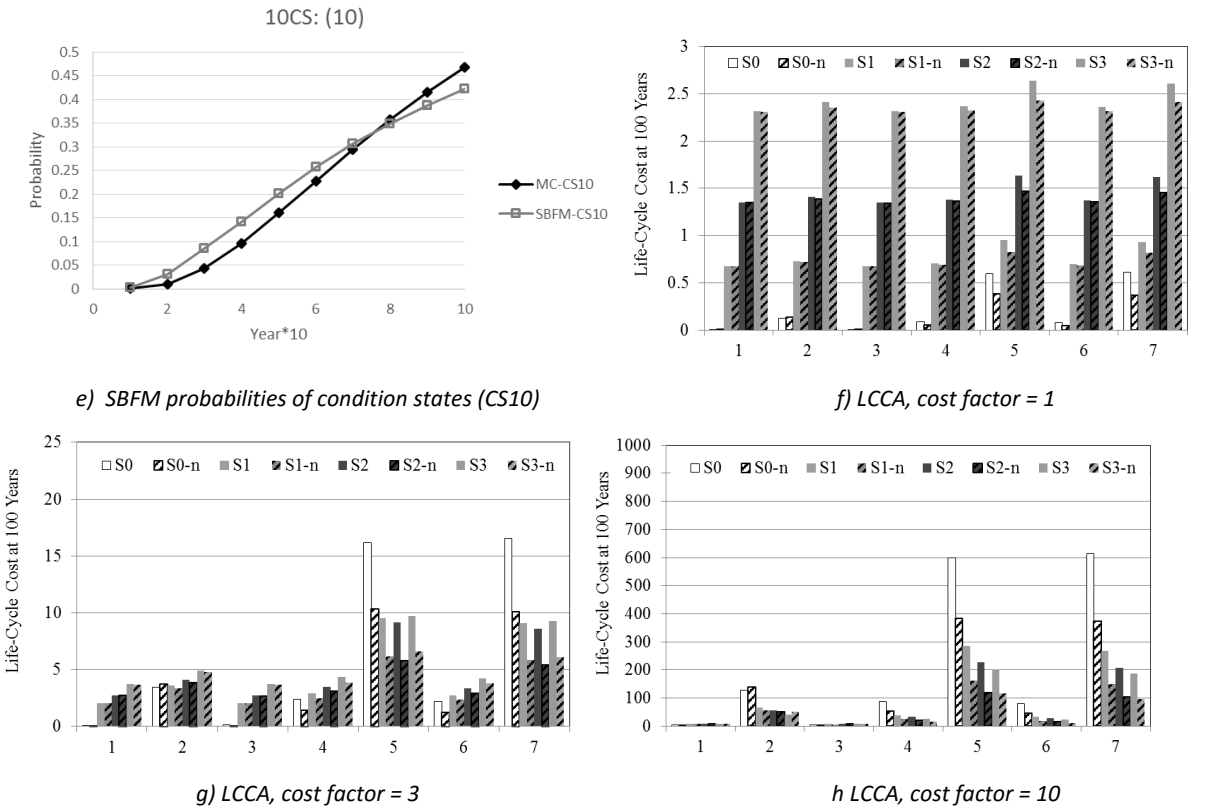

e) SBFM probabilities of condition states (CS10)

f) LCCA, cost factor = 1

g) LCCA, cost factor = 3

h LCCA, cost factor = 10

Figure 4.17: 10CS Calibration comparison using SBFM crack growth data

The calibration to SBFM crack growth data results in a very accurate 97.7% S-N curve, particularly for the reference point, however the gap between the 97.7% and 50% curve is larger than the other two methods. As noted before, the S-N curves can be drawn at much higher stress levels due to some of the transition probabilities reaching 1.0 later. The SBFM CS curves are very accurate again, and again it is interesting to note that the calibration of all CS results in a closer fit for the failure probability than just calibrating to the failure CS. For the life cycle cost, however, the Markov model predicts significantly lower costs. Note that as with the 5CS model, the initial probabilities have been modified to the 10CS equivalent of [0.968, 0.032, 0, 0, 0] to match the [Walbridge et al, 2012] paper.

The cause of this difference is dealing with very small probabilities of movement in Markov chains. Returning back to the original CSs to compare the 5CS and 10CS as they were both calibrated from the same set of data, Figure 4.18 shows the probability of failure for both five condition states (5CS) and ten condition states (10CS) for loading case 7, treatment strategy S0.

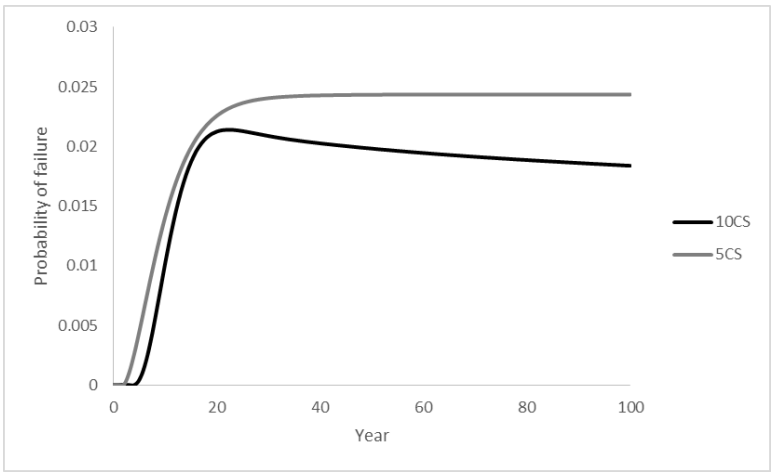

Figure 4.18: Probability of failure (end condition state)

As shown, both models rise to about the same result, around 0.22, but while the 5CS converges and stays constant, the 10CS decreases. This decrease in probability of failure is what caused the difference in cost for the life cycle cost comparison graphs. This decreasing trend continues, shown in Figure 4.19 over 2000 years.

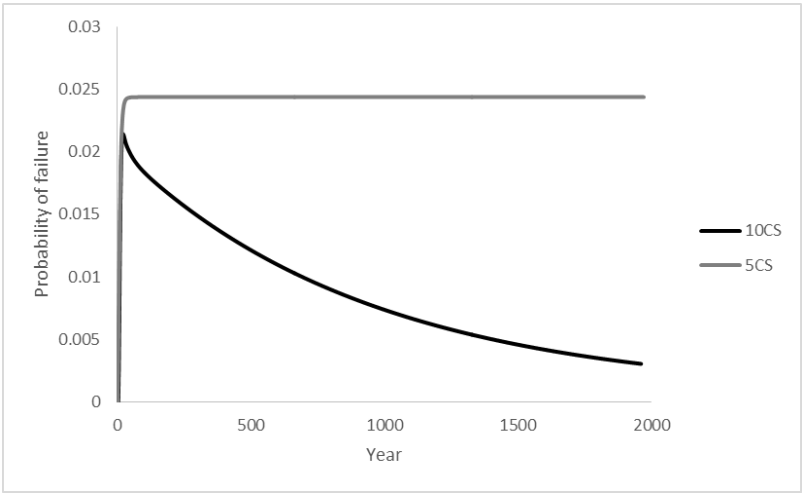

Figure 4.19: Probability of failure (end condition state), 2000 years

Markov chains modelling replacement action eventually converge on steady values, as shown in the 5CS model above. The 10CS model does not converge within a reasonable time frame, with the probability of failure steadily decreasing over time. This decrease is because the probability of being in CS1, or perfect, is rising to near 100% over the two thousand years. The reason for this is the probability of moving from CS1 into CS2 is very small, 0.00327%, compared to 55.5% moving from CS8 to CS9. This is a result of the low value from the calibration which is then modified by the higher stress range. This is normally not an issue as the initial condition specifies that only 4.9% starts in CS1. However, to model the replacement

action, which occurs every year, it is assumed that the element returns to initial conditions, and so 4.9% of the failed elements returns to CS1. This probability then has a very low chance of moving down to CS2, and so over the years this accumulates as failed elements are replaced.

This is not realistic, as continual replacement of welded elements will not eventually result in a weld which never fails. It is also not a valid Markov model for a 100 year time period, as the probabilities of residing in condition states do not converge. Therefore the first two probabilities of movement can be slightly modified until the probability of failure converges, as shown in Table 4.15.

Table 4.15: 10CS modified initial conditions

	Original	**Modified**
q1	0.00001	0.01
q2	0.007	0.03
q3	0.017	Same
q4	0.036	Same
q5	0.058	Same
q6	0.108	Same
q7	0.162	Same
q8	0.238	Same
q9	0.112	Same

The comparison graph between the 5CS and 10CS for probabilities of failure is now shown in Figure 4.20.

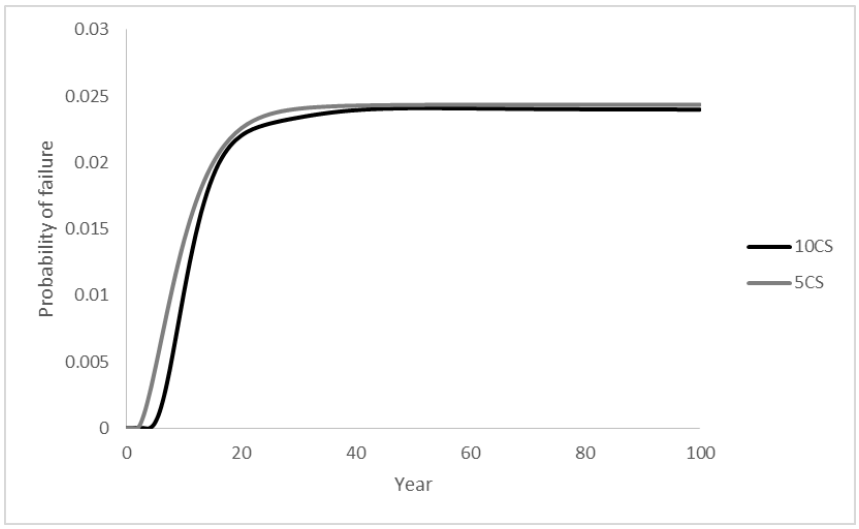

Figure 4.20: Probability of failure (end condition state) after modification of initial probabilities

This is now a much better fit. Using the equivalent initial conditions from [Walbridge et al] of [0.968, 0.032, 0, 0, 0], we get the life cycle cost comparison shown in Figure 4.21.

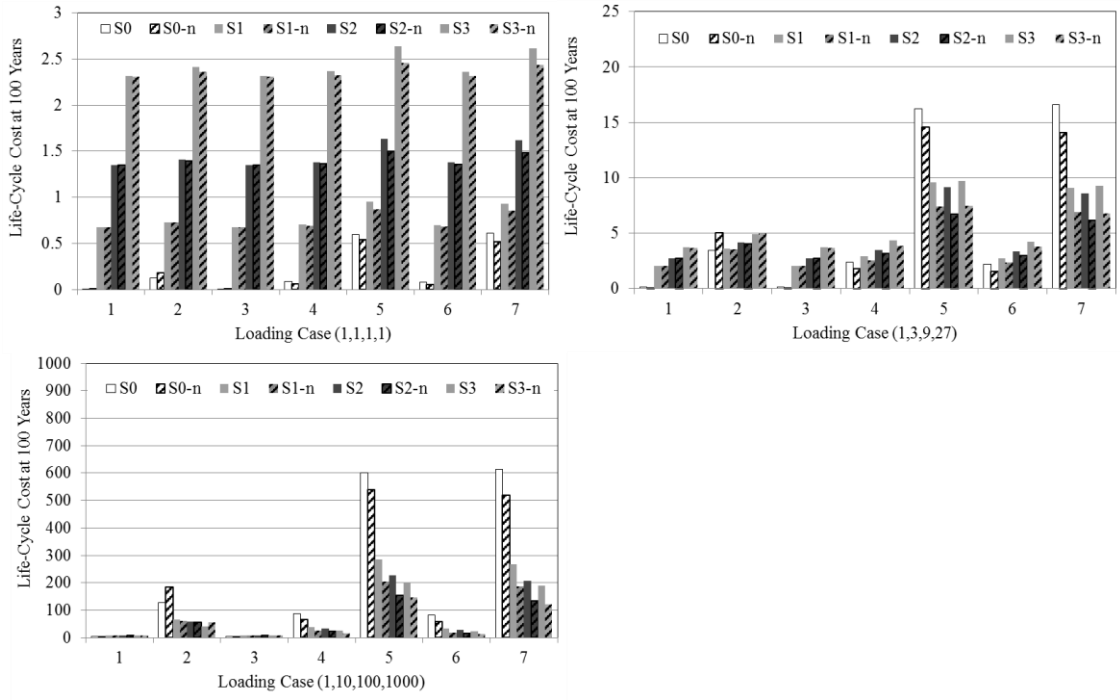

Figure 4.21: SBFM crack growth data calibration, life cycle costs after initial condition modification

This is closer than before, but the 10CS model still produces a lower estimate. The reason they are different now, with slightly lower cost indicated for the 10CS, is due to the nature of larger condition state models. Due to the fact that probabilities can only move one condition state at a time it simply takes longer for them to move from perfect to failure. This is shown by the slight offset in the lines in Figure 4.21 from years 5 to about 15 comparing the 5Cs and 10CS models. This problem is exacerbated when repair actions are introduced, as they often happen during this critical 6-30 year period. Figure 4.22 shows the probability of failure for maintenance strategy 3, repair and treatment every 20 years.

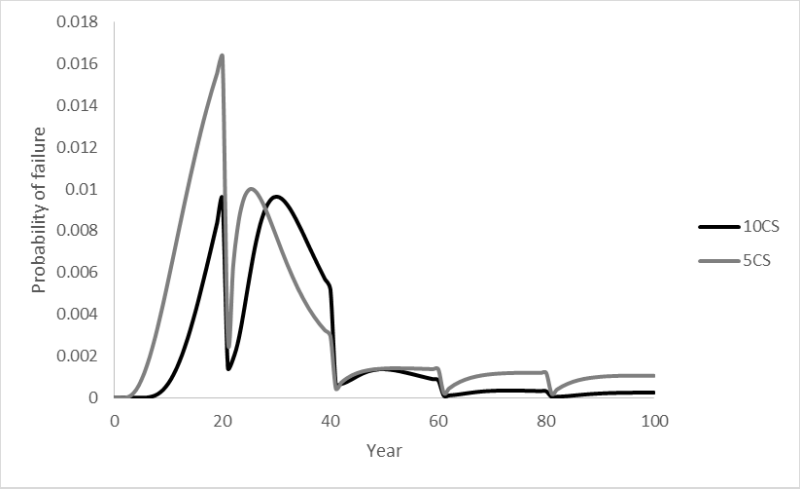

Figure 4.22: Probability of failure (end condition state), equivalent initial conditions as per [Walbridge et al], maintenance strategy S3

The repair at year 20 cuts the 5CS at near the peak of its probability of failure, whereas the 10CS is cut off about half way due to the lag. This creates a significant difference in the total cost, which is not a problem due to the modelling, simply a characteristic of larger Markov chains. This is shown by graphing the cumulative cost, shown in Figure 4.23.

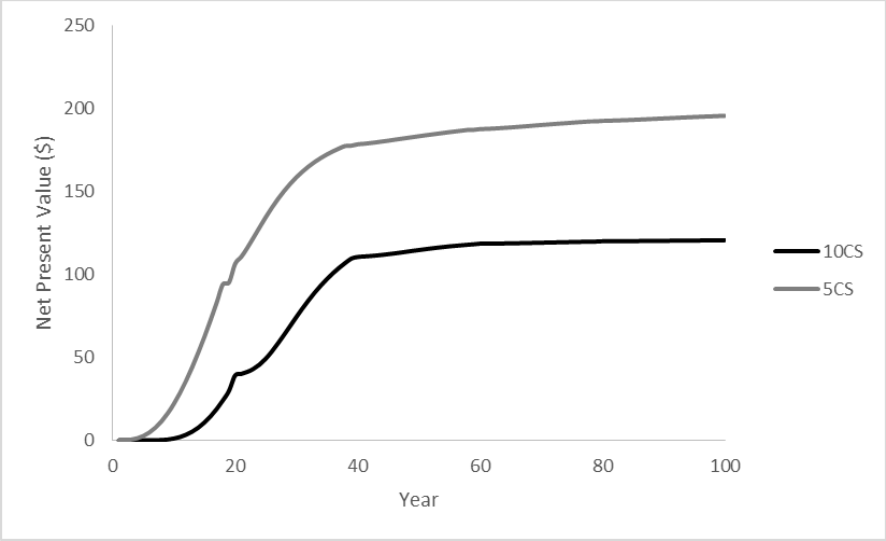

Figure 4.23: Cumulative net present value, maintenance strategy 3

The difference in cost occurs during years 6-36, after which the difference stays level. Therefore this is why the comparison between 10CS and 5CS life cycle costs are different.

4.4.3 Discussion

In general, each of the calibrated methods performed the best on the graph for which they were calibrated from, which was expected. The curves from the S-N calibration matched the closest, and the condition states calibrated to SBFM output matched the best to the SBFM results. The exception to this was the Markov chain calibrated to SBFM failure data; the Markov chain calibrated to SBFM crack growth data performed better in that case. The difference occurs when each method was graphed against the other calibration data, the SBFM crack growth data calibration performed adequately on the S-N curves: the 97.7% line was a very close fit, only the 50% line was off by a small amount. However, the S-N curve calibrated data performed very poorly when compared to SBFM condition state probabilities.

The new method of checking the calibration accuracy, life cycle cost analysis, was an independent method of comparing the calibration methods, and there was a clear trend from design S-N to SBFM failure to SBFM crack growth data in terms of increasing accuracy. The more complex the calibration process, the more accurate the results were. Not only did the S-N calibration and calibration to SBFM failure data have different absolute values, but they also often predicted other optimal maintenance strategies, which would lead to non-optimal use of funds. The calibration to SBFM crack growth data

resulted in a close fit, and with some tweaking resulted in a near exact fit. This also speaks to the flexibility of non-uniform Markov chains and their ease of modification. The 5CS model matches very well with the graphs from [Walbridge et al, 2012] once the initial conditions are modified to match that of the paper. The 10CS model does not match as well when using the equivalent initial conditions from [Walbridge et al, 2012], which was due to very small probabilities of movement in the Markov chain. Once this was fixed the 10CS model match was closer, but still not exact. This was due to the nature of larger Markov chains, as it simply takes longer for the probabilities to move down condition states simply due to the superior number of CSs. The relative values were still the same, and all models predicted the same optimal maintenance strategy.

Despite the 5CS and 10CS Markov models returning slightly different absolute values, the relative change was the same for all maintenance strategies, and the optimal ones were the same predicted by both. Therefore both models are equivalent for predicting life cycle costs, however it is important to not mix or compare them directly, as the differences in the Markov chains result in slightly different absolute values.

4.5 Local stress approach

The calibration process described in the previous section only applies for Category C welds, which while useful does not apply to all welds. Therefore a method of transforming between different detail categories is required. This section will discuss the local stress approach, which relates different detail categories by a stress concentration factor (SCF).

It is assumed that from a fatigue standpoint the only difference between various detail categories is the SCF, which relates the global or nominal stress to the higher local stress due to the change in geometry. This factor is calculated by comparing the stress range on the S-N curve at a set number of cycles, with the data coming from Table 4.1. Equation (4.1) was then used to determine the stress at 1E6 cycles. The SCF for Detail Category A was used as the reference, and so was set as 1, with the remaining SCFs a factor of that number. Table 4.16 shows the stress concentrations used.

Table 4.16: Stress concentration factors

Detail Category	Fatigue life constant γ	CAFL point	Stress Range at 1E6 cycles (Mpa)	SCF
A	8.19E+12	165	202	1.00
B	3.93E+12	110	158	1.28
C	1.44E+12	69	113	1.79
D	7.21E+11	48	90	2.25
E	3.61E+11	31	71	2.83

Next, the transition probabilities calculated in section 4.3 were modified to shift from Category C to A, so that the SCFs in Table 4.16 could be used. To do this, a reference number of cycles was chosen, 2 million used, and the stress range associated for detail category A was calculated, 159.9 MPa. Next, the stress range associated with the Markov chain at 2 million cycles was calculated, with the ratio of the two calculated. This ratio was then used in Equation (4.8), taken from [Lassen 1991]:

$$q_{i,1} = \frac{1}{\left(\Delta S_0 / \Delta S_1\right)^m \cdot \left(1 + \left(1 - q_{i,0}\right) / q_{i,0}\right)} \tag{4.8}$$

Where $q_{i,0}$ is the transition probability for a reference stress range, ΔS_0, and m is the S-N curve slope. For this case, the nominal stress (ΔS_0) was replaced with the ratio ($SCF \cdot \Delta S_0$). From there, the transition probabilities for each detail category were calculated also using Equation (4.8). The resultant transition probabilities are shown in Table 4.17.

Table 4.17: Transition probabilities after applying SCF

Det. Cat.	A	B	C	D	E
SCF	1.000	1.277	1.785	2.248	2.831
DS0	165	110	69	48	31
m	3	3	3	3	3
q1	0.0209	0.0129	0.0087	0.0058	0.0031
q2	0.0469	0.0290	0.0195	0.0131	0.0071
q3	0.1078	0.0665	0.0448	0.0301	0.0162
q4	0.1217	0.0751	0.0506	0.0340	0.0183

Note that the transition probabilities for Detail Category C are not the same as the ones used for the initial calibration. This is due to the initial laboratory results on which the SBFM code was calibrated to, which transverse stiffeners that was supposed to represent a Det. Cat. 'C' or FAT-80 detail. Analysis of the test data suggested that the tested detail had a slightly higher SCF than the one associated with Det. Cat. 'C' in Table 4.17. Specifically, the SCF for this detail, based on a comparison with the Det. Cat. 'A' design curve was calculated to be 2.223, placing it somewhere in between Det. Cats. 'C' and 'D'. In [Ghahremani, Walbridge, & Topper 2015], SCFs for the tested stiffener detail are obtained using finite element (FE) analysis, and SCF definitions based on the structural and notch stress fatigue design methods frequently discussed in the literature on weld fatigue. According to this analysis, the SCF for this detail was found to be 1.35 for use with the structural stress method and 2.37 for use with the notch stress method. The SCF based on the comparison of the design S-N curves presented herein falls in the middle of this range.

A similar process can be used on the treated probabilities as well, with results shown in Table 4.18.

Table 4.18: Treated transition probabilities after applying SCF

Det. Cat.	**A**	**B**	**C**	**D**	**E**
ΔS_0 (MPa)	165	110	69	48	31
m	5.0	5.0	5.0	5.0	5.0
q_1	0.0001	0.0001	0.0000	0.0000	0.0000
q_2	0.0100	0.0045	0.0023	0.0012	0.0004

The remaining transition probabilities, q_3 and q_4, are the same as the untreated probabilities.

These transition probabilities were then used to produce S-N curves, shown in Figure 4.24, overlaid on original S-N curves:

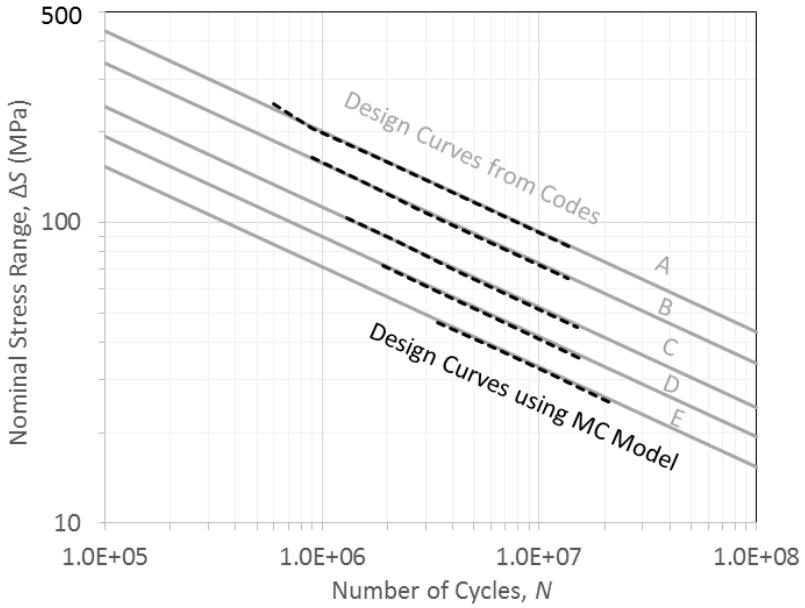

Figure 4.24: S-N curves, applying SCF

As shown, the curves fit very closely with the original results, and therefore the method of using stress concentration factors to relate the transition probabilities of detail category Markov chains to one other is valid. The calibrated Markov chains calculated in Section 4.2 therefore can be applied to a wide range of welds.

4.6 Consideration of corrosion effects

Typical BMSs look at the deterioration of each element, such as fatigue, in isolation. However, this is often not the case, as the bridge is one complete structure, and often the deterioration of elements affects how others behave. For example, the corrosion of girders has been shown to affect the fatigue life of the structure. As corrosion occurs, loss of thickness increases local stresses, which decreases fatigue life. Corrosion is also very uneven, and causes pits and ruts, which in turn cause stress concentrations, which also decreases fatigue life. When considering maintenance strategies, it is therefore important to consider how an action, or inaction, will affect the deterioration for other elements. Painting steel girders will decrease maintenance requirements due to corrosion, but the additional benefit of decreased fatigue maintenance requirements must also be considered.

4.6.1 Modelling interactions

The procedure for considering correlated Markov chains is discussed in [Cesare et al, 1992]. It defines an element *A*, for example fatigue, which is affected by the condition of an element *B*, or corrosion. At a simple level, *B* is defined as being either in a good or a bad state. For a 5 condition state Markov chain, good could be defined as condition states 1 through 3, with 4 and 5 defined as bad. The probability of *B* being good, therefore, is

$$P_{good} = B_1+B_2+B_3$$
$$P_{bad} = B_4+B_5 \quad (4.8)$$

Where B_i is the probability of a *B* element being in the i^{th} condition state. Two transition probability matrices for *A* are required, one for which *B* is in a good state, defined as A_{good}, and one for which *B* is in a bad state, or A_{bad}. The transition probability matrix to be used for *A* is therefore:

$$T_A = T_{A,good} \cdot P_{good} + T_{A,bad} \cdot P_{bad} \quad (4.9)$$

This procedure can be extended to having 5 levels of good and bad, one corresponding to each condition state of *B*.

4.6.2 Corrosion deterioration modelling

Atmospheric corrosion is a process by which the iron in steel oxidises to produce rust [Kucera & Mattson, 1987][Uhlig & Revie, 1985][Schweitzer, 1989]. This requires both oxygen and a source of moisture to act, and if left unchecked can deteriorate a steel section completely. The source of water can come from a variety of sources including, rain, dew, fog, snow, and does not require direct precipitation, but can also reach the steel via capillary action, pores and cracks. There are other substances which can increase the rate of corrosion, such as salts either from salting trucks for ice control or exposure to marine environments, or from pollution in the air, particularly sulfur dioxide from fossil fuels.

There have been many studies performed on rates of corrosion, ranging in steel types, environments, durations, treatments, and other factors. [Albrecht & Hall, 2003] have provided a summary of many of these studies. The paper divides the results into three environments: rural, industrial and marine in order of increasing corrosion rates, and several types of steel: carbon steel, copper steel, and different types of weathering steel, including A558 and A242 steel. Some of the figures are shown here in Figure 4.25:

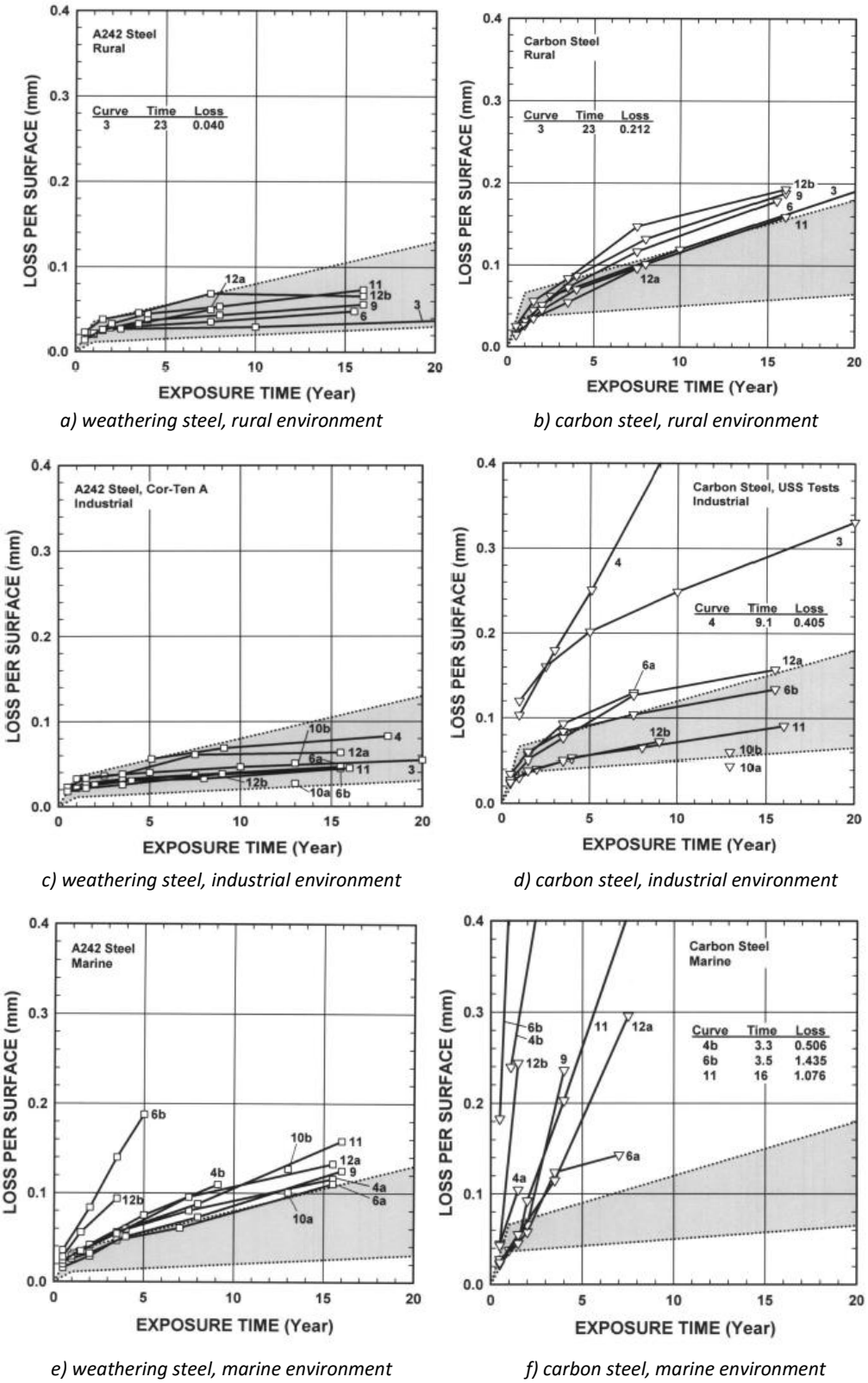

a) weathering steel, rural environment

b) carbon steel, rural environment

c) weathering steel, industrial environment

d) carbon steel, industrial environment

e) weathering steel, marine environment

f) carbon steel, marine environment

Figure 4.25: Corrosion rates, loss per surface over time. [Albrecht & Hall, 2003]

The figures are ordered from rural, industrial and marine from top to bottom, and weathering to carbon steel from left to right. Each of the data lines corresponds to the results from a study performed, the grey shaded area is the medium corrosivity band according to ISO standard 9224. The vertical axis is loss per surface in mm, and horizontal axis is time. There are two trends, the first as the atmosphere contains more pollutants and salts, the rate of corrosion increases. The second trend is as the steel contains corrosion retardant agents, such as copper, chromium, manganese, nickel, and other elements, the rate of corrosion decreases. Given the wide range it is difficult to determine one model to represent all studies for one steel within one environment, and so an average was chosen for calibration. For less severe environments or for steel with higher resistances the spread was significantly less, but at higher corrosion rates the average became less accurate of all studies.

A Markov chain was then calibrated to these averages for the three environments and two steels, using a similar process to the calibration to SBFM failure data, with the full process described in [Walbridge et al, 2013]. These chains can then be used to predict corrosion based on a certain type of steel in a specific environment. These corrosion Markov chains included the opportunity to model anti-corrosion paints, and so CS1 and CS2 model the deterioration of the paint, and the remaining CSs, three through five, modelled the deterioration of the steel due to corrosion. Therefore the calibrated Markov chains, shown in Table 4.19, only contain two transition probabilities for the remaining CSs.

Table 4.19: Corrosion transition probabilities

Steel type	**Environment**	**q3**	**q4**
Carbon	Marine	0.0270	0.1174
A242 Weathering	Marine	0.0124	0.0652
Carbon	Industrial	0.0045	0.0313
A242 Weathering	Industrial	0.0001	0.0143
Carbon	Rural	0.0000	0.0143
A242 Weathering	Rural	0.0001	0.0143

4.6.3 Modelling combined effects of fatigue and corrosion

Corrosion has been shown to have an adverse effect on fatigue life, the most striking example is the collapse of the Mianus River Bridge in Connecticut, in which severe corrosion buildup lead to fatigue

fracture of a support pin, resulting in the collapse of a section and the death of 3 people [NTSB, 1984]. The effects of corrosion on fatigue is discussed in [Fisher et al, 1998], starting with corrosion notching. Corrosion notching often occurs where dirt and debris build up to create an active corrosion cell, as this traps water and prolongs wetness. This can significantly reduce cross section in a localized area, which can have a fatigue resistance as low as Category E [Fisher et al, 1987][Fisher et al, 1990]. During the beginning stages of corrosion, pitting of the metal occurs, in which small corrosion pockets occur. This causes stress concentrations, which often initiate fatigue cracking. During the later stages of corrosion, as corrosion byproduct has a larger volume than the original steel, it can cause packout pressure, in which the expanding volume pushes plates apart, which can increase local stresses, in particular tension stresses, which cause fatigue cracks to grow even quicker [Fisher et al, 1998].

A study performed by [Palin-Luc et al, 2010] immersed samples for 600 hours in a salt fog, then cleaned to remove the oxide layer, revealing many corrosion pits. These were then fatigue tested in the high-cycle range, and it was discovered that there was a loss of 74% at 10^8 cycles, which is attributed to easier fatigue crack initiation phase due to the corrosion pits. More long-term tests have been performed, such as [Albrech, 1982], which compared specimens with transverse stiffeners for up to 4 years outside. The weathering process reduced the fatigue life by 62% for Category A, 44% for Category B, and 26% for Category C. [Albrecht and Cheng, 1983] compares specimens weathered over a four and eight year period, and found 42% and 54% loss in fatigue life, respectively. The weathering process involved placing the specimens outdoors in an area described as having above average atmospheric pollution. The specimens were placed on a 15° slope to avoid water pooling, and experienced about 525 wet-dry cycles over the first three years of weathering due to rainfall and condensation during humid dawn hours. The loss in fatigue life was also attributed to rust pitting, which aids in the formation of fatigue cracks. It was noted that despite the losses in fatigue life, the specimens were still above the allowable Category C line due to the high initial fatigue strength, attributed to excellent welds, and the reduction of standard deviation after weathering.

Other studies have investigated slightly different aspects of corrosion and fatigue relationships. [Albrecht and Cheng, 1983] also considered alternating weathering and fatigue testing, to better simulate the conditions of an operating bridge girder. The specimens were left to weather for three years, and the alternatively cycled one-eighth of the mean life and left to weather for six more months. This resulted in no significant difference in loss of life when compared to samples exposed to straight three years of weathering.

The previous studies have all examined the effects of weathering on fatigue life, which have shown that rust pitting increases the fatigue crack initiation phase. To investigate the effects of corrosion on the fatigue crack growth phase, studies have been performed in which the fatigue testing portion is performed with the sample immersed in a salt water environment as opposed to air. [Yadanzi and Albrecht, 1989] report that stress cycling a specimen in fresh or salt water increased fatigue crack propagation by a factor of about two compared to cycling in air. [Albrecht and Sidani, 1989] compared weathering steel exposed eight years to the outdoors in a medium corrosively environment, and reported 23% loss in stress range when cycled in salt water, compared to 8% loss when cycled in air. This still has an impact on the crack initiation life, [Novak, 1983] reports a 62% reduction in the initiation phase compared to stress cycling in salt water as opposed to air.

The weathering process in these studies involved simple exposure to atmospheric conditions. It was noted in several of the papers that should the specimens be exposed to salt water, such as runoff from de-icing methods frequently found near bridges, the corrosion rates would be more severe, and therefore the fatigue life even more adversely affected.

The correlated Markov chain procedure described in Section 4.6.1 can now be applied to the correlation between corrosion and fatigue. Three TPM for fatigue deterioration were modelled, one for normal, one associated with CS4 of corrosion deterioration (1.5mm of section loss), and one for CS5 of corrosion deterioration (2.5mm of section loss), recalling that CS1 and CS2 were reserved for protective treatment modelling, such as painting. The probabilities of residing in CS3 through CS5 over a hundred year life span were calculated using the Markov chains. For the calculation of fatigue deterioration, the equivalent TMP used was the sum of the probability of residing in CS3 of corrosion multiplied by the appropriate TPM, plus the probability of residing in CS4 of corrosion multiplied by the appropriate TPM, plus the fifth.

There are several ways to calculate the new TPM for fatigue relating to some level of corrosion deterioration. One such method is to use the decrease in fatigue life due to the increase in stress due to loss in cross section from corrosion according to the graphs from Figure 4.25. Using cross section analysis of a typical I girder, assuming plates 25.4 mm thick, and using the CS definitions from the corrosion Markov chains of 1.5mm for CS3 and 2.5mm for CS4, the increase in stress is 8.5% and 15.0% respectively.

The resultant interaction can also be graphed in a couple of ways. One option is to look at the total cost of both corrosion and fatigue. As both corrosion and fatigue act on the same girders, the replacement cost for both will be the same. Inspection, treatment, and repair of corrosion are not modelled, simply a replacement cost, in which the probability of failure is multiplied by the associated cost of failure, and the girder is assumed to be repaired to its original state. The total costs, assuming the worst corrosion case (carbon steel in a marine environment), are shown in Figure 4.26.

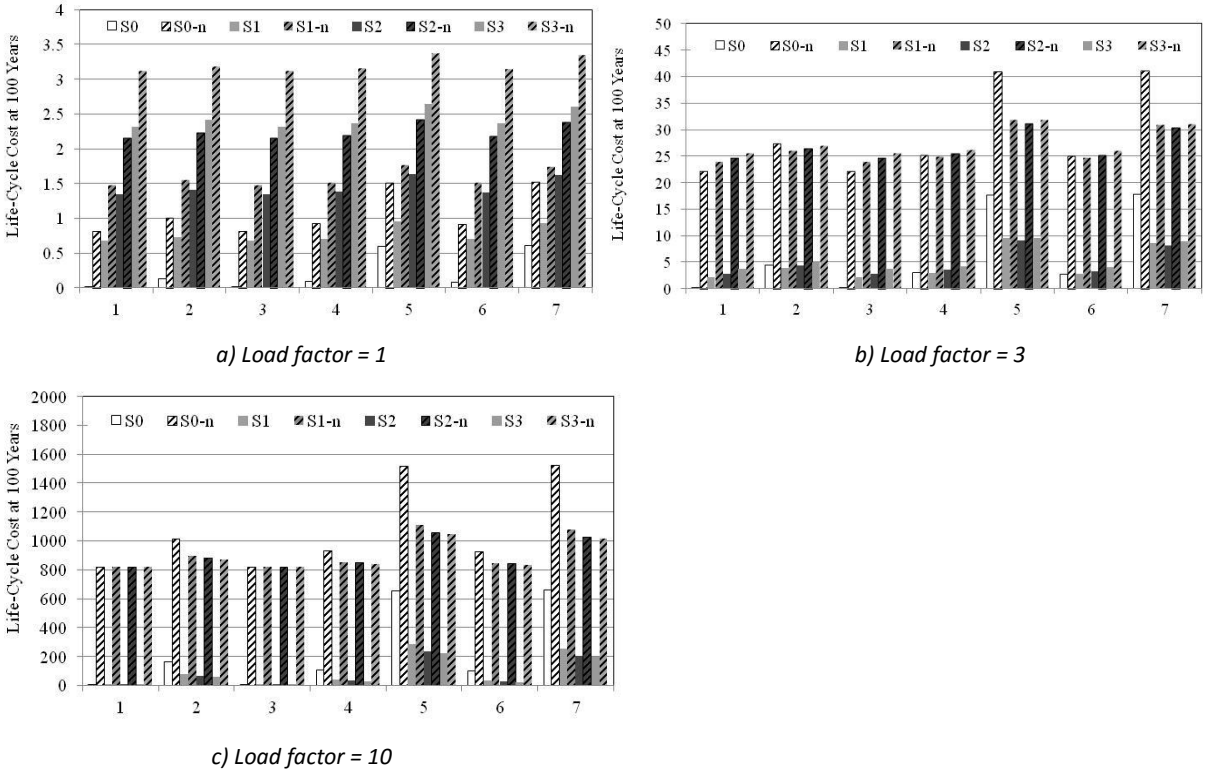

Figure 4.26: Life cycle cost, corrosion + fatigue cost

In these figures, the original graphs are the results from the uncorrelated Markov chain, with the new, or dashed bars, the results from considering corrosion.

All the graphs are simply shifted up by the base corrosion cost, which does not change with the loading case or the fatigue maintenance strategy. This value is $0.81, $21.9 and $812.5 for the cost factors of 1, 3, and 10 respectively. We can also just look at the cost of fatigue, which will change slightly due the consideration of corrosion, shown in Figure 4.27.

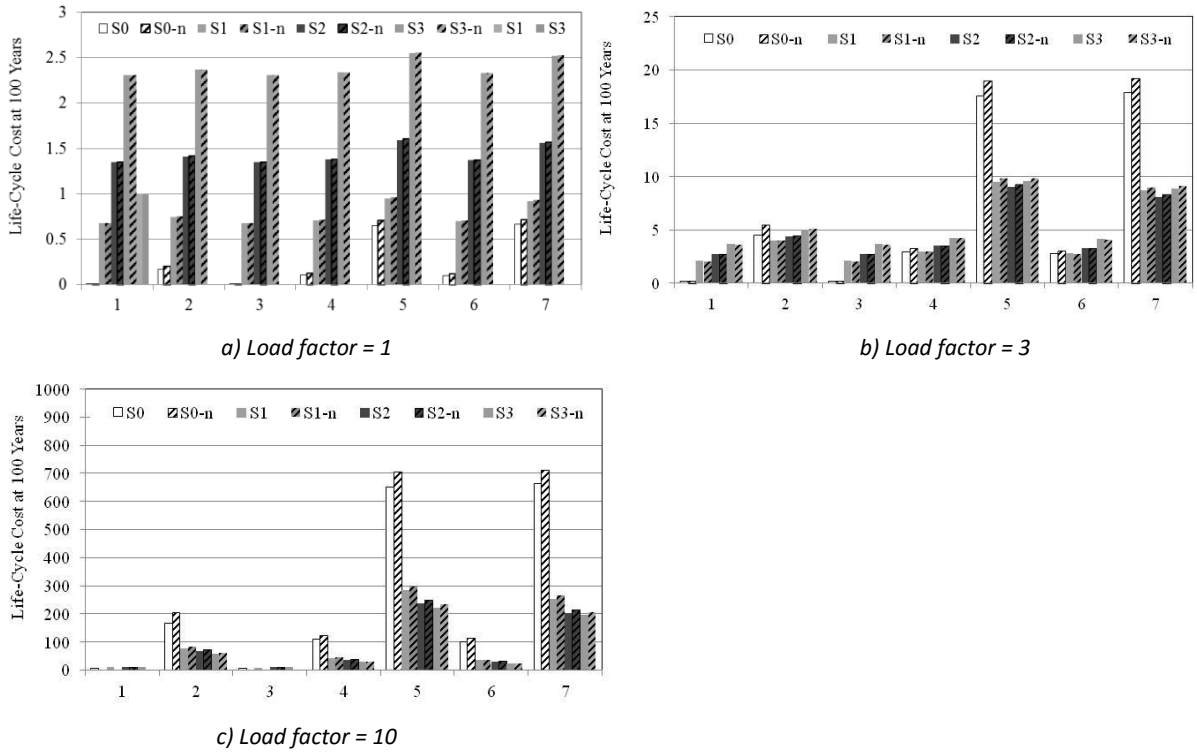

Figure 4.27: life cycle cost, fatigue after consideration of correlation with corrosion

Again, the original graphs are the 5CS Markov chain just for fatigue, with the new diagonal line bars the result from considering the correlation of fatigue as stated above.

As shown, considering corrosion has an impact on the fatigue life, although small. For the most part the increase is relative, where all maintenance strategy costs increase by the same amount, except for the load factor of 3, for loading case 2, 4 and 6, where strategy S0 is now more expensive than S1 or more. This then changes the optimal maintenance strategy, and so is important to consider.

However, the correlation model used above is not complete, it only assumes in increase in stress due to section loss, when in reality the relationship is more complex, There have been many studies performed to investigate this, with many different results. A summary of several of these studies is reported in Table 4.20.

Table 4.20: Literature summary of correlation between corrosion and fatigue

Study	**Loss in fatigue life**	**Comments**
Palin-Luc et al, 2010	74%	
Albrecht, 1982	62%, 44% 26%	Category A, B, C, respectively
Novak, 1983	62%	loss in initiation phase
Albrecht & Sidani, 1989	23%, 8%	loss in stress range, as opposed to fatigue life

The average of the first three studies is a 54% decrease in fatigue life, the fourth study is not included as it presents the results as a loss in stress range as opposed to fatigue life. There is no input in the current Markov models for decrease in fatigue life, therefore an equivalent increase in stress range is calculated. For example, for loading case one at a SR of 84MPa and DSL at 1,000,000 cycles, a 54% loss results in 540,000 cycles to failure instead. Using the same slope as the plots on the S-N graph, we can determine the equivalent stress range, which is 105.6MPa which would result in a 54% loss of fatigue life. This process is shown in Figure 4.28.

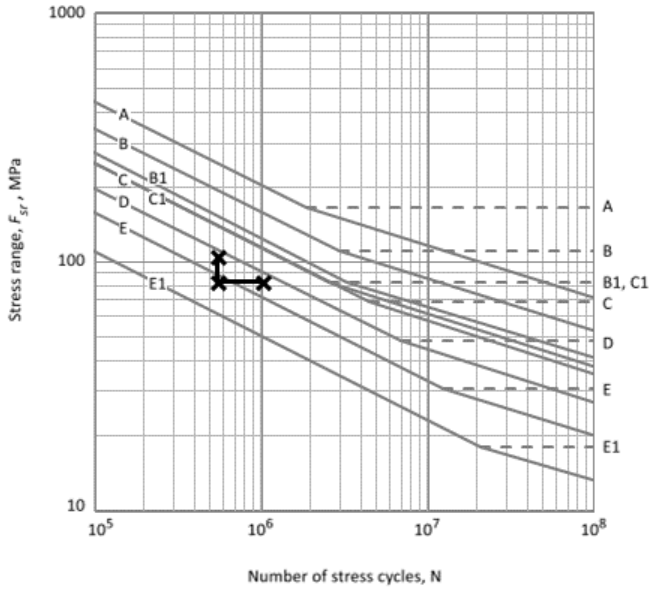

Figure 4.28: Calculation of loss of fatigue life, loading case 1

The bottom right point is the input point for loading case one, at 84MPa and 10^6 cycles. The one directly to the left is the 54% loss in number of cycles, and the one above is plotted on the same slope as the rest

of the S-N curves, which is the equivalent stress range that also represents a 54% loss, at 105.6MPa. This result is assumed to occur at severe corrosion, represented by CS5, and therefore for CS4 the associated stress range is (1.5/2.5) · (105.6-84) + 84 = 97.0 MPa. This process is repeated for the remaining loading cases, with results shown in Table 4.21.

Table 4.21: Stress range calculations

Loading Case	Stress Range	Design Service Life	SR at corrosion CS3	SR at corrosion CS4
1	84	1.00E+06	97.0	105.6
2	120	1.00E+06	135.2	145.3
3	43	1.00E+07	48.9	52.8
4	60	1.00E+07	67.8	73.0
5	84	1.00E+07	95.3	102.8
6	30	1.00E+08	33.9	36.5
7	43	1.00E+08	48.9	52.9

The stress range increase for the loading cases ranges between 17% and 20%, which is within the range reported from the last paper from Table 4.20, [Albrecht & Sidani, 1989].

Plotting the correlated fatigue with corrosion we now get plots shown in Figure 4.29.

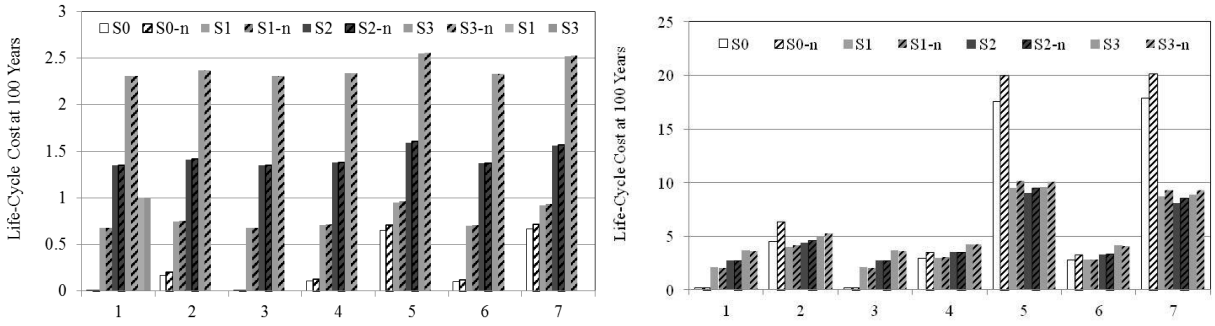

a) Load factor = 1

b) Load factor = 3

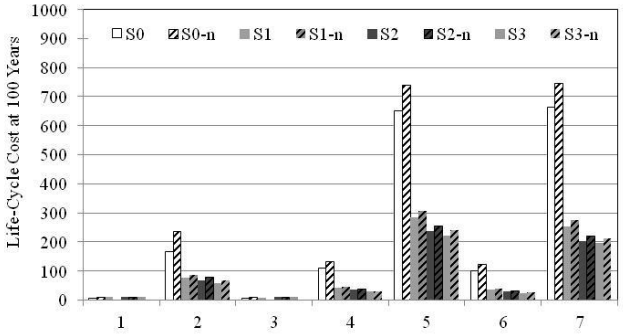

c) Load factor = 10

Figure 4.29: Life cycle cost, fatigue plus correlated corrosion, higher corrosion correlation

Slightly more net change than the previous method, but similar conclusions, that most of the changes are relative, where all costs rise by the same amount, except for some loading cases, in particular loading case 2, 4, and 6 from the cost factor of 3 graph. Again we see the importance of considering corrosion, as it does change the optimal maintenance strategy.

All these figures have been assuming that corrosion monitored, that as failure occurs it is replaced. However, if we assume that corrosion is not monitored, then we get plots as shown in Figure 4.30:

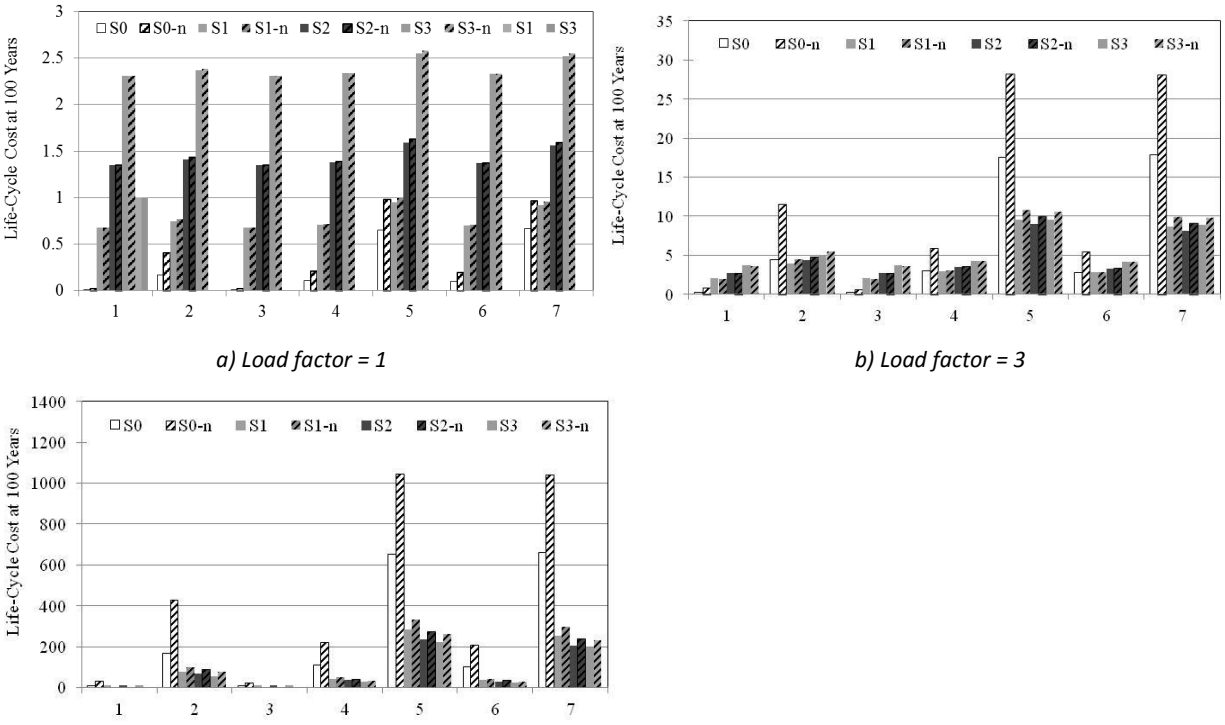

a) Load factor = 1

b) Load factor = 3

c) Load factor = 10

Figure 4.30: Life cycle cost, fatigue plus correlated corrosion, higher corrosion correlation, no corrosion maintenance

We can now see a drastic change, with the optimal strategy now changing in the cost factor of 1 graph as well. Note that the vertical axes have been changed to accommodate the increase in some of the costs. Therefore not only is it important to monitor corrosion for corrosion purposes, but also for fatigue purposes, as it can drastically increase the fatigue deterioration and cost.

In conclusion, it has been shown that it is possible to model correlated elements, in this case corrosion and fatigue, as long as there is research available on the interactions. It is important to consider the correlation, as in some cases the optimal strategy has changed from the original graphs. The models also allow us to consider other cases, such as neglecting to maintain corrosion deterioration, and the impact on life cycle costs.

5.0 Example application

Optimizing maintenance strategies for general situations is difficult due to the large number of variables. Costs by themselves are complicated, with each bridge having different access, inspection, repair, and replacement cost for each element. In trying to determine an optimal maintenance strategy for all bridges, perhaps the true lesson in what can be achieved with preventative maintenance is missed. Therefore for this thesis a theoretical bridge was designed and effects of preventative maintenance studied. In order to be applicable, the bridge was similar to ones seen in Ontario, with inspiration taken from the steel girder bridges over the 401 between London and Windsor, specifically the Furnival Rd Bridge.

Figure 5.1:Furnival road underpass [Google, 2015]

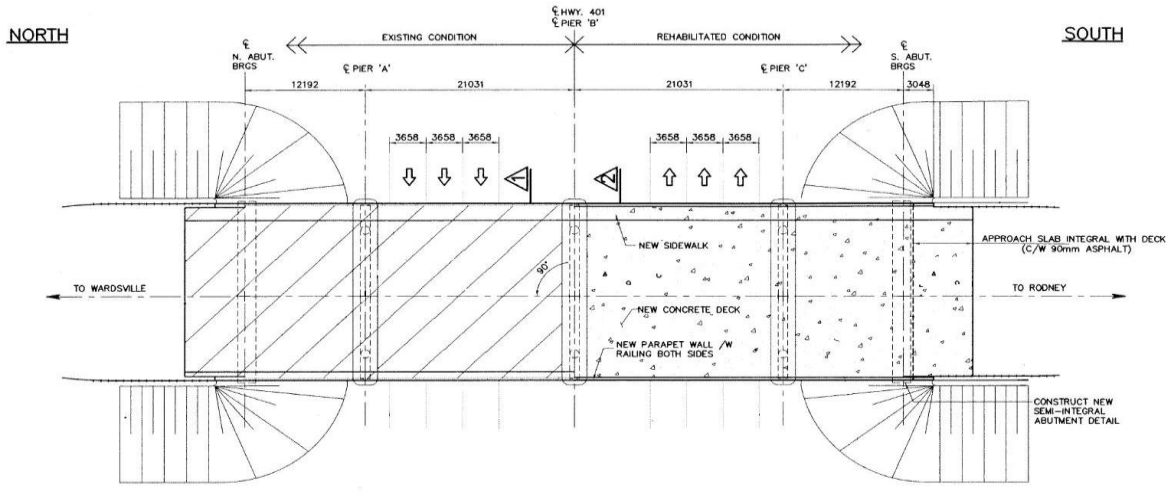

Figure 5.2: Furnival road underpass plan [MTO, 2012]

5.1 Bridge design

The bridge has 4 spans, the 2 outside spans with a length of 12.192 m, and the main spans 21.031 m. The width is 16.8 m, divided by 6 girders. The bridge was designed using the Canadian Highway Bridge Design Code (CSA S6, CHBDC) [CSA, 2006]. Figure 5-3 shows the dimensions of the interior girders.

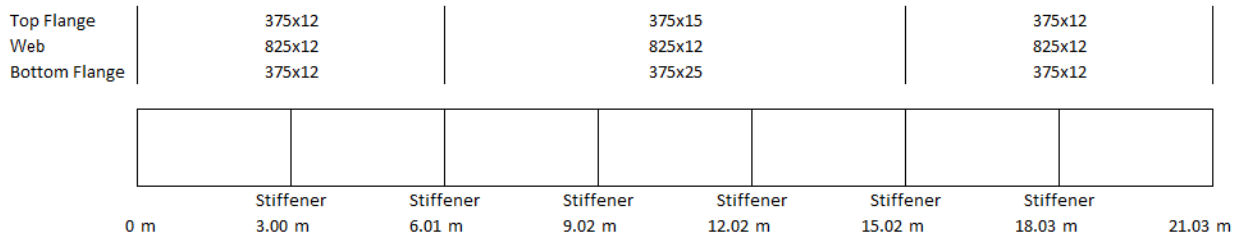

Figure 5.3: Girder details

The concrete deck was 200 mm thick, reinforced with #16 reinforcement bars spaced at 200 mm. The loads were calculated using the process outlined in the CHBDC, with shored construction assumed. The width of 16.8 m requires 4 design lanes. The full results from loading are shown in Figure 5.4, where DL = dead load, SDL = superimposed dead load, AxleLL = axle live load, and LaneLL = lane live load.

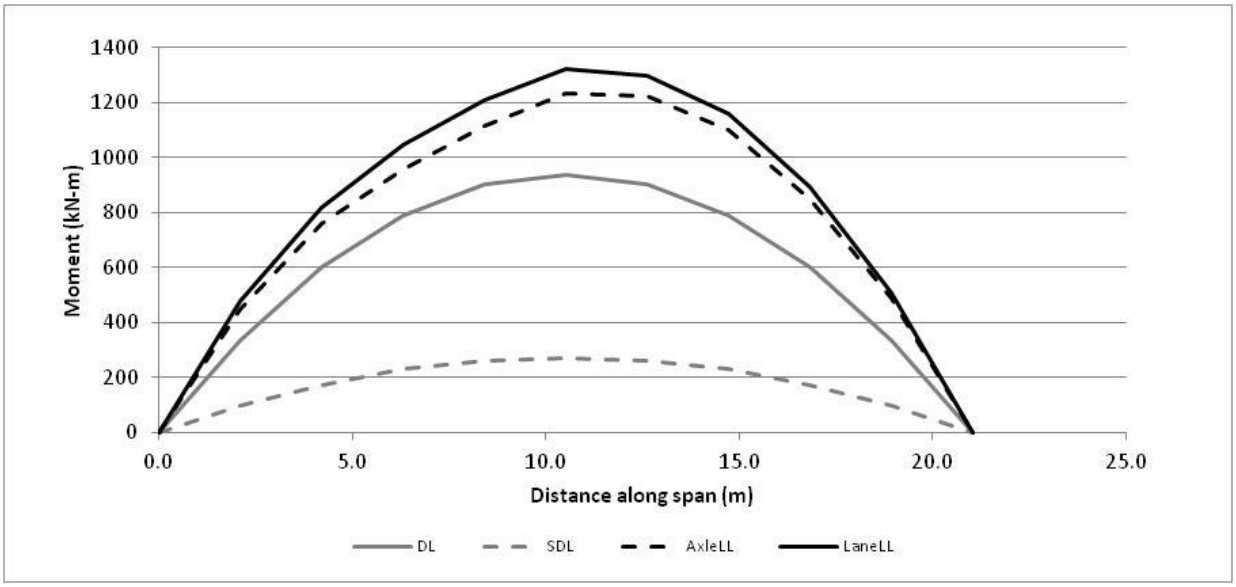

Figure 5.4: Bridge loads

The dead loads included the self-weight of all materials, including steel beams, concrete deck, reinforcement, 75 mm thick asphalt wearing surface, 100 mm thick sidewalk, and concrete barriers. The

live load includes the maximum of lane or truck load as per CSA S6 Section 3 [CSA, 2006], and as shown in Figure 5.4, the lane load is larger. These loads were then combined as per CSA S6 Table 3.1 [CSA, 2006] to achieve the maximum load. The resistances of each section with regards to moment, shear, and bearing were calculated, and by comparing the ratio of applied load to resistance, a resistance fraction was obtained. A fraction of one means that the stresses caused by the applied load meet the maximum resistance by the girder precisely, therefore a factor less than one corresponds to a safe design. Figure 5.5 graphs the resistance fraction over ten equally spaces stations along the span:

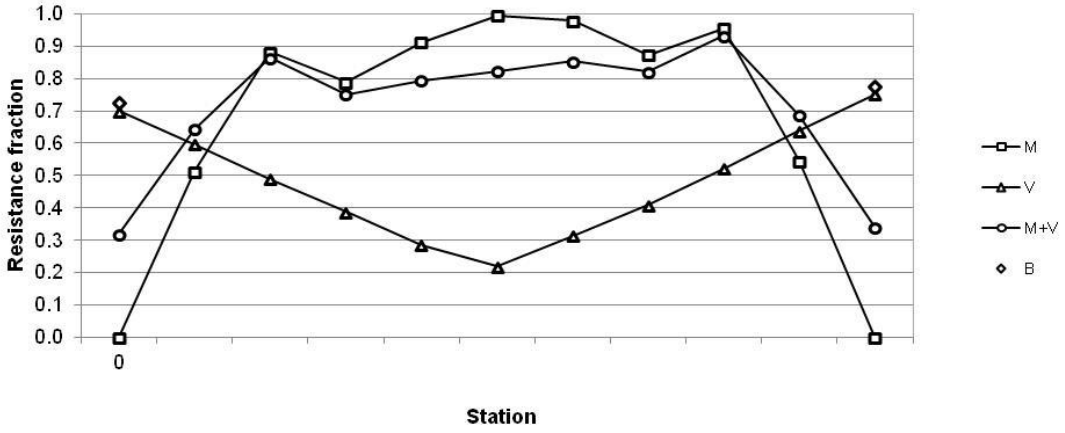

Figure 5.5: Bridge resistance fraction

As shown, all resistance fractions are below 1, and therefore the design is within code.

The sections were also checked for fatigue using CSA S6 Section 10.17 [CSA, 2006]. The critical fatigue section was the connection between the stiffeners welded to the bottom flange of the girders, which is a Detail Category C connection. A Class A highway with an ADTT of 4000 as per Table CSA S6 10.6 [CSA, 2006] was assumed with a 100 year life span. This results in a total Design Service Life of $4000 \cdot 365 \cdot 100 = 1.46 \cdot 10^8$ stress cycles. The load case for fatigue is a single truck, which produces a maximum moment of 660 kN·m. This causes a stress at the critical location in the girder of f_{sr} = 27.37 MPa which was less than the calculated F_{sr} of 41.5 MPa, and so the bridge passed the fatigue check. The stresses due to the live load passage of a single truck in the stiffener locations are summarized in Table 5.1.

Table 5.1: Stresses at fatigue critical locations

Stiffener location (m)	**Moment (kN-m)**	**Stress (MPa)**
3.00	314	25.5
6.01	532	43.2
9.02	643	52.2
12.02	647	52.5
15.02	545	44.3
18.03	336	27.3

For the analysis the stiffeners were divided into three groups of approximately equal stress ranges, the two interior (midspan) stiffeners, the two intermediate (quarter point) stiffeners, and the two exterior (end) stiffeners. This was done to simplify the analysis.

The analysis for this thesis was only to design the steel girders such that a fatigue analysis could be performed. As such, the design of the piers, foundations, bearings, concrete deck, etc, were not considered, as they did not affect the behaviour of the welds.

5.2 Action costs

In order to use the Markov chain model developed in this thesis for optimizing maintenance strategies, detailed costs for each of the actions must be calculated. The first of these is the total cost of the bridge.

Figure 5.6 shows the relationship between bridge length and cost per square meter. As this paper was written in Switzerland, the values on the vertical axis are Swiss Francs, converted to Canadian dollar the upper limit on the vertical axis is around $4000.

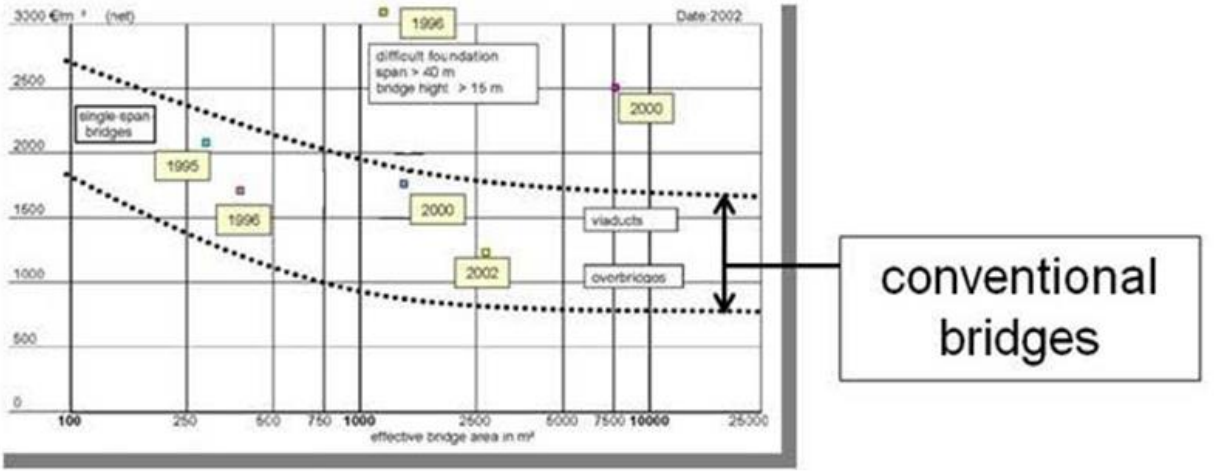

Figure 5.6: Bridge cost vs bridge area [Veselcic et al, 2003]

The dimensions of the main bridge span presented here are 16.8 m x 21.0 m, or an area of 336 m^2, which according to Figure 5.6 results in a cost per m^2 between \$1700 and \$3000. However, this figure is from 2003 and outdated, and discussions with local engineers have revealed the cost of a simple bridge with no complications to be around \$4500/m^2. Therefore the total cost of constructing one span is assumed to be \$1,590,000.

The next cost required is the replacement cost due to fatigue, which is the cost of replacing an entire girder. In [Walbridge et al, 2012], a bridge totalling 1,547,500 CHF was assigned a girder replacement cost of 550,000, or 35.5% of the total cost. Using the same ratio, the cost of replacement for the bridge in this thesis is \$564,450 per girder.

For treatment cost, [Walbridge, 2005] relates the cost of needle peening treatment to the cost of steel. It was assumed to take 0.16 minutes to treat one mm of weld in the field, and the ratio between material and labour cost in developed countries is 2.0 kg/min. [Okasha et al, 2011] specify a cost for fabricated carbon steel girder to be between \$3.30 and \$3.42 per kg, which includes fabrication, initial painting, shop inspection and transportation, with a value of \$3.35 per kg chosen for this thesis. Each stiffener has 738 mm of welding where the stiffener is attached to the bottom flange. In addition to this, part of the attachment to the web is also treated. The interior stiffeners were welded to a point where the stress was less than the exterior stiffeners, and for simplicity the other stiffeners were treated the same amount, for a total of 2338 mm per stiffener. The total cost per stiffener for treatment is therefore:

$$\frac{\$3.35}{kg} \cdot \frac{2\ kg}{min} \cdot \frac{0.16\ min}{mm} \cdot 2338\ mm = \$2{,}506$$

Therefore the cost of treating an entire girder with six stiffeners is $15,036.

Repair is assumed to consist of gouging out the weld containing the fatigue crack and rewelding it resulting in a new weld with properties similar to an as-received weld, which can be modelled with a similar deterioration matrix as the applied stresses are still the same. If treatment has already been performed, then treatment is assumed to be also performed on the repaired weld with properties and cost assigned accordingly. The cost of performing repair is similar to that of treatment, but instead of one pass over the weld required for treatment, roughly three or four passes for gouging are required, followed by around three or four welding passes, for a total of around seven. Therefore the repair cost per millimetre of weld is roughly seven times the treatment cost, or $7.50/mm. Using the same weld length, the total cost of repair is $105,252 for the entire girder.

Inspection costs vary significantly based on bridge location and ease of access. This value will be relative to the treatment cost, as both require personal to access the bridge, but less than treatment, as no equipment or significant time is required. A ratio of one fifth of the total girder treatment cost was chosen for this thesis, for an inspection cost of $3007.

A summary of action costs is provided in Table 5.2:

Table 5.2: Summary of maintenance actions

Action	**Cost**	**Rational**
Replace	$ 564,450	Ratio of girder replacement to bridge cost from [Walbridge, Fernando, & Adey, 2012]
Repair	$ 105,252	Seven times as expensive as treatment, as gouging and rewilding are similar in principle to treatment but require more passes
Treatment	$ 15,036	Cost per mm from [Walbridge, 2005] and [Okasha et al, 2011]
Inspection	$ 3,007	One fifth of treatment

To analyze the full girder, the girder was divided into elements equally spaced with each element containing one stiffener. The exterior stiffeners were each 21.4% of the length, and the remaining stiffeners were each 14.3%. The costs were then divided by the relative length of each of the elements,

and the life cycle costs of each element were summed together to calculate the total life cycle cost for the girder. As there are six girders in the bridge, the cost was multiplied by six to obtain the total bridge cost.

5.3 Cost analysis

Using the costs provided, a life cycle cost of 100 years of this bridge with respect to fatigue was calculated using the Markov chains calibrated in Chapter 4. Four maintenance strategies are used as specified in Section 4.3.5, for reference they are listed again here:

S0: base case, no inspection (MPI), repair (gouging and rewelding), or needle peening
S1: needle peening after 20 years of service loading
S2: inspection, repair (if needed), and needle peening after 20 years of service loading
S3: inspection, repair, and needle peening as needed after every 20 years of service loading

The results of the analysis are shown in Figure 5.7.

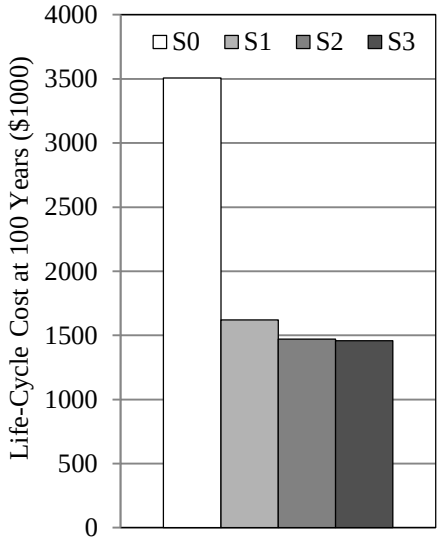

Figure 5.7: Life cycle cost of bridge:

As shown, for the sample bridge calculated for this thesis, there are large cost savings to be obtained by performing maintenance on the girders with respect to fatigue, up to $2,050,000 over the 100 year lifetime of the bridge. The difference in each of the treatment strategies which include treatment is small, but treatment followed by repair every 20 years is optimal.

The consideration of correlation of corrosion and fatigue as described in Section 4.6 can also be applied to this bridge. In Section 4.6.3 the condition states for corrosion were defined as 1.5 mm and 2.5 mm loss for CS3 and 4 respectively, which correlated to an 8% and 15% increase in the stress range. Using the girder described, the losses correspond to a 12% and 19% increase in the stress range for CS3 and CS4.

However, that method only considers the effects of stress increase due to loss of section. As explained in Section 4.6.3, an equivalent stress range equal to the average decrease in stress lives based on the studies in Table 4.20 was calculated, equal to 65 MPa for CS5. The stress at CS4 is therefore 59.7 MPa.

For the current analysis, three cases were considered, the first considering only fatigue. The second, Corrosion 1, considers correlation with corrosion deterioration, but only considering the increase in stress range due to reduced cross section. The third, Corrosion 2, also considers correlation with corrosion deterioration, but uses average loss in cycles to failure presented by the studies outlined in Table 4.20.

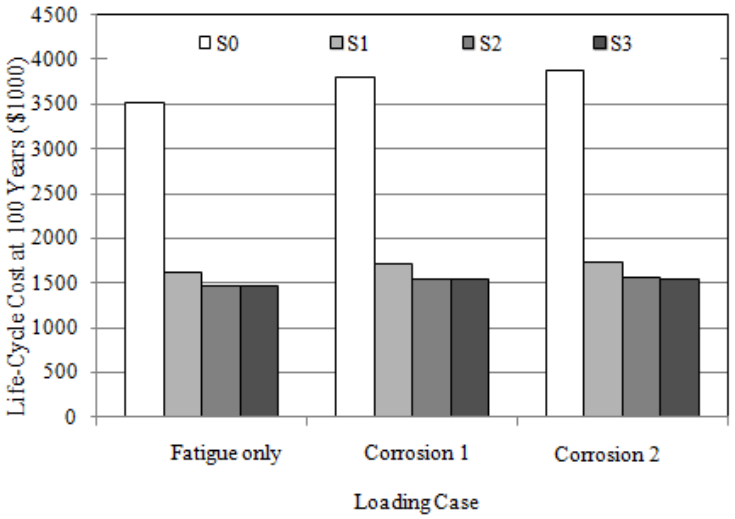

Figure 5.8: Life cycle cost of bridge including consideration of corrosion

The analysis results in Figure 5.8 show that the consideration of corrosion increases the total life cycle cost consideration of fatigue by a maximum of $365,000 for a 100 year service period, but does not change the relative values by a significant amount, or the optimal strategy.

Further studies were performed by changing some of the properties of the bridge. The first change performed was reducing the class of the road from A to B, C, and D, which according to Table 10.6 in CSA S6 [CSA, 2006] correspond to an ADTT of 4000, 1000, 250, and 50 respectively. As the bridge was

designed for Class A, the worst case scenario, the bridge will still be within code for lower traffic volumes.

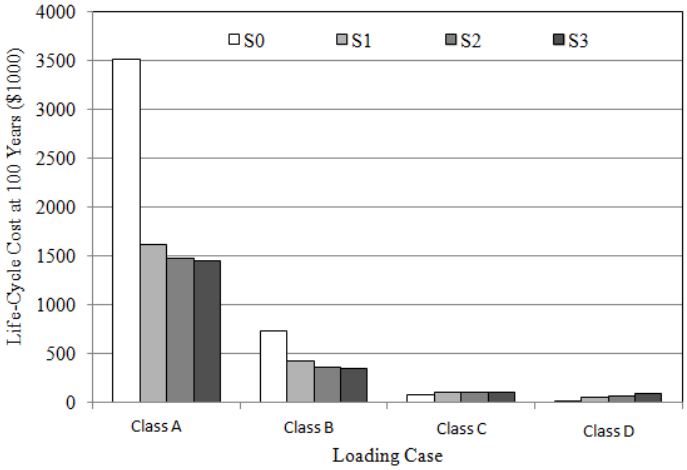

Figure 5.9: Life cycle cost compared to traffic volume

As shown previously, for Class A roads the optimal maintenance strategy is S3, with the option of doing nothing over twice as expensive. This is due the large number of trucks which cause significant fatigue damage. For Class B roads the cost related to fatigue has decreased to about 25% of the previous amounts, and the gap between S3 and S0 has diminished, however it is still optimal to perform strategy S3. For Class C roads we see a shift, it is now optimal to do nothing, $85,400 compared to $105,800 for S3. For Class D this trend continues, with the cost of doing nothing at $2,000 compared to $61,800.

The effects of corrosion on the relative optimal fatigue maintenance strategy as shown in Figure 5.8 are small, this is because fatigue completely dominates the costs at high traffic volumes. If we compare the effects of corrosion correlation at lower traffic volumes we get costs shown in Figure 5.10.

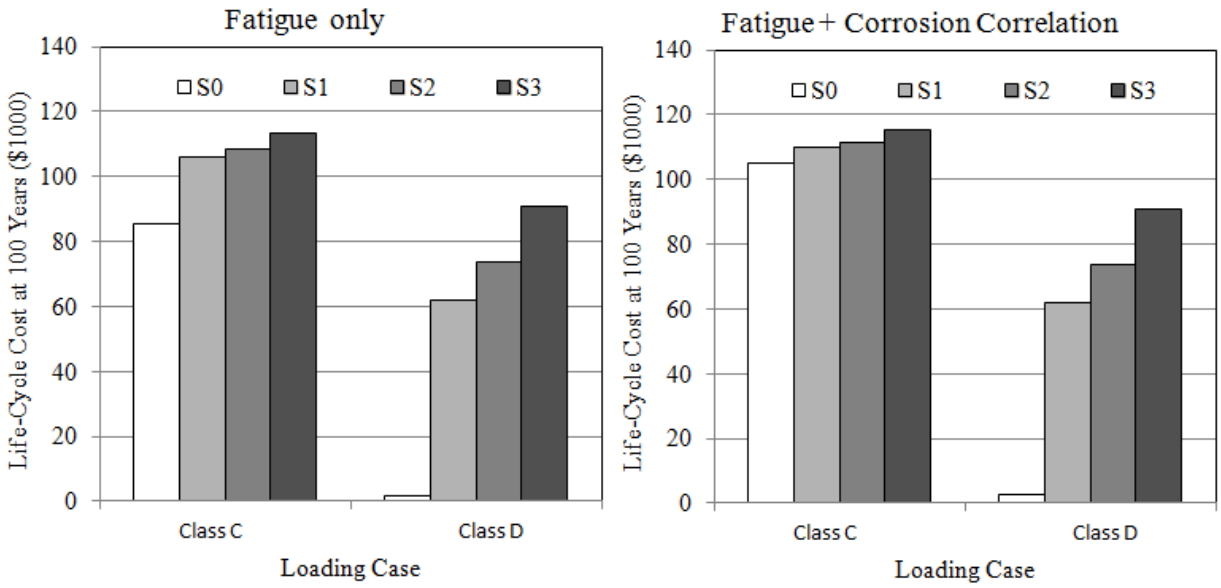

a) Fatigue only *b) Fatigue + corrosion correlation*

Figure 5.10: Life-cycle cost at low traffic volumes with consideration of corrosion

As shown, particularly for Class C roads, considering corrosion comes very close to changing the optimal strategy, and with slightly different costs could result in a different optimal choice.

Due to the different stress ranges at different stiffeners, it may not be optimal to consider the entire girder as one decision to treat or repair, but do selective treatments. The following new maintenance strategies are added:

- S4: inspection, repair, and needle peening as needed after every 20 years of service loading only on interior stiffeners
- S5: inspection, repair, and needle peening as needed after every 20 years of service loading only on interior and intermediate stiffeners.

The costs of treatment for each strategy were changed to reflect how much treatment was being performed. Figure 5.11 shows the results including these new maintenance strategies, each on individual graphs to easily distinguish changes at lower costs.

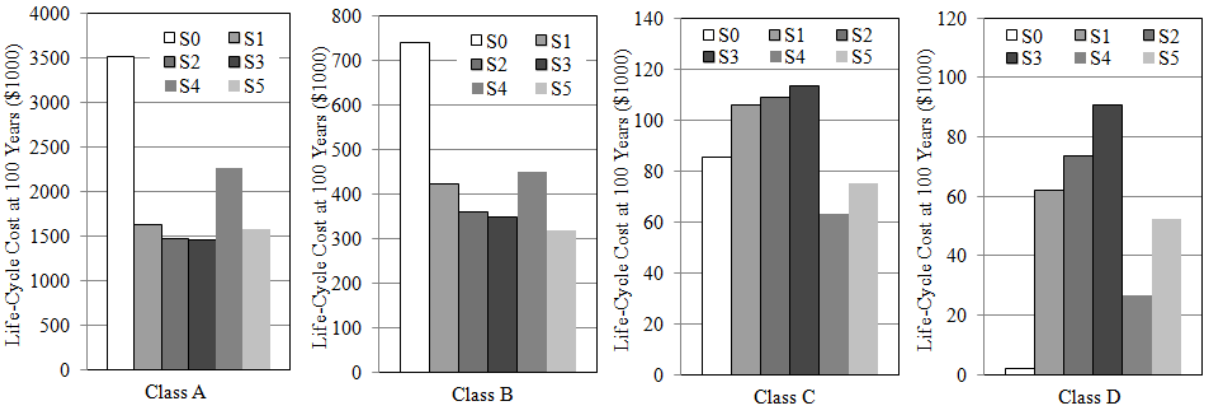

Figure 5.11: Live cycle cost including new maintenance strategies

For Class A, the traffic load is high enough that it is cost effective to treat all the stiffeners. For Class B, we can see that Strategy S5 is now the cheapest, which means it is no longer cost effective to treat the exterior stiffeners. For Class C roads, S4 is now the cheapest, meaning is it now optimal to only treat the interior stiffeners. For Class D roads, it remains optimal to do nothing, as there is not enough traffic to cause significant fatigue deterioration.

The largest factor in the decision of whether or not to treat is often the cost of treatment. Therefore a sensitivity analysis was performed on the treatment comparing the options of do nothing vs the optimal treatment strategy, as summarized in Table 5.3.

Table 5.3: Critical treatment cost

	Critical treatment cost	**Critical treatment cost per mm of treatment**
Class A	$ 512,966.31	$ 1,316.42
Class B	$ 191,757.01	$ 492.11
Class C	$ 33,742.30	$ 86.59
Class D	$ 0.00	$ 0.00

For Class A, B, and C roads, as the cost of doing nothing is larger than the treatment cost, the value in Table 5.3 represents the maximum treatment cost, as long as the cost of treatment is lower than the one shown it is cost effective to perform treatment. For Class D roads the optimization returned a negative value, which means that there is no scenario under which treatment will be less expensive than doing nothing.

In conclusion, the Markov chains developed in this thesis can be used to predict life-cycle costs for different maintenance strategies, and therefore can be used to select the optimal and most cost-effective strategy. The ease of use of Markov chains over MCS or M-DRM allows for the ability to quickly set up and calculate the effects of different loading cases and maintenance actions, which makes it a very powerful tool for planning bridge maintenance. Using the bridge designed in this section, a maximum total cost saving of $2,050,000 was obtained over the 100 year life span.

6.0 Conclusions and recommendations

6.1 Conclusions

The conclusions presented in this chapter are divided according to the three main areas of the research work: those resulting from (i) probabilistic fracture mechanics analysis of fatigue crack growth using Monte Carlo Simulation (MCS) and the Multiplicative Dimension Reduction Method (M-DRM), (ii) modelling fatigue deterioration and retrofitting using Markov chain models, and (iii) the application of the developed Markov chain models to compare fatigue management strategies for a full-scale bridge.

6.1.1 Probabilistic fracture mechanics using MCS and M-DRM

In Chapter 3 of this thesis, a probabilistic strain-based fracture mechanics (SBFM) model is successfully implemented with MCS and M-DRM to predict the statistics of fatigue crack growth. Based on this work, the following conclusions are drawn:

- For MCS, a convergence test was performed to determine the minimum amount of trials required to achieve a sufficient level of accuracy. Based on this test, it was found that 50,000 trials per stress range was sufficient to accurately establish the 50% and 97.7% S-N curves, which are commonly used by practicing engineers for fatigue assessment and design.
- The problem of SBFM simulations resulting in infinite lives for some trials at the lower stress levels can be easily dealt with in the MCS analysis by sorting the results and using their rank in the sorted list to obtain the survival probabilities directly, rather than calculating statistical parameters such as the mean and standard deviation.
- Solving this problem in the M-DRM analysis is a bigger challenge. To do this, known points were used to create a line of best fit and estimate where the final point would be if it weren't for the infinite life results. This approach only allowed the S-N curve in the finite life domain to be extended slightly. A better approach proved to be modifying the SBFM code so that the output was the threshold stress range limit (between finite and infinite life), rather than the number of cycles to failure. The S-N curve can then be completed by conservatively assuming that the curves from the finite and infinite life analysis can be extended until they intersect.
- A comparison of analyses performed using three loading histories – constant amplitude (CA) loading with a load ratio ($R = S_{min} / S_{max}$) of 0.1, and two variable amplitude (VA) loading

histories, one at the midspan of a simply supported 40 m bridge, and one at the support of a continuous 15 m bridge) – showed that the loading history does affect the position of the S-N curve. In general, the two VA loading curves fell below the CA loading curve.

Comparing the MCS and M-DRM results, the following additional conclusions are drawn:

- M-DRM can accurately predict the statistics of fatigue crack growth, both for as-welded and treated specimens, within 1% error at high stress ranges.
- The difference between the MCS and M-DRM analysis results at the lower stress ranges (where the M-DRM analysis could only be performed to obtain the statistics of the threshold stress range) was less than at the higher stress ranges, but still within 5%.
- The M-DRM analysis was performed using a fraction of the time required to perform the MCS analysis. Approximately 2 full days were required to calculate one S-N curve using MCS, compared to under one hour for M-DRM.
- M-DRM was also able to perform sensitivity analysis on the variables, with the Paris constant C having the highest sensitivity for most of CA and VA loading, followed by the load for VA and variation in the stress concentration factor for CA loading.
- While M-DRM resulted in a significant increase in the analysis speed, it is suspected that the large number of input parameters required by the probabilistic SBFM model and the high level of technical knowledge required to select these parameters means that the SBFM analysis implemented with M-DRM is probably still too complex and time consuming to be used routinely by practitioners to analyze many bridges in a large infrastructure network.

6.1.2 Modelling fatigue deterioration and retrofitting using Markov chain models

Both MCS and M-DRM require relatively complex equations and understanding to use effectively. Therefore a relatively simpler Markov chain model was investigated. This model is similar to the Markov chain models typically used to simulate deterioration due to other mechanisms (e.g. corrosion, wear) in existing bridge management systems (BMSs). In order to be applicable to a wide range of BMSs, two Markov chain sizes – five and ten condition states (CSs) – were considered. Three methods were used for calibration of the Markov chains with varying degrees of success: 1) calibration using design S-N curves (plots from CSA S16 [CSA, 2014] were used as a basis and a uniform Markov chain calibrated from

specific points), 2) calibration using failure data obtained by SBFM analysis (MCS output was used to determine the probability of failure in a given year, and the probability of being in the last condition state of the Markov chain, or failure, calibrated to that data), and 3) calibration using crack growth data from SBFM analysis (the MCS output was divided into CSs defined by crack lengths, and a non-uniform Markov chain calibrated to the probability of residing in each condition state). Following the calibration of these models, it was shown how they could be modified to simulate management actions (e.g. inspection, repair, and treatment). Based on this work, the following conclusions are drawn:

- Of the three calibration methods, calibration using the probabilistic SBFM crack growth data performed the best when comparing plots of individual CS probabilities and based on subsequent life-cycle cost analysis (LCCA). This method resulted in adequate predictions when evaluated based on comparisons with the design S-N curves. The other methods resulted in a closer fit, particularly for the 50% survival probability curve, but the fit from this calibration method was still close. Therefore the use of crack growth data (obtained by testing or fracture mechanics) is recommended when calibrating Markov chains to model fatigue deterioration.
- In comparing the life-cycle costs associated with several fatigue management strategies, the calibrated Markov chain model predicted the same optimal strategy as the probabilistic SBFM model, with a small fraction of the computational effort.
- Of the two Markov models used in this thesis, using five and ten condition states, both predicted the same optimal strategy with similar absolute values. There were small differences which were attributed to characteristics of larger CS models. Specifically, it takes a minimum of 10 years in the 10CS model for failure to begin, compared to 5 years for the 5CS model.
- The correlation between corrosion and fatigue was also studied and modelled using the Markov chain approach, and it was found that high levels of corrosion can have a significant impact on life-cycle cost, and can even change the optimal fatigue management strategy.

6.1.3 Application of Markov chain models for a full-scale bridge

The calibrated Markov chains models were then used on an example application to predict the fatigue deterioration of a full-scale steel-concrete composite highway bridge with a 21 m main span. Several different management strategies were modelled, including a mixture of impact treatment, inspection, and repair, in 20 year increments during the life of the bridge, and realistic costs were assigned to each management action. Based on this work, the following conclusions are drawn:

- In comparing the various management strategies, a cost savings of as much as $2,050,000 over the 100 year life span was obtained by choosing the optimal management strategy.
- Under realistic conditions and cost assumptions, optimal management strategies were identified that involved treatment of the critical fatigue details by impact treatment, including selective treatment of stiffeners at lower traffic volumes for additional savings. This demonstrates that such treatments can serve as a useful tool for the fatigue management of bridges.
- The flexibility and ease of use of the Markov chain models was exploited to easily analyze and modify a number of alternative management strategies, thus demonstrating the usefulness of this approach for modelling the fatigue deterioration and retrofitting of bridges.

6.2 Recommendations for future work

At the end of this project, a number of promising areas for future research to extend the findings of this study have been identified. They can be summarized as follows:

- For the example full-scale bridge application, certain assumptions could be more fully explored, such as the intervention costs (which were estimated), and the attribution of these costs. For example, in this analysis, if fatigue failure occurred on an element representing a certain percentage of a bridge girder, then an equal percentage of the girder replacement cost was incurred. In reality, it may be necessary to replace the full girder in this case, or perform a reinforcing repair that may be cheaper than the assumed amount.
- The full-scale example could also be improved with a more careful consideration of indirect costs, such as user delay costs due to full bridge or lane closure.
- The presented Markov chain models could be calibrated to test data for a wider range of fatigue life-improving treatments, such as grinding and other impact treatments.
- Fatigue problems in bridges often occur at locations where the applied stress range is difficult to assess using normal design models (e.g. distortion fatigue cracks at web stiffener ends). How to consider these cases in a BMS framework is an area requiring further investigation.
- In this research it was assumed that fatigue failure can be defined as crack growth to a critical depth related to the plate thickness. The facts that cracks of this size may not result in imminent failure and that fatigue failure does not have the same consequence in all locations on a bridge were not considered. These issues could be investigated in future research.

- The approach used to model correlations between element deterioration rates can be applied to other bridge elements to model such things as the effect of the wearing surface condition state on concrete deck deterioration, or the effect of joint waterproofing on bearing corrosion, etc., to improve the prediction accuracy of BMSs and result in better allocation of maintenance funding.

7.0 References

AASHTO. (2011). Manual for Bridge Evaluation, 2nd edition. *American Association of State Highway and Transportation Officials.*

ABBOTT S. P. (1998). Benefits of BRIDGIT Software. *TR News Special Issue — Hichwa Bridges: Progress and Prospects.* (194).

Adey, B. T., Klatter, L., & Kong, J. S. (2010). Overview of existing bridge management systems. *The IABMAS Bridge Management Committee*, *99*.

Albrecht, P. (1982). Fatigue behavior of weathered steel bridge components. *No. FHWA/MD-81/02 Final Rpt.*

Albrecht, P., & Cheng, J. G. (1983). Fatigue tests of 8-yr weathered A588 steel weldment. *Journal of Structural Engineering*, *109*(9), 2048-2065.

Albrecht, P., & Sidani, M. (1989). Fatigue of eight-year weathered A588 steel stiffeners in salt water. *Journal of Structural Engineering*, *115*(7), 1756-1767.

American Society of Civil Engineers. (2013). Report Card for America's Infrastructure. www.infrastructurereport.org

Ang, A. H. S., & Tang, W. H. (1984). *Probability concepts in engineering planning and design.*

Anthes, R. J. (1997). Modified rainflow counting keeping the load sequence. *International Journal of Fatigue*, *19*(7), 529-535.

Balomenos, G. P., and Pandey, M. D. (2013). Multiplicative Dimensional Reduction Method.

Bisby, L.A. and Briglio, M.B. (2004). ISIS Canada Educational Module No. 5: An Introduction to Structural Health Monitoring, *Prepared by ISIS Canada*, 3.

Bogdanoff, J. L., & Kozin, F. (1985). *Probabilistic models of cumulative damage*. John Wiley & Sons, Ltd, New York.

Bu, G., Lee, J., Guan, H., Blumenstein, M., & Loo, Y. (2014). Development of an Integrated Method for Probabilistic Bridge Deterioration Modelling. *Journal of Performance of Constructed Facilities*, *28*(2) 330-340. doi:10.1061/(ASCE)CF.1943-5509.0000421

Canadian Standards Association (CSA). (2006). Canadian Highway Bridge Design Code. *CAN/CSA S6-06*

Canadian Standards Association (CSA), (2014). Design of Steel Structures. *CAN/CSA S16-14*

Carnahan, J., Davis, W., Shahin, M., Keane, P., & Wu, M. (1987). Optimal maintenance decisions for pavement management. *Journal of Transportation Engineering*, *113*(5), 554-572.

Cesare, M. A., Santamarina, C., Turkstra, C., & Vanmarcke, E. H. (1992). Modeling bridge deterioration with Markov chains. *Journal of Transportation Engineering*, *118*(6), 820-833.

Grinstead, C. M., & Snell, J. L. (2012). *Introduction to Probability*. American Mathematical Society,

Dowling, N.E. (2007). *Mechanical Behaviour of Materials*. Upper Saddle River, NJ: Pearson Education Inc.

Downing, S. D., & Socie, D. F. (1982). Simple rainflow counting algorithms. *International Journal of Fatigue*, *4*(1), 31-40.

Elbehairy, H., Hegazy, T. and Soudki, K. (2009). Integrated Multiple-Element Bridge Management System. *Journal of Bridge Engineering, ASCE, Vol. 14, No. 3*, pp. 179-187.

Elhakeem, A. and Hegazy, T. (2005). Improving Deterioration Modeling using Optimized Transition Probability Matrices for Markov Chains. *TRB 84th Annual Meeting, January 10-14, Washington, D.C.*

Fisher, J. W., Kaufmann, E. J., & Pense, A. W. (1998). Effect of corrosion on crack development and fatigue life. *Transportation Research Record: Journal of the Transportation Research Board*, *1624*(1), 110-117.

Fisher, J. W., Kulak, G. L., & Smith, I. F. (1998). *A fatigue primer for structural engineers* (No. IMAC-BOOK-1998-002). National Steel Bridge Alliance, American Institute of Steel Construction.

Fisher, J. W., Yen, B. T., & Wang, D. (1990). Fatigue strength of riveted bridge members. *Journal of Structural Engineering*, *116*(11), 2968-2981.

Fisher, J. W., Yen, B. T., Wang, D., & Mann, J. E. (1987). Fatigue and fracture evaluation for rating riveted bridges. *NCHRP Report No. 302.*

Ghahremani, K. (2010). *Predicting the effectiveness of post-weld treatments applied under load* (Doctoral dissertation, University of Waterloo).

Ghahremani, K., & Walbridge, S. (2011). Fatigue testing and analysis of peened highway bridge welds under in-service variable amplitude loading conditions. *International Journal of Fatigue*, 33(3), 300-312.

Ghahremani, K., Walbridge, S., & Topper, T. (2015). High Cycle Fatigue Behaviour of Impact Treated Welds under Variable Amplitude Loading Conditions, *International Journal of Fatigue.*

Google. (2015) [streetview of Furnival Underpass] Accessed from maps.google.ca, December 03, 2015

Hajdin, R. (2001). KUBA-MS: The Swiss bridge management system. In *Structures 2001—A Structural Engineering Odyssey*, American Society of Civil Engineers, Washington, D.C.,

Hammad, A., Yan, J., & Mostofi, B. (2007). Recent development of bridge management systems in Canada. In *2007 Annual Conference and Exhibition of the Transportation Association of Canada: Transportation-An Economic Enabler (Les Transports: Un Levier Economique)*.

Hasofer, A., & Lind, N. (1974). Exact and invariant second-moment code format. *ASCE Journal Engineering Mechanics Division, 100*(1), 111–121.

Hawk, H. (2003). *Bridge life-cycle cost analysis* (No. 483). Transportation Research Board.

Hawk, H., & Small, E. P. (1998). The BRIDGIT bridge management system. *Structural Engineering International*, *8*(4), 309-314.

Hobbacher, A. (2009). IIW recommendations for fatigue design of welded joints and components, WRC Bulletin 520. *New York: The Welding Research Council*.

Holt, R., & Hartmann, J. L. (2008). *Adequacy of the U10 & L11 gusset plate designs for the Minnesota Bridge No. 9340 (I-35W over the Mississippi River)*. Federal Highway Administration, Turner-Fairbank Highway Research Center.

Inverardi, P., & Tagliani, A. (2003). Maximum entropy density estimation from fractional moments. *Communication in Statistics - Theory and Methods*, *32*(2), 327–345.

Jaynes, E. (1957). Information theory and statistical mechanics. *Physical Review Letters*, *108*(2), 171–190.

Jiang, Y. & Sinha, K. C. (1989). Bridge service life prediction model using the Markov chain. *Transportation Research Record, 1223, 24-30.*

Johnson, P. M., Couture, A., & Nicolet, R. (2007). *Commission of Inquiry Into the Collapse of a Portion of the de la Concorde Overpass: October 3, 2006-October 15, 2007: Report*.

Kennedy, C., & Lennox, W. (2001). Moment operations on random variables, with applications for probabilistic analysis. *Probabilistic Engineering Mechanics*, *16*(3), 253–259.

Khalil, M., & Topper, T. H. (2003). Prediction of crack-opening stress levels for 1045 as-received steel under service loading spectra. *International Journal of Fatigue*, *25*(2), 149-157.

Kozin, F., & Bogdanoff, J. L. (1989). Probabilistic models of fatigue crack growth: results and speculations. *Nuclear Engineering and Design*, *115*(1), 143-171.

Kucera, V., and Mattson, E. (1987). Atmospheric corrosion. Chapter 5, *Corrosion mechanisms*, 211–284.

Kuehn, B., Lukić, M., Nussbaumer, A., Guenther, H. P., Helmerich, R., Herion, S., Kolstein, M.H., Walbridge, S., Androic, B., Dijkstra, O., & Bucak, Ö. (2008, February). Assessment of existing steel structures: recommendations for estimation of remaining fatigue life. In *Joint Research Centre-European Convention for Constructional Steelwork Report*.

Lam, T. S., Topper, T. H., & Conle, F. A. (1998). Derivation of crack closure and crack growth rate data from effective-strain fatigue life data for fracture mechanics fatigue life predictions. *International Journal of Fatigue, 20*(10), 703-710.

Lassen, T. (1991). Markov modelling of the fatigue damage in welded structures under in-service inspection. *International Journal of Fatigue*, *13*(5), 417-422.

Li, G., Rosenthal, C., & Rabitz, H. (2001). High dimensional model representations. *Journal of Physical Chemistry A*, *105*(33), 7765–7777.

MacDougall, C., & Topper, T. H. (1997). The influence of variable amplitude loading on crack closure and notch fatigue behaviour. *International Journal of Fatigue*, *19*(5), 389-400.

McCalmont, D. (1990). *A Markovian model of bridge deterioration*, Bachelor of Science in Engineering thesis

MDOT (2007). PONTIS bridge inspection manual. *Michigan Department of Transportation.*

Micevski, T., Kuczera, G., & Coombes, P. (2002). Markov Model for Storm Water Pipe Deterioration. *Journal of Infrastructure Systems*, ASCE, *8*(2), 49-56.

Milev, M., Inverardi, P., & Tagliani, A. (2012). Moment information and entropy evaluation for probability densities. *Applied Mathematics and Computation*, *218*(9), 5782–5795.

Morcous, G. (2006). Performance prediction of bridge deck systems using Markov chains. *Journal of Performance of Constructed Facilities*, *20*(2), 146-155.

Morcous, G., and Hatami, A. (2011). Developing deterioration models for Nebraska bridges. Final report, *Nebraska Department of Roads*, pp. 182

MTO (1995). Ontario commercial vehicle survey, *Ministry of Transportation*

MTO (2012). Furnival Road Overpass Rehabilitation, *Ministry of Transportation*

National Transportation Safety Board (NTSB) (1984). Collapse of a Suspended Span of Route 95 Highway Bridge over the Mianus River, Greenwich, Connecticut. *HAR-84/ 03*

Newman, J.C. (1984). A Crack Opening Stress Equation for Fatigue Crack Growth. *International Journal of Fracture*, Vol. 24, pp. R131-R135.

Novak, S. R. (1983). Corrosion Fatigue Crack Initiation Behavior of Four Structural Steels. *Corrosion Fatigue: Mechanics, Metallurgy, Electrochemistry, and Engineering, ASTM STP 801*, pp 26-63.

Okasha, N. M., Frangopol, D. M., Fletcher, F. B., & Wilson, A. D. (2011). Life-cycle cost analyses of a new steel for bridges. *Journal of Bridge Engineering*, *17*(1), 168-172.

Palin-Luc, T., Pérez-Mora, R., Bathias, C., Domínguez, G., Paris, P. C., & Arana, J. L. (2010). Fatigue crack initiation and growth on a steel in the very high cycle regime with sea water corrosion. *Engineering Fracture Mechanics*, *77*(11), *1953-1962. doi:10.1016/j.engfracmech.2010.02.015*

Rahman, S., & Xu, H. (2004). A univariate dimension-reduction method for multi-dimensional integration in stochastic mechanics. *Probabilistic Engineering Mechanics*, *19*(4), 393–408.

Ranjith, S., Setunge, S., Gravina, R., & Venkatesan, S. (2013). Deterioration Prediction of Timber Bridge Elements Using the Markov Chain. *Journal of Performance of Constructed Facilities*, *27*(3), 319-325.

Robert E. Melchers. (1999). *Structural reliability analysis and prediction*.

Rosenblueth, E. (1981). Two point estimates in probabilities. *Applied Mathematical Modelling*, *5*(5), 329–335.

Schuëller, G., & Pradlwarter, H. (2007). Benchmark study on reliability estimation in higher dimensions of structural systems: an overview. *Structural Safety*, *29*(3), 167–182.

Schweitzer, P. A. (1989). Atmospheric corrosion. *Corrosion and Corrosion Protection Handbook*, 2nd

Shen G, Glinka G. (1991). Weight functions for a surface semi-elliptical crack in a finite thickness plate. *Theory of Applied Fracture Mechanics;15(3):247–55*

Standard, A. S. T. M. (2009). E23-09: Standard Test Method for Notched Bar Impact Testing of Metallic Materials. *Annual Book of ASTM Standards, ASTM*

Statistics Canada. (2009). Age of Public Infrastructure: A Provincial Perspective. www.statcan.gc.ca/pub/11-621-m/11-621-m2008067-eng.htm.

Taguchi, G. (1978). Performance analysis design. *International Journal of Production Research*, *16*(6), 521–530.

Thompson, P. D., Small, E. P., Johnson, M., & Marshall, A. R. (1998). The Pontis Bridge Management System. *Structural Engineering International*, *8*(4), 303-308.

Topper, T. H., & Lam, T. S. (1997). Effective strain–fatigue life data for variable amplitude fatigue. *International Journal of Fatigue*, *19*(93), 137-143.

Tran, H. D. (2007). Investigation of deterioration models for stormwater pipe systems. (Doctoral dissertation, Victoria University).

Uhlig, H. H., & Revie, R. W. (1985). Corrosion and corrosion control.

Veshosky, D., & Beidleman, C. (1996). Closure to "Comparative Analysis of Bridge Superstructure Deterioration" by David Veshosky and Carl R. Beidleman. *Journal of Structural Engineering 122*(6), 710-71.

Walbridge, S. (2005). A probabilistic study of fatigue in post-weld treated tubular bridge structures. *PhD Thesis.*

Walbridge, S. & Nussbaumer, A. (2008). Probabilistic assessment of the effect of post-weld treatment on the fatigue performance of tubular truss bridges. *Engineering Structures*, *30*(1), 247-257.

Walbridge, S., Dilum, F., & Adey, B. T. (2012). Probabilistic models to evaluate effectiveness of steel bridge weld fatigue retrofitting by peening. *Transportation Research Board*, (2285), 27-35. doi:10.3141/2285-04

Walbridge, S., Fernando, D., & Adey, B. T. (2012). Modelling inspection and fatigue retrofitting by post-weld treatment in bridge management systems. In *6th International Conference on Bridge Maintenance, Safety and Management* (pp. 3960-3967).

Walbridge, S., Fernando, D., & Adey, B. (2013). Total Cost-Benefit Analysis of Alternative Corrosion Management Strategies for a Steel Roadway Bridge. *Journal of Bridge Engineering*, *18*(4), 318–327.

Wirahadikusumah, R., Abraham, D., & Iseley, T. (2001). Challenging Issues in Modeling Deterioration of Combined Sewers. *Journal of Infrastructure Systems*, *7*(2), 77–84.

Xu, H., & Rahman, S. (2004). A generalized dimension-reduction method for multidimensional integration in stochastic mechanics. *International Journal for Numerical Methods in Engineering*, *61*(12), 1992-2019.

Yazdani, N., & Albrecht, P. (1989). Crack growth rates of structural steel in air and aqueous environments. *Engineering Fracture Mechanics*, *32*(6), 997-1007.

Zhang, X. (2013), Efficient Computational Methods for Structural Reliability and Global Sensitivity Analyses. *PhD Thesis*,

Zhao, Y., & Ono, T. (2001). Moment methods for structural reliability. *Structural Safety*, *23*(1), 47–75.